COMPARISON OF THE BETA-SPECTRA OF BORON 12 AND NITROGEN 12

Thesis by

Henry H. Hilton

In Partial Fulfillment of the Requirements

for the Degree of

Doctor of Philosophy

California Institute of Technology

Pasadena, California

1960

ACKNOWLEDGEMENTS

The author is indebted to Professors M. Gell-Mann and R. P. Feynman for proposing this problem, and to Professors T. Lauritsen, C. A. Barnes, R. F. Christy, W. A. Fowler, and C. C. Lauritsen for helpful discussions and encouragement throughout the course of this work. He is particularly indebted to Dr. Volker Soergel of the University of Freiberg and to Dr. Cornelis Van der Leun of the University of Utrecht, whose collaboration made this research possible, and to his wife, for her encouragement and patience.

The research was assisted by the joint program of the Office of Naval Research and the Atomic Energy Commission.

ABSTRACT

This thesis, a "Comparison of the Beta-Spectra of Boron 12 and Nitrogen 12," is an attempt to test the nature of the vector interaction in beta-decay. The ratio of the matrix elements of the Boron 12 and Nitrogen 12 beta-decays is expected theoretically to have an energy dependence of the form $(1 + 16/3\ aE)$, where a is of the order of $2/M$ for the Conserved Vector Current Theory in which the virtual pions surrounding the nucleons carry the beta-decay charge, and is of the order of $2/5M$ for the Fermi Theory in which the virtual pions do not. Inserting for M the value of the nucleon mass, the expected energy dependences are 1.4%/Mev and 0.3%/Mev. Two separate determinations of this energy dependence were made by measuring the momentum spectra of the two beta-decays. The first gave $+0.2 \pm 1.2$%/Mev, and the second gave 3.1 ± 1.2%/Mev. About half of these errors are systematic, and are the same for both experiments. Hence it seems wiser not to average the two experiments. The Conserved Vector Current Theory seems slightly favored by these two experiments.

TABLE OF CONTENTS

I. INTRODUCTION

This thesis, a "Comparison of the Beta-Spectra of B^{12} and N^{12}," was suggested by Dr. Gell-Mann to test the nature of the vector interaction in beta-decay (1). The fundamental form of the beta-interaction was proposed by Fermi in 1934 (2), and is discussed in detail by Konopinski and Uhlenbeck (3).

A comprehensive review of beta-decay theory and experiments may be found in three articles in Siegbahn's "Beta and Gamma Ray Spectroscopy," published in 1955. Rose discusses the theory of allowed beta-decay (4), Konopinski the theory of forbidden beta-decay (5), and Wu experiments on the shapes of beta-spectra (6).

The interaction is believed to be a point interaction between four fermions, two nucleons and two leptons. Letting a be the positive energy solution of the Dirac equation, and $\underline{a}$ the negative energy solution of the Dirac equation, i.e.,

$$\begin{aligned} (\not{p} - m)\, a &= 0 \,, \\ (\not{p} + m)\, \underline{a} &= 0 \,, \end{aligned} \tag{1}$$

the matrix elements for neutron decay H_n and for proton decay H_p may be expressed as follows:

$$H_n = \sum G_i (\bar{p} O_i n)(\bar{e} O_i \underline{\nu})$$
$$H_p = \sum G_i (\bar{n} O_i p)(\bar{\nu} O_i \underline{e}) \qquad (2)$$

The appropriate sums over spins and the nucleons, if more than one, are implied. The O_i represent operators, of which there are five types whose products are relativistically invariant scalars, corresponding to the scalar, vector, axial vector, tensor, and pseudoscalar interactions. Defining the γ matrices as follows:

$$\gamma_o = \begin{pmatrix} 1 & 0 \\ 0 & 1 \end{pmatrix}$$
$$\gamma = \begin{pmatrix} 0 & \vec{\sigma} \\ -\vec{\sigma} & 0 \end{pmatrix} \qquad (3)$$
$$\gamma_5 = \gamma_0\gamma_1\gamma_2\gamma_3 = -i\begin{pmatrix} 0 & 1 \\ 1 & 0 \end{pmatrix}$$

the five operators are defined as follows:

Scalar	1
Vector	γ_μ
Tensor	$i/2(\gamma_\mu\gamma_\nu - \gamma_\nu\gamma_\mu) = T_{\mu\nu}$ (4)
Axial vector	$i\gamma_\mu\gamma_5 = A_\mu$
Pseudoscalar	γ_5

These are defined so that $\gamma_o O^+ \gamma_o = O$.

Anticipating the violation of parity conservation, as proposed by Lee and Yang(7), we may write down the total matrix element for beta decay in the following manner:

$$
\begin{aligned}
M = \quad & g(\bar{p}\, 1\, n)\,(\bar{e}\,|\, C_S\, 1 - C'_S\, i\gamma_5\,|\,\nu) \\
& + g(\bar{p}\,\gamma_\mu\, n)\,(\bar{e}\,|\, C_V\,\gamma_\mu - C'_V\,\gamma_\mu\, i\gamma_5\,|\,\nu) \\
& + \tfrac{1}{2} g(\bar{p}\, T_{\mu\nu}\, n)\,(\bar{e}\,|\, C_T\, T_{\mu\nu} - C'_T\, T_{\mu\nu} i\gamma_5\,|\,\nu) \\
& - g(\bar{p} A_\mu\, n)\,(\bar{e}\,|\, C_A\, A_\mu - C'_A\, A_\mu\, i\gamma_5\,|\,\nu)
\end{aligned}
\qquad (5)
$$

The pseudoscalar interaction has been neglected, and a summation over μ and ν is implied. The gC's are the parity conserving couplings, and the gC's are the parity non-conserving couplings.

The parity conserving operators, as defined in equation 4, may be divided into two groups: those which couple large components of the wave functions, and those which couple small components. The division is as follows:

Operator	Large	Small
1	$1 = \begin{pmatrix} 1 & 0 \\ 0 & 1 \end{pmatrix}$	-
γ_μ	$\gamma_o = \gamma \begin{pmatrix} 1 & 0 \\ 0 & -1 \end{pmatrix}$	$\gamma_k = \begin{pmatrix} 0 & \sigma_k \\ -\sigma_k & 0 \end{pmatrix}$
$T_{\mu\nu}$	$T_{ij} = \begin{pmatrix} \sigma_k & 0 \\ 0 & \sigma_k \end{pmatrix}$	$T_{ok} = i \begin{pmatrix} 0 & \sigma_k \\ \sigma_k & 0 \end{pmatrix}$
A_μ	$A_k = \begin{pmatrix} \sigma_k & 0 \\ 0 & -\sigma_k \end{pmatrix}$	$A_o = \begin{pmatrix} 0 & 1 \\ -1 & 0 \end{pmatrix}$

For non-relativistic nucleons, we may consider only the coupling between large components in the nucleon spinors, leading to the Fermi matrix element $\int 1$ for scalar and vector couplings, and to the

Gamow-Teller matrix element $\int \vec{\sigma}$ for tensor and axial vector couplings. In this approximation the total matrix element becomes:

$$
\begin{aligned}
M = \; & (\textstyle\int 1)\left\{(\bar{e}\, C_S \begin{pmatrix} 1 & 0 \\ 0 & 1 \end{pmatrix} - C_S' \begin{pmatrix} 0 & 1 \\ 1 & 0 \end{pmatrix} \nu)\right. \\
& \left. + (\bar{e}\, C_V \begin{pmatrix} 1 & 0 \\ 0 & -1 \end{pmatrix} - C_V' \begin{pmatrix} 0 & 1 \\ -1 & 0 \end{pmatrix} \nu)\right\} \\
+ \; & (\textstyle\int \vec{\sigma}) \cdot \left\{(\bar{e}\, C_T \begin{pmatrix} \vec{\sigma} & 0 \\ 0 & \vec{\sigma} \end{pmatrix} - C_T' \begin{pmatrix} 0 & \vec{\sigma} \\ \vec{\sigma} & 0 \end{pmatrix} \nu)\right. \\
& \left. + (\bar{e}\, C_A \begin{pmatrix} \vec{\sigma} & 0 \\ 0 & -\vec{\sigma} \end{pmatrix} - C_A' \begin{pmatrix} 0 & \vec{\sigma} \\ \vec{\sigma} & 0 \end{pmatrix} \nu)\right\} .
\end{aligned}
\tag{6}
$$

Until the proposal by Lee and Yang of parity non-conservation, the determination of the relative strengths of the four parity conserving couplings was the subject of experimental investigation. Since then one has had all eight to determine. It should be noted that no interference between the parity conserving and parity non-conserving couplings manifests itself unless one measures a pseudoscalar quantity such as $\vec{\sigma}_e \cdot \vec{p}_e$ or $\vec{p}_e \cdot (\vec{p}_e \times \vec{p}_\nu)$. Jackson, Treiman, and Wyld (8) have worked out several decay probabilities for electron emission as a function of the eight coupling constants, for the case of plane waves for electron and neutrinos. They find that the probability of decay for an electron of energy E, into a solid angle $d\Omega$, and having a spin direction $\vec{n}$ in its rest frame is:

$$
\begin{aligned}
& \omega(\vec{n}, E, \Omega)\, dE\, d\Omega \\
& = \frac{g^2}{(2\pi)^4}\, pE\, (E^o - E)^2\, dE d\Omega \\
& \quad \times \xi \left[1 + b\, {}^{m}/_{E} + G \vec{n} \cdot \frac{\vec{p}}{E}\right] .
\end{aligned}
\tag{7}
$$

Furthermore, they find that the probability of decay for an electron from an oriented nucleus for an allowed transition $J = J' = J, J\pm1$, where $\langle\vec{J}\rangle$ is the expectation value of the vector angular momentum of the original nucleus, is:

$$\omega(\langle\vec{J}\rangle, E, \Omega)\, dE\, d\Omega$$

$$= \frac{2g^2}{(2\pi)^4}\, pE\,(E^o - E)^2\, dE\, d\Omega$$

$$\times \xi \left[1 + b\,\frac{m}{E} + A\,\frac{\langle\vec{J}\rangle}{J} \cdot \frac{\vec{p}}{E}\right] . \qquad (8)$$

The quantities in equations 7 and 8 have the following values, the upper signs referring to electrons, the lower to positrons.

$$\xi = |M_F|^2 \left\{|C_S|^2 + |C_S'|^2 + |C_V|^2 + |C_V'|^2\right\} \qquad (9a)$$

$$+ |M_{GT}|^2 \left\{|C_T|^2 + |C_T'|^2 + |C_A|^2 + |C_A'|^2\right\}$$

$$b\xi = \pm 2\mathrm{Re}\left\{|M_F|^2 (C_S C_V^* + C_S' C_V'^*) + |M_{GT}|^2 (C_T C_A^* + C_T' C_A'^*)\right\} \qquad (9b)$$

$$G\xi = \pm 2\mathrm{Re}\left\{|M_F|^2 (C_S C_S'^* - C_V C_V'^*) + (M_{GT})^2 (C_T C_T'^* - C_A C_A'^*)\right\} \qquad (9c)$$

$$A\xi = 2\mathrm{Re}\left[\pm |M_{GT}|^2 \lambda_{JJ'} (C_T C_T'^* - C_A C_A'^*)\right. \qquad (9d)$$

$$\left. + \delta_{J'J} |M_F||M_{GT}| \left(\frac{J}{J+1}\right)^{\frac{1}{2}} (C_S C_T'^* + C_S' C_T^* - C_V C_A'^* - C_V' C_A^*)\right]$$

$$\lambda_{JJ'} = \begin{cases} 1 & J \to J' = J - 1 \\ \dfrac{1}{J+1} & J \to J' = J \\ -\dfrac{J}{J+1} & J \to J' = J + 1 \end{cases} \qquad (9e)$$

The Fierz interference term, $b\xi$, had been known to be effectively zero (9), and in 1957 it was believed that the interaction was S and T (9). Wu et al. (10) measured the electron distribution from oriented $Co^{60}(5^+ \rightarrow 4^+)$ and found nearly the maximum asymmetry, with the emission of electrons more favored in the direction opposite to that of the nuclear spin. With reference to equation 8, the conclusion is that $C'_T = -C_T$, or $C'_A = C_A$. Boehm et al. (11) studied the positron polarization from N^{13} by measuring the circular polarization of the high-energy annihilation-in-flight quanta. The ratio of the square of the Gamow-Teller and Fermi matrix elements is 0.40, and so this checks the Fermi part of the interaction. They obtained a polarization of $(0.93 \pm .20)$ v/c, and assuming it is exactly v/c, the following relations hold as a consequence of equation 7, $C'_S = -C_S$, or $C'_V = C_V$.

Burgy et al. (12), by measuring the asymmetries in the decay of polarized neutrons, in particular the correlation between the momentum of the neutrino and the neutron spin, and the correlation between the momentum of the electron and the neutrino spin, concluded that the coupling was V-A, and that $-\frac{C_A}{C_V} = 1.25 \pm .04$. Comparison of the O^{14} and neutron lifetimes gives $\left|\frac{-C_A}{C_V}\right| = 1.19 \pm .04$ (13).

It should be stated that there were many experiments performed, and repeated, before coming to the firm conclusion that the beta-decay coupling is V-A, where $C_V = C'_V$, $C_A = C'_A$, and $C_A = -1.2\, C_V$. However, that appears to be the present situation (13, 14).

Define $gC_V = gC'_V = \frac{G_V}{\sqrt{2}}$, and $gC_A = gC'_A = \frac{G_A}{\sqrt{2}}$, the matrix element for beta-decay, equation 5, may be rewritten as follows:

$$M = \frac{G_V}{\sqrt{2}} (\bar{p}\gamma_\mu n)(\bar{e}\gamma_\mu(1 - i\gamma_5)\nu)$$

$$- \frac{G_A}{\sqrt{2}} (\bar{p}\, i\gamma_\mu\gamma_5)(\bar{e}\, i\gamma_\mu\gamma_5(1 - i\gamma_5)\nu) \quad , \tag{10}$$

or $$M = \frac{1}{\sqrt{2}} [\bar{p}(G_V\gamma_\mu - (-G_A) i\gamma_\mu\gamma_5) n] (\bar{e}\gamma_\mu(1 - i\gamma_5)\nu) . \tag{11}$$

The matrix element for muon-decay is given by (14)

$$M_\mu = \frac{1}{\sqrt{2}} [\bar{\mu}(G\gamma_\alpha - Gi\gamma_\alpha\gamma_5)\nu] \overset{+}{} [\bar{e}\gamma_\alpha(1 - i\gamma_5)\nu] . \tag{12}$$

Feynman and Gell-Mann (15) were led to propose a universal V-A interaction of this type by observing that the Dirac equation for an electron

$$(i \not{\nabla} - \not{A})\psi = m\psi \tag{13}$$

where $$\psi = \begin{pmatrix} \theta + \phi \\ \theta - \phi \end{pmatrix}$$

may be written as

$$[(i\nabla_\mu - A_\mu)(i\nabla_\mu - A_\mu) + \vec{\sigma}\cdot\vec{B} - i\vec{\alpha}\cdot\vec{E}]\chi = m^2\chi \tag{14}$$

where $$\psi = \frac{1}{m}(i \not{\nabla} - \not{A} + m)\chi . \tag{15}$$

Now since $i\gamma_5$ commutes with $\vec{\sigma}$ and $\vec{\alpha}$, there are solutions of equation 14 for which

$$i\gamma_5 = \mp \chi \ .$$

Therefore, $$\chi = \frac{1}{2}(1 \mp i\gamma_5)\psi$$

or $$\chi = \begin{pmatrix} \phi \\ -\phi \end{pmatrix} , \begin{pmatrix} \theta \\ \theta \end{pmatrix} \ . \qquad (16)$$

Furthermore, by simplifying equation 14, one obtains two second order two component equations:

$$\begin{aligned} [(i\nabla_\mu - A_\mu)^2 + \vec{\sigma} \cdot (\vec{B} + i\vec{E})]\,\phi &= m^2\phi \\ [(i\nabla_\mu - A_\mu)^2 + \vec{\sigma} \cdot (\vec{B} - i\vec{E})]\,\theta &= m^2\theta \end{aligned} \qquad (17)$$

Arguing that the θ's and ϕ's are fundamental, since the ψ's from equation 15 involve gradients, they proposed to use θ or ϕ as the field operators in beta-decay. This amounts to replacing ψ by $\frac{1}{2}(1 \mp i\gamma_5)\psi$ in the usual coupling. Furthermore, they suppose that this rule applies to the wave functions of all the particles entering the interaction. Defining $a = \frac{1}{2}(1 \mp i\gamma_5)$, $\bar{a} = \frac{1}{2}(1 \pm i\gamma_5)$, this means that in each term of the interaction are terms of the form $\bar{a} O_i a$, when the O_i represent the five couplings of equation 4. Since γ_5 anti-commutes with γ_μ, $\mu = 0, 1, 2, 3$, the scalar, tensor, and pseudo-scalar interactions give $\bar{a} O_i a = O_i \bar{a} a = 0$, and the vector and axial vector interaction give $\bar{a} O_i a = O_i a\, a = O_i a$, and hence these couplings survive. Furthermore, for vector coupling $O_i = \gamma_\mu$, and $O_i a = \gamma_\mu \dfrac{(1 \mp i\gamma_5)}{2}$, and for axial vector coupling $O_i = i\gamma_\mu\gamma_5$, and hence $O_i a = \mp \gamma_\mu(1 \mp i\gamma_5)$, and thus the vector and axial vector couplings

are the same. The $\mp$ sign in the above discussion gives left-handed or right-handed particles, and experiments have shown that the minus sign is correct (13).

Returning to equations 11 and 12, it is clear that in μ-decay one can be reasonably sure of measuring the Fermi coupling constant G, unaltered by the effects of strong couplings. In nuclear beta-decay one measures effective coupling constants, G_V and $-G_A$, which contain the effects of the strong interactions of the nucleons. The measured values of G_V and $-G_A$ are $G_V = 0.99\ G$, and $-G_A = 1.2\ G$ (14). For the latter this is as yet no explanation, and the former has led to the speculation that there is a conserved vector current (1,14).

In electromagnetism all charged elementary particles have the same charge $\pm e$. This universality is not disturbed by strong interactions, the reason being that the electromagnetic current j_μ is a conserved quantity. Now the vector operator describing nucleons in beta-decay is $\bar{n}\gamma_\mu p$, which is not, in the Yukawa theory of strong interactions, a conserved quantity. It is, however, one term of a conserved quantity, the $x \mp iy$ component of the isotopic spin current, which includes the current due to pions. By analogy with electromagnetism one argues that the nucleon operator $G\gamma_\alpha(1 - i\gamma_5)$ must be replaced by

$$G_V F_1(q^2)\gamma_\alpha - (-G_A)F_2(q^2)\gamma_\alpha i\gamma_5 + AF_3(q^2)\sigma_{\alpha\beta}q_\beta - BF_4(q^2)i\gamma_5 q_\alpha \qquad (18)$$

where q_a is the momentum transfer, and the form factors $F_i(q^2)$ all have $F_i(0) = 1$ (14).

The interaction with coefficient A is called "weak magnetism," and in the conserved vector current theory $A = \frac{\mu_p - \mu_n}{2M} = \frac{-\mu_V}{2M}$ where μ_p and μ_n are the anomalous moments and M is the nucleon mass. In the Fermi theory A = O by definition (16). The interaction with coefficient B is called the induced pseudoscalar, and may be evaluated exactly.

The test of the conserved vector current is the determination of the coefficient A. Consider the isobaric triplet B^{12}, C^{12}, and N^{12}, of which an energy level diagram is shown in fig. 1. The ground state of C^{12} is $0^+(T=0)$ and the ground states of B^{12} and N^{12} are $1^+(T=1)$. The corresponding state in C^{12} is at 15.1 Mev and is $1^+(T=1)$. For the $\beta^{\mp}$ transition, an evaluation of the beta-decay transition probability shows that it is proportional to (1)

$$p^2(E^o-E)^2\, dp\, \left(1 \pm 8/3\ \frac{\eta}{2M}\ E\right), \qquad (19)$$

where $\eta = \frac{1 + \mu_V}{\lambda}$ for the conserved vector current theory, and $\eta = 1/\lambda$ for the Fermi theory. $\mu_V = \mu_p - \mu_n = 3.7$, and $\lambda = \frac{-C_A}{C_V} \approx 1.2$. If a is defined as $\eta/2M$, $a \approx 2M^{-1}$ in the conserved vector current theory, and $a \approx 2/5\ M^{-1}$ in the Fermi theory. These estimates treat the transition magnetic moment as if it were due entirely to the intrinsic moments of the nucleons, and ignore orbital moments and more complicated effects.(31) An experimental determination of a for the conserved

vector current theory may be made from the γ-ray width of the 15.1-Mev state in C^{12}, leading to (1)

$$|a| = (2.34 \pm 0.25)M^{-1} \tag{20}$$

Now we are in a position to write down the complete transition probabilities for the beta-decay of B^{12} and N^{12}

$$N_B(p)dp = \frac{g^2}{2\pi^3} (1^+|M|0^+)^2 \mathcal{F}(+Z,p) (1 + 8/3\ aE)p^2(E^o-E)^2dp \tag{21}$$

$$N_N(p)dp = \frac{g^2}{2\pi^3} (1^+|M|0^+)^2 \mathcal{F}(-Z,p) (1 - 8/3\ aE)p^2(E^o-E)^2dp \tag{22}$$

g^2 is the coupling constant, $(1^+|M|0^+)$ is the nuclear matrix element, which is the same for the two transitions, $(1 \pm 8/3\ aE)$ the weak magnetism or conserved vector current factor, and $(2\pi^3)^{-1}p^2(E^o-E)^2dp$ the statistical factor. $\mathcal{F}(\pm Z,p)$ is the coulomb factor, which arises from the fact that electron wave functions must satisfy the Dirac equation. This factor is conventionally written as (17, 18)

$$\mathcal{F}(\pm Z,p) = F(\pm Z,p) \left[1 \mp 2\alpha Zr \left[\frac{5E + E^{-1}}{6}\right]\right], \tag{23}$$

where $F(\pm Z,p)$ is defined in the NBS tabulations (19), and the second factor has become known as the finite DeBroglie wavelength correction. α is the fine structure constant and r is in units of $\hbar/mc$.

Knowing the energies of the two decays, one may divide out the statistical factors and coulomb factors, and then divide the two spectra, leading to

$$R(B/N) \propto (1 + 16/3\, aE) \qquad (24)$$

This gives an energy dependence in the ratio of about 1.4%/Mev for the conserved vector current theory, and about 0.3%/Mev for the Fermi theory. The purpose of comparing the beta-spectra of B^{12} and N^{12} is to look for this energy dependence and to see with which theory it is consistent.

II. THE EXPERIMENT

As explained in the preceding section, the test of the conserved vector current hypothesis involves the comparisons of the nuclear matrix elements of the beta decays of B^{12} and N^{12}. Experimentally, one measures the electron momentum spectra of these two decays, and an appropriate analysis then yields the matrix elements.

B^{12} and N^{12} were produced in the two reactions (20)

$$B^{11}(d,p)B^{12} \qquad Q = 1.138 \text{ Mev}$$

$$B^{10}(He^3,n)N^{12} \qquad Q = 1.46 \text{ Mev}$$

B^{12} has a half-life of 20.34 ± 0.05 msec, and a disintegration energy of 13.378 Mev ($E_{\beta max}$ = 13.378 Mev). N^{12} has a half-life of 11.43 ± 0.05 msec, and a disintegration energy of 17.46 Mev ($E_{\beta max}$ = 16.44 Mev) (20).

Figure 2 is a schematic diagram of the experimental apparatus. The 3 Mv Van de Graaff generator was used to produce a beam of d or He^3 ions, which were magnetically analyzed in a 90° double focusing magnetic analyzer. The target, either natural boron (B^{11}) or enriched B^{10} (B^{10}) was at the focal position of a beta-ray spectrometer.

This spectrometer was a thin-lens type, axially-symmetric and iron-free, as discussed by Siegbahn (21), Thomas (22), and Hornyak (23). Details of the design, alignment, and calibration are discussed in Appendix A. The momentum resolution was about 1%, the solid angle

approximately 1% of a sphere, and the maximum focusing energy about 18.5 Mev. The momentum analyzed electrons were detected either with a Geiger-Müller counter and a thin anthracene crystal in coincidence, or with a plastic scintillator.

A standard beam current integrator, accurate to about 1%, was used to measure the amount of charge collected on the target. The energy of the beam was regulated to about 1 part in 1000 by controlling the magnetic analyzer current. For a fixed amount of charge collected with the beam energy held constant, the number of electrons detected was recorded for a sequence of electron momenta. To eliminate any systematic effects due to slow drifts in the electronic circuitry or to deterioration of the target, each set of data consisted of a sequence of momentum points taken twice, first in one order and then in the reverse order. No such effects were observed.

The range of electron energies over which it is practical to take data is severely limited. On the high-energy end of the B^{12} spectrum any uncertainty in the target backing and thickness, through which the electrons must pass before they are analyzed by the spectrometer, affects greatly the $(W_o-W)^2$ term in the statistical factor. For example, at 12.4 Mev, a 10 kev error in the target thickness will make a 2% error in the matrix element. Both B^{12} and N^{12} decay not only to the ground state of C^{12}, but also to excited states of C^{12}. Although the branching ratios are small, due to the shape of the statistical factor, the correction

to obtain only the ground state transition becomes quite large at lower energies, about 12% for N^{12} at 5.0 Mev. This correction is discussed more fully in section III. For these reasons the comparison of the two matrix elements was made between 5 and 12 Mev.

The experiment was performed twice, the first time with Dr. Volker Soergel of the University of Freiberg, and the second time with Dr. Cornelis Van der Leun of the University of Utrecht. Although both experiments were basically the same, the details were somewhat different, and hence the experiments will be discussed separately. Table I shows the main similarities and differences.

For the first experiment with Dr. Soergel, targets were made by depositing amorphous boron from an alcohol suspension on a 1 mil copper backing. This was supported by a lucite holder, consisting of two pieces of 1/16" lucite 1/4" x 1/2", with a 1/4" hole in the center of each. Natural boron was used for the B^{12} experiment and enriched B^{10} for the N^{12} experiment. The original targets were broken before they were weighed to determine their thickness, so an effort was made to make two more in the same manner. The new deposits of B^{11} and B^{10} on a circular area 1/4" in diameter were about 8 mg and 16 mg respectively, with an uncertainty of about $\pm$ 50%. These weights give thicknesses of 13 mg/cm^2 and 26 mg/cm^2 respectively. The energy lost by an electron or positron passing through these targets is determined by the value of dE/dx. At 9 Mev $\frac{-dE^+}{dx} \approx -\frac{dE^-}{dx} \approx 1.9$ kev-

TABLE I

Experimenters:	Soergel Hilton	Van der Leun Hilton
Counters:	Geiger-Müller Counter and 2"x1/2" anthracene crystal in coincidence with 1 Mev lucite absorber between	2" x 3" plastic scintillator with 100 Channel Pulse Height Analyzer
Beam:	Continuous	60 cycle chopped with gated counter
Background:	Interposed brass valve in beam	Interposed quartz disc in beam
Targets:	12-38 kev (B^{12}) 40-120 kev (N^{12}) Deposited	1/2 kev (B^{12}) 1/2 kev (N^{12}) Cracked diborane
Range of Electron Energies:	5.2 to 11.8 Mev (30 to 65 mv.) 15 points	6.1 to 10.9 Mev (35 to 60 mv.) 5 points
Statistics:	10,000 counts/point	80,000 counts/point

cm^2/mg. These values are obtained by interpolation from values for beryllium and carbon (24). Thus the target for B^{12} was about 25±13 kev thick, and that for N^{12} was about 50±25 kev thick. The 1 mil copper backing was about 35 kev thick for 9 Mev electrons and positrons (24).

To estimate the effective target thickness for the bombarding particles (d and He^3), we note that the ranges of two particles with the same charge Z and the same initial velocity v in the same material have the ratio (25)

$$R_1 R_2 = \left(\frac{M}{Z^2}\right)_1 \quad \left(\frac{M}{Z^2}\right)_2^{-1} .$$

If the capture and loss of electrons has the same velocity dependence for particles of different charge, this formula is valid for particles of different charge but with the same initial velocity. For the bombarding particles and energies used this relationship is approximately true. From tables of the energy loss of charged particles in matter (26), and using the above range formula, it is found that the range of 0.5 Mev deuterons in boron is approximately 0.9 mg/cm^2, and that of 3 Mev He^3 is approximately 2.2 mg/cm^2. It is thus seen that the targets were much thicker than necessary to obtain the full yield of the reaction, and introduced an unnecessary energy loss for the electrons, a situation which was corrected in the second experiment.

The electron detection was accomplished by using a two-windowed Geiger-Müller counter and a 2-1/2" x 1/2" anthracene crystal in

coincidence. The GM counter was made from a 2" brass tube 5/8" long, with the two end windows of 2 mil aluminum, cemented on with araldite. The wire, approximately 2 mil tungsten, was inserted radially through a Stupakoff fitting and extended about 7/8 of the diameter. A 1/8" tube was soldered on a radius for filling the counter. Optimum operation was obtained with a mixture of 2 cm of argon and 2 cm of alcohol. This counter was placed between the ring focus and end plate of the beta spectrometer. In contact with the GM counter was a 2 mil copper vacuum seal, and then a 0.2" lucite absorber, which is about 1 Mev thick for 9 Mev electrons and positrons (24). The purpose of this absorber was to stop low energy electrons which might have been scattered through the GM counter.

The anthracene counter was covered with a 2 mil aluminum reflector and placed snugly against the absorber. A 19" long 1-1/2" diameter lucite light pipe was optically connected to the anthracene crystal and to a 5819 photomultiplier with vacuum grease. Finally, the 5819 was placed inside a compensating coil, whose current was in parallel with the beta spectrometer field current.

The pulses from the GM counter and those from the anthracene crystal were fed into standard 10T2 pulse amplifiers. The discriminator outputs were fed to two univibrators to give a standard pulse size and length of 10 microseconds, and the coincidence was obtained with a standard Rossi circuit. In essence the counting arrangement consisted

of two GM counters, as the anthracene crystal is of the order of 2.5 Mev thick for electrons in the range of 6 to 11 Mev and was biased at approximately 500 kev.

In practice at each momentum setting of the beta-spectrometer the following data was taken: the time of the run, the number of GM counts, the number of crystal counts, and the number of coincidence counts. Further each point was taken twice, with the gain of the photomultiplier output changed by a factor of two, which effectively changed the cutoff-bias from 500 kev to 250 kev, as a check of the low energy background. This usually changed the crystal singles rate by a factor of two, but had little effect on the coincidence rate. The high and low gain coincidence counts for the points between 30 mv. and 65 mv. (the voltage drop across a current measuring resistance), corresponding to 5.2 and 11.8 Mev, and their ratios are shown in Table II. The weighted ratio for the B^{12} is 1.006, and for the N^{12} is 1.010. It appears that the fluctuations are approximately random, and the final curves were obtained by adding the high and low counts together.

As can be seen from Table II, the number of counts in the boron spectrum varies from about 14000 at 45 mv. to about 3300 at 65 mv. The variation in the nitrogen spectrum is from 10000 counts at 52.5 mv. to 5300 at 30 mv. This data, from 30 mv. to 65 mv., is that on which the comparison between the two matrix elements was made. Some additional data was taken to energies above the end-points of both spectra for completeness. The corrected momentum spectra and Kurie plots are shown in figures 3, 4, 5, 6.

TABLE II

	Boron 12			Nitrogen 12		
Mv.	High Gain Counts	Low Gain Counts	Ratio	High Gain Counts	Low Gain Counts	Ratio
30.0	5009	4857	1.031	2680	2616	1.024
32.5	5537	5546	.998	3026	2945	1.028
35.0	6078	5875	1.075	3453	3535	.977
37.5	6553	6463	1.014	3831	3842	.997
40.0	6871	6611	1.039	4128	4135	.998
42.5	6893	6949	.992	4559	4421	1.031
45.0	6911	6997	.988	4651	4674	.995
47.5	6674	6690	.998	4810	4849	.992
50.0	6301	6455	.976	4944	4925	1.004
52.5	5710	5792	.986	4948	5011	.987
55.0	5194	5035	1.032	5042	4836	1.043
57.5	4366	4281	1.017	4842	4686	1.033
60.0	3394	3446	.985	4668	4542	1.028
62.5	2422	2546	.951	4347	4330	1.004
65.0	1695	1611	1.052	3960	3918	1.011
Avg.			1.006			1.010

The background counting rate was determined by closing the valve of the beam tube, and measuring the number of coincidence counts per crystal count at various gain settings and momentum settings. Typical rates were 5 to 10 per 1000, to be compared with approximately 500 true counts per 1000.

The GM counter had a dead-time of 200 μsec, and the counting rate was kept low enough so that the dead-time correction did not exceed 1%. This resulted in the accidental coincidence rate being negligible.

The regulation signal for the Van de Graaff generator was taken from two slits about 8" from the target, and about 20" from the exit of the magnetic analyzer. The beam was required to enter the beta spectrometer on axis, and trimmed by two sets of tantalum slits to give a source size of about 1-1/2 mm square. It was discovered that the beam spot moved horizontally as the beta-spectrometer field was changed. The stray field of the spectrometer in the space below the Van de Graaff and above the magnetic analyzer apparently was strong enough to deflect the beam slightly. The displacement at the target position was about 5 mm at the highest beta-spectrometer field, and of course changed in sign and magnitude for the d and He^3 beams. This is due to the different energies used, and the fact that opposite senses of the beta-spectrometer field are necessary to focus electrons and positrons. To compensate for this a coil was placed above the magnetic analyzer, and the two vertical trimming slits (about 8" from the target) were connected

to a difference amplifier. The beam was kept centered by varying the compensating field, keeping the difference signal nil. With only one compensating coil the trajectory of the incident beam will move slightly in the magnetic analyzer. Since this is a double focusing magnetic analyzer, the change in bombarding energy, and hence the change in yield, will be second order effects.

The second experiment with Dr. Van der Leun was performed several months later and attempted to improve several aspects of the experiment. As has been stated, the deposited boron targets were much thicker than necessary to stop the incident beam of deuterons or the He^3 ions and hence obtain the maximum yield of the reactions. J. Overly had made several boron targets by cracking diborane gas, and offered to make some for us. A piece of 1 mil copper 1/2" in diameter was clamped between a 1/4" diameter by 1/8" thick copper backing and a 1/4" O.D. by 7/16" I.D. by 1/8" thick copper "washer." This jig was screwed together and placed in a quartz tube. An induction heater was used to bring the copper to red heat, and then diborane gas was admitted from a flask. When the copper had cooled off the uncracked diborane was returned to the flask by reducing it to liquid nitrogen temperature, and the process was repeated. About ten repetitions gave targets estimated to be about 1/2 kev thick for 9 Mev electrons. The 1 mil copper was then removed and placed in the same lucite holder as used in the first experiment. It should be noted that the 1/2 kev of boron is small

compared with the 35 kev of copper backing (both for 9 Mev electrons), and hence the uncertainty in the target thickness due to the boron was negligible. It appeared that thinner copper backings would not stand the heat of the cracking process.

Since Dr. Van der Leun and I had the benefit of Dr. Soergel's and my experiment, it was decided to concentrate on a few points of the momentum spectra, and get better statistics. Five momenta were chosen, corresponding to 35, 37.5, 47.5, 57.5, and 60 mv., the four end points essentially to determine the ratio of the matrix elements, and the central point as a check on the linearity of the ratio. About 80,000 cts per point were taken.

The electron detection was accomplished by using a 2" diameter x 3" long plastic scintillator, covered with a 2 mil aluminum reflector. Its axial displacement from the ring focus was determined by a knowledge of the electron trajectories in that region, which had been measured (see Appendix A). As before, a 19" long 1-1/2" diameter lucite light pipe, optically connected by vacuum grease, connected the scintillator to a 5819 photomultiplier. The same magnetic field compensation was used.

The pulses from the 10T2 pulse amplifier were fed to the Kellogg RIDL 100 channel pulse height analyzer (to be referred to as the 100 CHADD). The reasons for changing the detector were twofold: in the first place, one could then dispense with the GM counter and coincidence

circuit, and hence tolerate faster counting rates; and in the second place, it was thought that having the resulting electron and positron pulse-height spectra might aid in the analysis.

To reduce the background a gated or pulsed beam was used as follows. The RF of the ion source was gated on and off by a square wave pulse from the pancake generator at a frequency of about 63 cps. The resulting gated beam was "sniffed" below the mass-separating slit by a small piece of tantalum which intercepted the heavy ion beam. The square wave pulse from this "sniffer" was used to gate a series of univibrators which allowed one to gate the 100 CHADD on while the beam was off. Actually, the trailing edge of the beam pulse was used to trigger a variable delay pulse, whose trailing edge again triggered a variable count pulse. To monitor the frequency of the pancake generator and the lengths of the beam-on, delay, and count pulses, the following was done. The time of each run was recorded, as well as the number of beam-on pulses. Also, 30 kc oscillator pulses were fed into four scalars which were gated on and off absolutely by the beam integrator. The total oscillator scalar had no other gate, and measured the frequency of the oscillator. The beam-on, delay, and count scalars were additionally gated on by their respective gates, and used to measure these respective times. Variations in these times will affect the ratio of the number of disintegrations detected to the number of radioactive nuclei produced, as explained in Appendix B. All these gates were monitored

on an oscilloscope, as was the beam. The beam was held constant plus or minus about 10%, while the data for each momentum setting was taken.

Unfortunately, the He^3 discharge could not be gated by chopping the RF power in the ion source in this manner. After a few cycles the discharge would go out, and could be restored only by turning on the RF power without chopping. This led to electrostatically chopping the He^3 beam above the magnetic analyzer by applying a 5 kv 60 cps square wave to the top of the electrostatic analyzer. The rest of the circuitry remained the same.

As a result the B^{12} pulse height spectra were very clean with respect to background after a millisecond delay. But the N^{12} pulse height spectra had a large amount of low-energy background, since during the counting cycle the He^3 beam was deflected on to a tantalum strip at the entrance to the magnetic analyzer. To eliminate the background, each point was taken with the beam on the target and the pulse height spectrum recorded on the 100 CHADD. Then a quartz disc, used to visually align the beam, was placed about 1" in front of the target, and the spectrum subtracted from the beam on spectrum. Two such spectra at 47.5 mv. (9 Mev) for B^{12} and N^{12} are shown in figures 7 and 8. It is apparent that the two spectra, which have been normalized to the same peak value and same pulse height, are considerably different at low electron energies. The consideration of this difference has been the

cause of much analysis and is finally the source of most of the error in this experiment with Dr. Van der Leun.

As can be seen from figure 7, the B^{12} pulse height spectrum of momentum analyzed electrons has a low energy tail extending all the way down to zero pulse height. Actually, the N^{12} spectra subtracted very poorly in the lower few channels due to the high background counting rate, so the spectrum between 20% and 40% of the peak was used to extrapolate to zero pulse height in the case of N^{12}, and also for consistency in the case of B^{12}. Qualitatively, this tail is due to electrons which lose only part of their energy in the crystal, the remaining energy escaping from the crystal either in the form of bremsstrahlung quanta or electrons scattering from the crystal. These effects are difficult to estimate quantitatively, but the spectra appear reasonable.

The N^{12} pulse height spectrum, as shown in figure 8, has an appreciably higher low-energy tail, which could arise from the positrons annihilating in flight in the crystal - with the loss of the annihilation quanta, or from an insufficient background subtraction. The effect of the loss of the annihilation quanta is discussed in Appendix C, and is estimated to account for only a small part of the low-energy excess. It should be emphasized that if the positrons annihilated only at rest, and if the annihilation quanta escaped, the positron and electron pulse height spectra would be approximately identical. The difference in the two spectra arises from the possibility of the positron annihilating before

losing all its kinetic energy, and the remaining kinetic energy escaping from the crystal in the form of radiation.

The low energy excess then appears to be due to insufficient background subtraction. Apparently, there was more delayed background with the beam on the B^{10} target than on the quartz. It is uncertain what this was due to, and an attempt was made to circumvent this difficulty in the following manner. All the pulse height spectra were normalized so that the peaks had unit pulse height. This was done on the Datatron 205 computer by including on the data tape input an estimate of the peak pulse height, usually of the order of 60 volts. This estimate was lowered 5 volts, and then the ratio of the integrated areas from 95% to 100% and from 100% to 105% of this estimate was computed. This was done eleven times, increasing the estimate 0.5 volts each time. The peak was determined by averaging the two adjacent estimates which gave values of the ratio greater than and less than one. Using this value of the peak, the number of counts in each 5% interval was calculated, as well as the partially integrated spectra from each 5% interval over the peak. This made possible the addition of pulse height spectra at the same electron or positron energy to get better statistics, but was primarily done to study the background problem.

Since the nitrogen background appears mainly at low energies, the ratio of the partial areas at different energies might be expected to become constant as one raises the lower limit cut-off, hence reducing the background contribution. However, if one raises the cut-off too

high, the statistics due to the areas becoming too small increase the uncertainty. However, the analysis was performed at several values, which changes the value of the nitrogen matrix element, as shown in figure 9, and introduces the major uncertainty in this experiment with Dr. Van der Leun.

Two small changes were made in the beam regulating system. The beta-spectrometer beam compensating coil, mentioned earlier, was regulated electronically. Also, cross-field slits were installed at the entrance of the magnetic analyzer, which held the radial position of the beam constant. These, too, were electronically regulated.

III. CORRECTIONS

The corrections which must be applied to the experimentally measured momentum spectra fall into three classes: experimental, determinable, and theoretical. All but one of the experimental corrections have been discussed in the preceding section, but are mentioned here briefly. The measured spectra were corrected for the resolution of the beta-ray spectrometer by dividing the number of counts measured at a given momentum setting by the momentum. Dead time corrections were made for the GM counter (ρ = 200 μsec), and for the 100 CHADD (ρ = 20 μsec + 1/2 μsec/channel). These were negligible, as was the accidental coincidence rate in the experiment with Dr. Soergel. The nitrogen spectrum in the experiment with Dr. Soergel was corrected for positron annihilation in the absorber and crystal, as explained in Appendix C, page 61. The gating time correction for the gated beam, as explained in Appendix B, was also negligible. The background subtraction, which caused the major uncertainty in the analysis of the pulse height spectra with Dr. Van der Leun, has been explained earlier also.

The correction for the thickness of the target and backing, which will be referred to as the target thickness, was mentioned earlier, but will be explained in detail here, as it applies to both experiments. The energy loss of electrons in the target and backing displaces toward lower energies the measured spectrum with respect to the true spectrum. For the purposes of this discussion we will use the elementary statistical

momentum spectrum for beta-decay, but the extension to other distributions is straightforward. Define the true spectrum as follows:

$$N(p)dp = Ap^2(W-E)^2dp \tag{25}$$

where $E = \sqrt{1 + p^2}$, and W is the maximum energy available for the decay. As a result of the target thickness t, electrons which have an original momentum p will be measured as having a momentum $q(p,t) < p$. Thus, the measured spectrum $M(q)dq$ as a function of q is:

$$M(q)dq = N(p(q)) \frac{dp}{dq} dq \tag{26}$$

The true spectrum at the measured momentum q is $N(q)dq$, and hence the correction factor to obtain the true spectrum from the measured spectrum is

$$R(q) = N(q)/M(q) \tag{27}$$

The ratio R may be calculated for any target thickness t if we know it as a function of momentum or energy. For completeness $R(q)$ is expressed in two forms, for $t(q)$ and $t(F)$, where $F = \sqrt{1 + q^2}$. A straightforward calculation gives

$$R(q) = (1 + t/q)^{-2} \left\{ 1 - \frac{\sqrt{F^2 + 2qt + t^2} - F}{W-F} \right\}^{-2} (1 + dt/dq)^{-1} \tag{28}$$

for $q = p - t(q)$,

and

$$R(q) = \left(1 + \frac{2tF+t^2}{q^2}\right)^{\frac{1}{2}} (1 + t/F)^{-1} (1 - \frac{t}{W-F})^{-2} (1 + dt/dF)^{-1} \qquad (29)$$

for $F = E - t(F)$.

In the highly relativistic region, such as we have in this experiment, $t(q) \approx t(F)$, and if either is approximately constant, $dt/dF \approx dt/dq \approx 0$, and for both cases we find

$$R(x) \approx 1 + 4t/W \left(\frac{x - \frac{1}{2}}{x(1-x)}\right) \qquad (30)$$

where $x \approx F/W \approx q/W$.

In practice, the target thickness correction was made using equation 28. The values of t were 0.12 and 0.24 for the B^{12} and N^{12} spectra in the first experiment with Dr. Soergel, and 0.08 for both spectra in the second experiment with Dr. Van der Leun.

Table III shows values R for boron (W = 27.19) and for nitrogen (W = 33.18) for a small range of target thickness and momenta. As can be seen, the reduction of the target thickness, both in absolute value and in uncertainty, greatly reduces the size of the correction and its uncertainty in the second experiment.

Another correction in this experiment arises from the impossibility of determining the energy released in a beta-disintegration when one detects an electron or positron alone. As is well known, the beta-decay of B^{12} is complex, the main transition being to the ground state, and weaker transitions to the excited states. The branching ratios

TABLE III

Target Thickness Correction Factor R(q)

Boron (W = 27.19)

	t = .10		t = .20		t = .30	
q	Eq. 28, 29	Eq. 30	Eq. 28, 29	Eq. 30	Eq. 28, 29	Eq. 30
5	0.970	0.969	0.941	0.938	0.914	0.907
10	0.992	0.992	0.984	0.983	0.976	0.975
15	1.003	1.003	1.007	1.006	1.010	1.009
20	1.018	1.018	1.037	1.036	1.057	1.053
25	1.090	1.083	1.194	1.167	1.315	1.250

Nitrogen (W = 33.18)

	t = .10		t = .20		t = .30	
q	Eq. 28, 29	Eq. 30	Eq. 28, 29	Eq. 30	Eq. 28, 29	Eq. 30
5	0.968	0.967	0.938	0.934	0.909	0.901
10	0.989	0.989	0.978	0.977	0.967	0.966
15	0.998	0.998	0.996	0.995	0.994	0.993
20	1.005	1.005	1.011	1.011	1.016	1.015
25	1.017	1.016	1.034	1.033	1.052	1.049

log ft values to the ground state, 4.43-Mev state, and 7.65-Mev state are 97, 1.5, 1.3, and 4.1, 5.0, 4.0 (20). The information for the similar transitions in N^{12} is not well-known (20), but an experiment on the branching to the 4.43-Mev state is being performed in the laboratory at the time of this writing. However, because B^{12}, C^{12}, and N^{12} form an isobaric triplet, a reasonable assumption is that the matrix elements between B^{12} and C^{12}, and N^{12} and C^{12} are the same, and hence that the ratio of the total decay probabilities to corresponding states in C^{12} will be given by the F values, where

$$F = \int_0^{\sqrt{1+\eta_o^2}} \eta^2 \left(\sqrt{1+\eta_o^2} - \sqrt{1+\eta^2}\right)^2 F(Z,\eta)\,d\eta . \qquad (31)$$

$F(Z,\eta)$ is the Fermi function, and is equal to

$$F(Z,\eta) = \left|\frac{\Gamma(3)}{\Gamma(3+2S)}\right|^2 \left(\frac{2mc\eta R}{\hbar}\right)^{2s} e^{\pm \pi\delta} \times$$

$$\left|\Gamma(1+S+i\delta)\right|^2 (1+S/2)$$

where $S = \sqrt{1 - Z^2/137^2} - 1$

$\delta = \dfrac{Zc}{137\,v}$

η = momentum of electron

R = nuclear radius = $1.37\,A^{1/3} \times 10^{-13}$ cm.

These have been tabulated (19) in the form

$$f(Z,\eta) = \eta^2 \frac{F(Z,\eta)}{\phi(Z)} = \eta^{2+2S} e^{\pm \pi\delta} \left| \Gamma(1 + S + i\delta) \right|^2 \qquad (32)$$

Hence, for the same final Z, we must compute

$$f = \int_0^{\sqrt{1+\eta_o^2}} (\mathcal{E}_o - \mathcal{E})^2 \, f(Z,\eta) \, d\eta \qquad (33)$$

In the limit of high η and Z = 0, this gives the fifth power law.

Adding two arguments to f, i.e., N or B to distinguish the decay, and E to distinguish the energy of the state of C^{12} in question, we find by numerical integration

$$\frac{f(N,O)}{f(B,O)} = 2.057 = 1.000\ (2.057)$$

$$\frac{f(N,4.43)}{f(B,4.43)} = 3.112 = 1.513\ (2.057) \qquad (34)$$

$$\frac{f(N,7.65)}{f(B,7.65)} = 5.689 = 2.766\ (2.057)$$

It is interesting to note that the fifth power law gives 2.706, 4.082, and 7.388, respectively. If one normalized so that the ground state in B^{12} is 100.0, the expected values of the N^{12} branching ratios are given by multiplying the B^{12} ratios by the constants 1.000, 1.513, and 2.766, as given in equation 34.

Since one is investigating an effect in the ground state transitions only, one must correct the measured spectra for the excited state transitions. From a knowledge of the branching ratios and theoretical momentum spectra one may calculate the number of electrons or positrons appearing at a given momentum from each of the three states in question. That is to say, N(total) = N(ground) + N(4.43) + N(7.65). The ratio

$$R = N(\text{ground})/N(\text{total})$$

then gives the correction that must be applied to the B^{12} and N^{12} spectra. These are tabulated and graphed in Tables IV and V and figures 10 and 11. Spectra to the various states (normalized to unit area) are also tabulated and graphed in Tables VI and VII and figures 12 and 13.

The errors in this correction arise from the absolute errors in the B^{12} data, which may be as large as 50%, and from the assumed, but not yet verified experimentally, equality of the B^{12} and N^{12} matrix elements to the same states in C^{12}.

The theoretical corrections are two: the effect of the finite de-Broglie wavelength of the electron, and the effect of inner bremsstrahlung. A brief statement of the origin of the former, and a formula (eq. 23) for it is given in the introduction. The effect of inner bremsstrahlung, the emission of soft photons and a corresponding loss in the energy of the emitted leptons, has been calculated for this experiment by Dr. S. Berman (27). The correction factor is $1 + \delta$, where δ is given by

TABLE IV

B^{12} Branching Correction

N(ground)	1.0000	1.0000	1.0000	1.0000	1.0000
N(4.43)	0.0078	0.0124	0.0155	0.0186	0.0233
N(7.65)	0.0067	0.0107	0.0134	0.0161	0.0201
η					
0	-	-	-	-	-
2	.923	0.882	0.858	0.833	0.801
4	.937	0.903	0.882	0.861	0.832
6	.952	0.926	0.909	0.892	0.869
8	.968	0.946	0.937	0.925	0.908
10	.981	0.971	0.964	0.956	0.946
12	.990	0.934	0.981	0.977	0.971
14	.994	0.990	0.988	0.985	0.982
16	.997	0.996	0.995	0.994	0.992
18	1.000	1.000	1.000	1.000	1.000
20	1.000	1.000	1.000	1.000	1.000
22	1.000	1.000	1.000	1.000	1.000
24	1.000	1.000	1.000	1.000	1.000
26	1.000	1.000	1.000	1.000	1.000
27.17	1.000	1.000	1.000	1.000	1.000

TABLE V

N^{12} Branching Correction

N(ground)	1.0000	1.0000	1.0000	1.0000	1.0000
N(4.43)	0.0117	0.188	0.0234	0.0281	0.0351
N(7.65)	0.0185	0.296	0.0370	0.0445	0.0555
η					
0	-	-	-	-	-
2	0.887	0.830	0.796	0.765	0.723
4	0.897	0.845	0.814	0.784	0.744
6	0.909	0.862	0.833	0.806	0.769
8	0.922	0.881	0.856	0.831	0.798
10	0.937	0.902	0.881	0.860	0.831
12	0.952	0.925	0.908	0.892	0.868
14	0.967	0.949	0.937	0.925	0.908
16	0.981	0.970	0.963	0.956	0.946
18	0.980	0.985	0.981	0.977	0.971
20	0.994	0.990	0.988	0.985	0.982
22	0.997	0.996	0.995	0.994	0.992
24	1.000	1.000	1.000	1.000	0.999
26	1.000	1.000	1.000	1.000	1.000
28	1.000	1.000	1.000	1.000	1.000
30	1.000	1.000	1.000	1.000	1.000
32	1.000	1.000	1.000	1.000	1.000
33.16	1.000	1.000	1.000	1.000	1.000

TABLE VI

B^{12} Calculated Spectra

	To Grd	To 4.43	To 7.65
	$\eta_o = 27.17$	$\eta_o = 18.47$	$\eta_o = 12.16$
η	$N(\eta)$	$N(\eta)$	$N(\eta)$
0	0.0000	0.0000	0.0000
2	0.0052	0.0151	0.0463
4	0.0174	0.0467	0.1203
6	0.0327	0.0782	0.1547
8	0.0477	0.0981	0.1257
10	0.0598	0.1003	0.0529
12	0.0671	0.0844	0.0005
14	0.0689	0.0547	
16	0.0648	0.0219	
18	0.0552	0.0010	
20	0.0418		
22	0.0263		
24	0.0118		
26	0.0019		

TABLE VII

N^{12} Calculated Spectra

η	To Grd $\eta_o = 33.16$ $N(\eta)$	To 4.43 $\eta_o = 24.49$ $N(\eta)$	To 7.65 $\eta_o = 18.17$ $N(\eta)$
0	0.0000	0.0000	0.0000
2	0.0028	0.0067	0.0154
4	0.0101	0.0227	0.0483
6	0.0198	0.0419	0.0807
8	0.0303	0.0593	0.1005
10	0.0401	0.0716	0.1014
12	0.0483	0.0767	0.0834
14	0.0539	0.0735	0.0518
16	0.0565	0.0630	0.0184
18	0.0558	0.0465	0.0001
20	0.0519	0.0276	
22	0.0452	0.0103	
24	0.0362	0.0005	
26	0.0260		
28	0.0156		
30	0.0067		
32	0.0010		

$$\delta = \frac{2a}{\pi}\left\{(Z-1)\left[\ln\frac{K_o'}{K_o} + \frac{1}{3}\,\frac{K_o'-K_o}{E}\right] + \frac{Z}{24}\left(\frac{K_o'^2-K_o^2}{W^2}\right)\right\}$$

where $$Z = \frac{W}{p}\ln\frac{W+p}{m}$$

$$K_o' = (W_o^N - W)$$

$$K_o = (W_o^B - W)$$

This correction is to be applied to the ratio of the B^{12} to N^{12} spectra, and is presented in figure 14 and in Table VIII. It can be seen that except for extremely low energies, and near the B^{12} endpoint where there is a logarithmic divergence, the correction is very small.

TABLE VIII

Inner Bremsstrahlung Correction Factor

W	$1 + \delta$
1	1.068
2	1.028
4	1.012
6	1.008
8	1.007
10	1.006
12	1.006
14	1.006
16	1.007
18	1.008
20	1.009
22	1.011
24	1.015
26	1.026
27	1.050

IV. CONCLUSIONS

The measured momentum spectra of B^{12} and N^{12}, after having been corrected for the several experimental corrections and branching ratio correction discussed in Part III, yield the true momentum spectra of the ground state transitions for these decays. As explained in Part I, the true momentum spectra are given by a product of a matrix element for the transition, a Coulomb factor, and a statistical factor. For completeness, the inner bremsstrahlung factor, discussed in Part III, should be included, although it is small in the range of interest. The matrix element has been expressed as a product of a constant term and the energy dependent conserved vector current factor, the term of interest.

Figures 15, 16, 17, 18 show the experimental conserved vector current factor for B^{12} and N^{12} for the two discussed experiments, and figures 19, 20 show the ratio of B^{12}/N^{12}, which is the final result of this experiment. In the ratio the deBroglie wavelength correction is accurate to one higher order in e^2, as is the expected value of the conserved vector current term, due to the cancellation of higher order terms of the same sign.

The experiment with Dr. Soergel gives a value for the B^{12}/N^{12} ratio of $+0.2 \pm 1.2\%$ Mev. This probable error is the sum of a 0.2% statistical error, a 0.4% possible systematic error from the target thickness, a 0.4% possible systematic error from the branching ratio correction, and a 0.2% possible systematic error from the spectrometer

calibration (see Appendix A). The experiment with Dr. Van der Leun gives a value of $+3.1 \pm 1.2\%$/Mev, with errors of 0.5%, 0.1%, 0.4%, and 0.2% respectively. The large assigned statistical error arises from the interpretation of the N^{12} pulse height spectra, as explained in Appendix C. To examine the consistency of the two experiments, we may disregard the possible errors due to the branching ratio correction and the calibration, obtaining $+0.2 \pm 0.6\%$/Mev and $+3.1 \pm 0.6\%$/Mev. In terms of standard deviations these become $+0.2 \pm 0.9\%$/Mev and $+3.1 \pm 0.9\%$/Mev, where the conversion factor 0.675, obtained from the normal distribution, has been used.

If one assumes that the probability of measuring a given ratio x_i is normally distributed about a mean value μ, with variance σ_i^2, it can be shown that an unbiased estimate for μ is $\mu = \bar{X}$, where $\bar{X} \equiv \left(\sum X_i/\sigma_i^2\right)\left(\sum \frac{1}{\sigma_i^2}\right)^{-1}$. Further, if $n/\sigma^2 = \sum' \frac{1}{\sigma_i^2}$, one finds that $(\bar{X} - \mu)/\sigma$ has a normal distribution with mean 0 and variance $1/n$, and that $\chi^2 = \sum\left(\frac{X_i - \bar{X}}{\sigma_i}\right)^2$ has the chi-squared distribution with n-1 degrees of freedom.

Hence one finds that the average value of the ratio has a value 1.65%/Mev with a standard deviation of 1.0%/Mev. Converting this to probable error, and adding the possible systematic error of the branching ratio and calibration, we obtain a value for the ratio of $+1.65 \pm 1.3\%$/Mev. However, χ^2 has a value of 4.8, and for a χ^2 distribution with 1 degree of freedom there is only a 3% probability that χ^2 is greater than 4.8. This makes it seem likely that the estimate of the probable error

is too low or that some undetected error was present.

Either way it seems that one should accept the fact that the two experimental values obtained for the ratio of the B^{12}/N^{12} matrix elements are $+0.2 \pm 1.2\%$/Mev, and $+3.1 \pm 1.2\%$/Mev, and hesitate to average the two.

Theoretically, one expects to find a ratio of 0.3%/Mev in the absence of the conserved vector current interaction, and 1.4%/Mev with the conserved vector current interaction. As tempting as it is to take the average value of the two experiments, 1.65%/Mev, for a confirmation of the theory, it seems wiser in view of the analysis of the errors not to do so. Hence the final conclusion is that two somewhat inconsistent experiments perhaps favor slightly the conserved vector current theory.

It is clear that the largest source of error in the first experiment was the thickness of the target. In the second experiment this was corrected, but the background in the N^{12} spectrum caused a large error. This could be cured, I believe, by mechanically or electrically chopping the He^3 beam at the exit of the ion source in the Van de Graaff generator, which would not interfere with maintaining the discharge. This involves a fair amount of time during which the Van de Graaff is inoperative. Perhaps the easiest way to correct for this background is to have a movable absorber for positrons and electrons which could be placed in position directly behind the source. This would have to be

thick enough to stop the positrons, and give no neutron background. Then one should have essentially the same conditions as far as background is concerned, and hence should get a true subtraction.

One would hope that another experiment might reduce the statistical error, including background, to 0.2%, and the target thickness to 0.1% simultaneously. If the calibration constant were known accurately and the branching ratio were known to about 20%, the probable error in the ratio would be about 0.2%/Mev, giving a total error of about 0.5%/Mev. There would still be the inconsistency of the present experiments, which could be brought into better statistical agreement, if the experimental errors were somewhat arbitrarily increased by 50%.

APPENDIX A

Spectrometer Design:

The Beta-Ray Spectrometer used in this experiment was essentially the one designed and constructed by W. F. Hornyak (23). A more general discussion of beta-ray spectrometers is given by Siegbahn (21).

The trajectories of the electrons may be determined from the equation of motion in a magnetic field,

$$\frac{d\vec{v}}{dt} = \frac{e}{mc} (\vec{v} \times \vec{B}) \qquad (A1)$$

where m is the transverse mass, i.e., $m = m_o(1 - \beta^2)^{-1/2}$. The only case that can be solved easily is that of a uniform axial field, which is instructive as the qualitative features appear in all beta-spectrometers with axial fields. The derivations are given in Siegbahn, so only certain of the results will be quoted. For a magnetic field in the z-direction the radial equation of motion is

$$r = D \sin \alpha \sin \zeta \qquad (A2)$$

where $D = \frac{2mv}{B}$, $\zeta = \frac{z}{D \cos \alpha}$, and $v_{z_o} = v \cos \alpha$. Now it can be shown that $\frac{dr}{d\alpha} = 0$ for

$$\frac{\tan \zeta}{\zeta} = - \tan^2 \alpha \qquad (A3)$$

This is known as the Ring Focus condition, and means that electrons having angles of emission close to α will to first order be focussed in a ring of radius r. If the resolution is defined as $R^\circ = \frac{\Delta(B\rho)}{B\rho}$, where $B\rho$ is the momentum in gauss-cm, and the solid angle as T, the following relation may be established:

$$R^\circ = T^2/_2 \left[\frac{3}{\sin^2 \alpha} + \mathrm{ctn}^2 \alpha \tan^2 \zeta \right] . \qquad (A4)$$

In the case of a thin lens spectrometer, where the field is limited in space, the radial equation of motion for paraxial rays is given by

$$\frac{d^2 r}{dz^2} = - \frac{B_z^2(z,o)}{4(B\rho)^2} r \qquad (A5)$$

$B_z(z,o)$ is the axial component of the magnetic field, and $B\rho$ is the momentum in gauss-cm. This may be integrated following Hornyak to give

$$\frac{1}{u} + \frac{1}{v} = \frac{1}{f} \qquad (A6)$$

where $r_o = u \tan \alpha$, $r_o = - v \tan \beta$, and $f = \frac{1}{4(B\rho)^2} \int_{-\infty}^{\infty} B^2(z)\, dz$.

This is known as the Lens Equation, of which a more complete discussion is contained in Hornyak's thesis.

As designed by Hornyak, and modified by myself, the spectrometer is essentially a "thin" lens type, and the axial field is plotted in Figure 21.

For the purpose of this experiment, which reduces to a comparison of an electron spectrum and a positron spectrum, the emphasis during the alignment procedure was to produce a spectrometer which was identical for positrons and electrons. As monoenergetic positron sources are nonexistent, a Cs^{137} β^- emitter, kindly loaned to me by F. Boehm, was used. Now the requirement is to have the resolution and solid angle the same for the normal field and reversed field, which should only change the sense of the pitch of the helical trajectory. After this alignment was made, the trajectories were measured to determine the optimum design of various baffles, as described below.

The alignment of the beta-ray spectrometer consists in moving the geometric axis of the spectrometer until it is coincident with the magnetic axis of the coils. At the same time I had to adjust the vertical and horizontal compensating fields to give complete symmetry also. It would have been better to have eliminated the stray field by means of a magnetometer first, so as to have had fewer parameters to adjust. As a preliminary measurement, a strong thulium source was placed at the source position, two "pin-hole" baffles, made of 1/8" aluminum with centered 1/8" and 1/16" holes, were placed in the spectrometer, and an end window Geiger counter was placed at the detector position. This was covered with a brass cap having a 1/8" hole in the center. By adjusting the spectrometer tube with respect to the coils, and by adjusting the two compensating coils, it was attempted to have the counting rate

as a function of spectrometer field the same for both senses of the field. Quite good results were achieved, but the next step in the alignment procedure seemed to be even more sensitive.

At this point a three-ring baffle was placed at the center of the spectrometer. The baffle had three concentric openings of 1/4" width, with inner radii of 2-1/2", 3-1/4", and 4-3/4". The trajectories of the electrons passing through these shall be called the inner, central, and outer rays, respectively. A Cs^{137} source was placed at the source position, and then, with the same counter, the "spectrum" as a function of magnetic field was obtained. For the counter in a fixed position, the internal conversion line will be focussed at three different values of the magnetic field, corresponding to the three different trajectories. Again by successive adjustments the two senses of the magnetic field were required to give the same "spectrum." Figures 22, 23 show this matching toward the end of this process, and Figures 24, 25 show the final alignment.

The next step was to measure the pitch of the helical trajectories in order to construct a "helical baffle." The purpose of such a baffle is to allow one to measure electron spectra in the presence of positrons, and vice versa, and to reduce background from scattering. A twelve bladed helical baffle, with the blades 12" long and a 1/4" thick was suggested by Dr. T. Lauritsen, this being considerably larger and more opaque than the one formerly used. Although in the present experiment we were not worried about the simultaneous production of positrons and

electrons, it was felt that such a baffle would decrease the background from scattering, as was found to be the case. To determine the pitch a rotatable 1/8" aluminum baffle, which had two sets of eight 1/4" holes at radii of 2-1/2" and 4-3/4", was placed at the center of the coils. Another baffle with eight 1/4" radial grooves was placed behind this. With a fixed counter position and constant magnetic field the rotation necessary for maximum transmission was measured as a function of the axial displacement of the "radial" baffle. This was done for two counter positions corresponding to the inner and outer trajectories. The results of these measurements are shown in Figure 26 . A wooden model of the blades was then cut on a milling machine, with a pitch of 63° per foot. Then the twelve blades were cast from aluminum, and mounted with pivots on a 3-1/2" by 13" brass slug, in such a manner as to allow a variation of a few degrees of pitch to obtain maximum transmission.

The trajectories of the electrons near the source and counter positions were measured by suitable circular baffles which could be moved axially. At a constant field setting the location of the Geiger counter was determined for the inner, central, and outer rays, and the various circular baffles were moved until they intercepted the rays. The results of these measurements are shown in Figures 27 and 28. This permitted an optimum design for the ring forms baffle, cone baffle, and the two solid angle defining baffles. In practice the cone baffle, which effectively affects the resolution, and the outer aperture baffle, which

affects the solid angle, were movable, and were adjusted for optimum performance when the entire spectrometer was assembled.

At low energies there exist monoenergetic electron sources, the electrons being emitted as a result of internal conversion or K-capture. A Cs^{137} source, having a conversion line at 661 kev, was used to obtain one low energy point. Unfortunately, a thorium source, having a conversion line at 2.615 Mev, was not available. Due to the focusing effect of the earth's axial magnetic field, which is small (0.2 gauss) in magnitude but is uniform in shape, it was felt desirable to calibrate at a high energy. At the suggestion of Dr. Soergel, the following procedure was used. A thin carbon foil with an evaporated layer of gold was placed at the source position of the spectrometer. A set of stops was arranged so that it could be placed in two orientations, perpendicular to the axis of the spectrometer and at 40°5' to the axis. Then protons were scattered from the foil, and the scattered protons' momenta analyzed by the beta-ray spectrometer. The detector was a Faraday cup and electrometer. Knowing the incident energy of the protons, and the two momenta, corresponding to the two positions of the scattering foil, the calibration constant, and incidentally the foil thickness, can be determined.

The energy of the incident beam of protons was calibrated as follows. A thick target of F^{19} was placed directly in front of the scattering foil. Outside of the spectrometer was placed a NaI counter. Then the 669 kev (p,γ) resonance (20) was found by varying the magnetic

analyzer until the midpoint of the step of the 6.14-Mev gamma-ray yield was found. Then the magnetic analyzer was held constant, and the voltage of the Van de Graaff lowered until the mass 2 beam was focussed, and this beam was scattered. If E_i is the initial kinetic energy, the final kinetic energy per proton is

$$E_f = E_i/4 \left[1 + 3/8 \, E_i/M \right] \quad ,$$

where E and M are in Mev. The statistical error in measuring the two peaks and determining the calibration constant is estimated to be about 0.1%, and the proton resonance was taken to be at 669.6 ± 0.7 Mev, an average of 671.6 ± 0.7 (28) and 667.6 ± 1.1 (29). Hence the calibration was assumed to be good to about 0.2%.

APPENDIX B

Gating Time Correction Factors

When using a chopped beam and a delayed counting cycle to study a decay process, it is of interest to know how the ratio of the number of decays counted (N_C) to the total number of decays produced (N_T) varies with changes in the timing. To be specific, let us consider the following situation after equilibrium has been reached. Let I be the production rate per second, A the period of the cycle, B the time during which the production is taking place, D the delay time, C the counting time, and λ the decay rate. Then the following relations hold:

$$0 \leq B \leq B + D \leq B + D + C \leq A$$

$$\frac{dN}{dt} = -\lambda N + I \qquad 0 \leq t \leq B$$

$$\frac{dN}{dt} = -\lambda N \qquad B \leq t \leq A$$

These immediately lead to

$$N_C = I/\lambda \; \frac{1}{1-e^{-\lambda A}} \; (1 - e^{-\lambda B})\,(1 - e^{-\lambda C})\, e^{-\lambda D}$$

$$N_T = IB$$

or
$$R = \frac{1}{1-e^{-\lambda A}} \left(\frac{1-e^{-\lambda B}}{\lambda B} \right) (1 - e^{-\lambda C})\, e^{-\lambda D} \qquad \text{(B1)}$$

The variations of R with respect to A, B, C, and D are

$$\left.\frac{dR}{R}\right|_A = -\frac{dA}{A}\left[\frac{\lambda A e^{-\lambda A}}{1-e^{-\lambda A}}\right] \tag{B2}$$

$$\left.\frac{dR}{R}\right|_B = -\frac{dB}{B}\left[\frac{1-(1+\lambda B)e^{-\lambda B}}{1-e^{-\lambda B}}\right] \tag{B3}$$

$$\left.\frac{dR}{R}\right|_C = \frac{dC}{C}\left[\frac{\lambda C e^{-\lambda C}}{1-e^{-\lambda C}}\right] \tag{B4}$$

$$\left.\frac{dR}{R}\right|_D = \frac{dD}{D}\left[\lambda D\right] \tag{B5}$$

These functions are tabulated in Table BI, and are graphed in figure 29.

TABLE BI

x	$\frac{dR/R}{dA/A}$ =λA	$\frac{dR/R}{dB/B}$ =λB	$\frac{dR/R}{dC/C}$ =λC	$\frac{dR/R}{dD/D}$ =λD
0.0	-1.000	-0.000	+1.000	-0.000
0.1	-0.951	-0.049	+0.951	-0.100
0.2	-0.903	-0.097	+0.903	-0.200
0.3	-0.857	-0.143	+0.857	-0.300
0.4	-0.813	-0.187	+0.813	-0.400
0.5	-0.771	-0.229	+0.771	-0.500
0.6	-0.730	-0.270	+0.730	-0.600
0.7	-0.691	-0.309	+0.691	-0.700
0.8	-0.653	-0.347	+0.653	-0.800
0.9	-0.617	-0.383	+0.617	-0.900
1.0	-0.582	-0.418	+0.582	-1.000
1.1	-0.549	-0.451	+0.549	-1.100
1.2	-0.517	-0.483	+0.517	-1.200
1.3	-0.487	-0.513	+0.487	-1.300
1.4	-0.458	-0.542	+0.458	-1.400
1.5	-0.431	-0.569	+0.431	-1.500
1.6	-0.405	-0.595	+0.405	-1.600
1.7	-0.380	-0.620	+0.380	-1.700
1.8	-0.356	-0.644	+0.356	-1.800
1.9	-0.334	-0.666	+0.334	-1.900
2.0	-0.313	-0.687	+0.313	-2.000

APPENDIX C

Annihilation of Positrons

In the present experiment the annihilation of positrons, in flight and at rest, manifests itself in two ways. Firstly, positrons may annihilate in passing from the source to the detector, resulting in an altered measured momentum spectrum. Secondly, all the positrons which enter the detector annihilate, converting their kinetic energy at the time of annihilation, and the rest mass energy of an electron and positron, into radiation.

As will be shown in detail below, the annihilation cross-section varies by about a factor of two between 5 Mev and 12 Mev kinetic energy. However, the absolute cross-section is about an order of magnitude too low to be detected in this experiment. This loss is based on the cross-section for annihilation per electron times the number of electrons/cm^2 between the source and detector, including the target, backing, air path in the spectrometer (at 10^{-5} mm Hg), and the reflecting foil of the photomultiplier.

To estimate the effect on the pulse height distribution of a positron in a crystal due to annihilation in comparison to that of an electron is a somewhat more subtle process. An electron loses its kinetic energy by collisions and by bremsstrahlung - the emission of high energy photons. If a source of monoenergetic electrons is at the

center of a crystal large enough to absorb all the radiation, a delta-function spectrum will result. In the case of positrons, a delta-function spectrum will result, only at 1.02 Mev higher in energy, due to the ultimate conversion of the rest mass of an electron and positron into radiation. The complication arises in this analysis because of the finite size of the crystal, which has two consequences: first, as a result of a collision the electron or positron may be scattered out of the crystal before losing all its kinetic energy, and second, the crystal is essentially transparent to quanta above a few hundred kev. Thus many electrons and positrons will lose only part of their kinetic energy in the crystal, and their maximum energy loss will be the same, due to the escape of radiation, particularly the annihilation radiation. The B^{12} pulse height spectra are used to estimate the fractional number of electrons having lost a specified fraction of their energy in the crystal. The assumption is then made that the positrons will have the same spectra, modified by the possibility of annihilation.

The cross-section for annihilation of a positron with total energy E is shown by Heitler (30) to be

$$\phi = \pi r_o^2 \frac{1}{\mathcal{E}+1}\left[\frac{\mathcal{E}^2+4\mathcal{E}+1}{\mathcal{E}^2-1}\ln\left\{\mathcal{E}+\sqrt{\mathcal{E}^2-1}\right\}-\frac{\mathcal{E}+3}{\sqrt{\mathcal{E}^2-1}}\right] \tag{C1}$$

where $\mathcal{E} = E/m_o$, the total energy in mass units, and r_o is the

classical electron radius. As $\mathcal{E}$ approaches 1, i.e., as the velocity v approaches 0, this reduces to

$$v\phi \rightarrow \pi r_o^2 c \qquad \text{(N.R.)} \tag{C2}$$

and for high energies it becomes

$$\phi \rightarrow \pi r_o^2 \, \mathcal{E}^{-1} \, [\ln 2\mathcal{E} - 1] \quad \text{(E.R.)} \tag{C3}$$

A graph of $\phi/\pi r_o^2$ vs. kinetic energy is shown in figure 30.

The probability per unit energy $\Phi(E)$ of a positron of kinetic energy E annihilating in a material of density ρ and stopping power -dE/dx, containing NZ electrons/cm^3 is given by

$$\Phi(E)dE = NZ\rho^{-1} \, \phi(E) \, (dE/dx)^{-1} \, dE \tag{C4}$$

where N is the number of atoms/cm^3, Z is their charge, ρ the density in gm/cm^3, $\phi(E)$ is the annihilation cross-section in cm^2, and (-dE/dx) is the stopping power in Mev-cm^2/gm.

If we consider a non-annihilating positron which has a kinetic E_o incident upon a crystal, it will lose an energy E' $(O \leq E' \leq E_o)$ in the crystal, and an energy $E_o - E'$ will escape by scattering and bremsstrahlung. To simplify the analysis, let us picture the process as follows: upon entering the crystal an energy $g(E_o - E')$ escapes $(O \leq g \leq 1)$, then an energy E' is lost in the crystal, and finally an energy $(1-g)(E_o - E')$

escapes. The number of positrons losing an energy E' is determined from the electron pulse height spectra.

If now we consider real positrons which will annihilate while losing energy in the crystal, it may be shown that the positrons, $m(E')dE'$ in number, which would have lost an amount of energy E' in the absence of annihilation now have a spectrum given by

$$n(E,E';E_o,g)dE = e^{-\int_o^E \Phi(E'',E';E_o,g)dE''} \quad \text{(C5)}$$

$$\times \quad [\Phi(E,E';E_o,g) + \delta(E-E')] \quad dE$$

where $O \leq E \leq E' \leq E_o$,

and $$\Phi(E,E';E_o,g) = \Phi(E_o[1-g] + gE' - E) . \quad \text{(C6)}$$

This distribution represents the numbers of positrons which have annihilated while losing an energy between E and $E + dE$ in the crystal, having had an incident energy of E_o. Two cases may be distinguished. When $g = 0$

$$\Phi(E,E';E_o,0) = \Phi(E_o - E) \quad \text{(C7)}$$

corresponding to the energy loss occurring between E_o and $E_o - E'$. When $g = 1$,

$$\Phi(E,E';E_o,1) = \Phi(E' - E) \quad \text{(C8)}$$

corresponding to the energy loss occurring between E' and 0. I believe that the actual process must lie between these two limits.

Now if the pulse height spectrum in the absence of annihilation is given by $m(E')dE'$, it is easy to show that the following is the expected spectrum with annihilation.

$$n(E;E_o,g)dE = \int_E^{E_o} m(E')dE'\, n(E,E';E_o,g)\, dE$$

$$= dE \int_E^{E_o} m(E')\, dE'\; e^{-\int_o^E \Phi(E'',E';E_o,g)\, dE''}\; \Phi(E,E';E_o,g)\; e^{-\int_o^E \Phi(E'',E;E_o,g)\, dE''} + m(E)\, dE \qquad \text{(C9)}$$

Furthermore, one notes that

$$\int_a^{E_o} n(E;E_o,g)\, dE = \int_a^{E_o} m(E')\, dE'\; e^{-\int_o^a \Phi(E'',E';E_o,g)\, dE''} \qquad \text{(C10)}$$

$\Phi(E)$ was calculated for styrene, which has a density $\rho = 0.9045$ gm/cm^3, and a molecular weight of 104.14. NZ equals 2.93×10^{23} electrons/cm^3. Values of $-dE/dx$ (in Mev-cm^2/gm) were taken from

tables of the energy loss and range of electrons and positrons (24). A graph of $(-dE/dx)^{-1}$ vs. E is shown in figure 31, and a graph of $\Phi(E)$ vs. E is shown in figure 32. Table CI gives values of $\Phi(E)$ vs. E, and Table CII gives values of $F(E) = \int_0^E \Phi(E')dE'$ vs. E. Further, expected pulse height distributions for monoenergetic positrons of 6.5 and 10.5 Mev kinetic energy with no escape loss except for annihilation quanta (i.e., $E' = E_o$) are shown in figures 33 and 34.

The relative effect of the annihilation process in the crystal is small, as at 6 Mev 11% annihilate in flight and 89% at rest, while at 11 Mev 14% annihilate in flight, and 86% at rest, a change of only 3%. The folding process was carried out at 9 Mev, as shown in figure 35.

Furthermore, one observes that the probability for annihilation depends upon the density of electrons, and hence the annihilation of positrons in flight in the spectrometer is far too low to be observed.

In the first experiment the positrons had to traverse a 1 Mev lucite absorber and lose 1/2 Mev in the crystal before being detected. From the tables presented here it can be shown that 1.7% of the 5 Mev positrons will annihilate while losing 1.5 Mev of energy, and 0.6% of the 12 Mev positrons will annihilate. The nitrogen spectra of the first experiment have been corrected for this.

TABLE CI

$\overline{\Phi}(E)$ for styrene

$\overline{\Phi}(E) = NZ\,\phi(E)\,\rho^{-1}\,(-dE/dx)^{-1}$

E(Mev)	$\overline{\Phi}(E)$ (Mev^{-1})
.25	0.032
.75	0.034
1.25	0.026
1.75	0.022
2.25	0.020
2.75	0.016
3.25	0.014
3.75	0.012
4.25	0.012
4.75	0.010
5.25	0.010
5.75	0.008
6.25	0.008
6.75	0.008
7.25	0.008
7.75	0.006
8.25	0.006
8.75	0.006
9.25	0.006
9.75	0.006
10.25	0.006
10.75	0.004
11.25	0.004
11.75	0.004

TABLE CII

$$F(E) = \int_{o}^{E} \Phi\,(E')\ dE'$$

E(Mev)	F(E)	1-F(E)
0.0	0.000	1.000
0.5	0.016	0.984
1.0	0.033	0.967
1.5	0.046	0.954
2.0	0.057	0.943
2.5	0.067	0.933
3.0	0.075	0.925
3.5	0.082	0.918
4.0	0.088	0.912
4.5	0.094	0.906
5.0	0.099	0.901
5.5	0.104	0.896
6.0	0.108	0.892
6.5	0.112	0.888
7.0	0.116	0.884
7.5	0.120	0.880
8.0	0.123	0.877
8.5	0.126	0.874
9.0	0.129	0.871
9.5	0.132	0.868
10.0	0.135	0.865
10.5	0.138	0.862
11.0	0.140	0.860
12.5	0.142	0.858
12.0	0.144	0.856

REFERENCES

1. M. Gell-Mann, Phys. Rev. 111, 362 (1958).

2. E. Fermi, Zeits. f. Phys. 88, 161 (1934).

3. E. J. Konopinski and C. E. Uhlenbeck, Phys. Rev. 60, 308 (1941).

4. M. E. Rose, "The Theory of Allowed Beta-Decay," Beta- and Gamma-Ray Spectroscopy, K. Siegbahn, ed., North Holland Publishing Company, Amsterdam (1955).

5. E. J. Konopinski, "The Theory of Forbidden Beta-Decay, "Beta- and Gamma-Ray Spectroscopy, K. Siegbahn, ed., North Holland Publishing Company, Amsterdam (1955).

6. C. S. Wu, "Experiments of the Shape of Beta-Spectra -- The Interaction in Beta-Decay," Beta- and Gamma-Ray Spectroscopy, K. Siegbahn, ed., North Holland Publishing Company, Amsterdam (1955).

7. T. D. Lee and C. N. Yang, Phys. Rev. 104, 254 (1956).
T. D. Lee and C. N. Yang, Phys. Rev. 106, 1371E (1957).
T. D. Lee and C. N. Yang, Phys. Rev. 105, 1671 (1957).

8. J. D. Jackson, S. B. Treiman, and H. W. Wyld, Jr., Phys. Rev. 106, 517 (1957).

9. L. Michel, Rev. Mod. Phys. 29, 223 (1957).

10. Wu, Ambler, Hayward, Hoppes, and Hudson, Phys. Rev. 105, 1413 (1957).

11. Boehm, Novey, Barnes, and Stech, Phys. Rev. 108, 1497 (1957).

12. Burgy, Krohn, Novey, Ringo, and Telegdi, Phys. Rev. 110, 1214 (1958).

13. C. S. Wu, Rev. Mod. Phys. 31, 783 (1959).

14. M. Gell-Mann, Rev. Mod. Phys. 31, 834 (1959).

15. R. P. Feynman and M. Gell-Mann, Phys. Rev. 109, 193 (1958).

16. M. Gell-Mann, Course Notes in Quantum Electrodynamics, California Institute of Technology (1958-1959).

17. M. Gell-Mann, private communication.

18. M. Morita, Phys. Rev. 113, 1584 (1959).

19. Tables for the Analysis of Beta Spectra, National Bureau of Standards Applied Mathematics Series, No. 13 (1952).

20. F. Ajzenberg-Selove and T. Lauritsen, "Energy Levels of Light Nuclei. VI," Nuclear Physics 11, 340 (1959).

21. K. Siegbahn, "Beta-Ray Spectrometer Theory and Design," Beta- and Gamma-Ray Spectroscopy, K. Siegbahn, ed., North Holland Publishing Company, Amsterdam (1955).

22. R. G. Thomas, Thesis, California Institute of Technology (1951).

23. W. F. Hornyak, Thesis, California Institute of Technology (1949).

24. A. T. Nelms, "Energy Loss and Range of Electrons and Positrons," National Bureau of Standards Circular 577 (1956).

25. R. D. Evans, The Atomic Nucleus (McGraw-Hill Book Company, Inc., New York, 1955), p. 649.

26. W. Whaling, Handbuch der Physik (J. Springer-Verlag, Berlin, 1958), Vol. 34, p. 274.

27. S. M. Berman, private communication. Also S. M. Berman, Phys. Rev. 112, 267 (1958) and M. Gell-Mann and S. M. Berman, Phys. Rev. Letters 3, 99 (1959).

28. S. E. Hunt and K. Firth, Phys. Rev. 99, 786 (1955).

29. J. Kuperus, P.J.M. Smulders, and P. M. Endt, Physica 25, 600 (1959).

30. W. Heitler, The Quantum Theory of Radiation, Third Edition (Clarendon Press, Oxford, 1954), p. 268.

31. H. Weidenmüller (private communication) of the Kellogg Laboratory finds that $\langle \| \ell \| \rangle \lesssim 0.1 \langle \| \sigma \| \rangle$ for the case of this triplet.

FIGURES

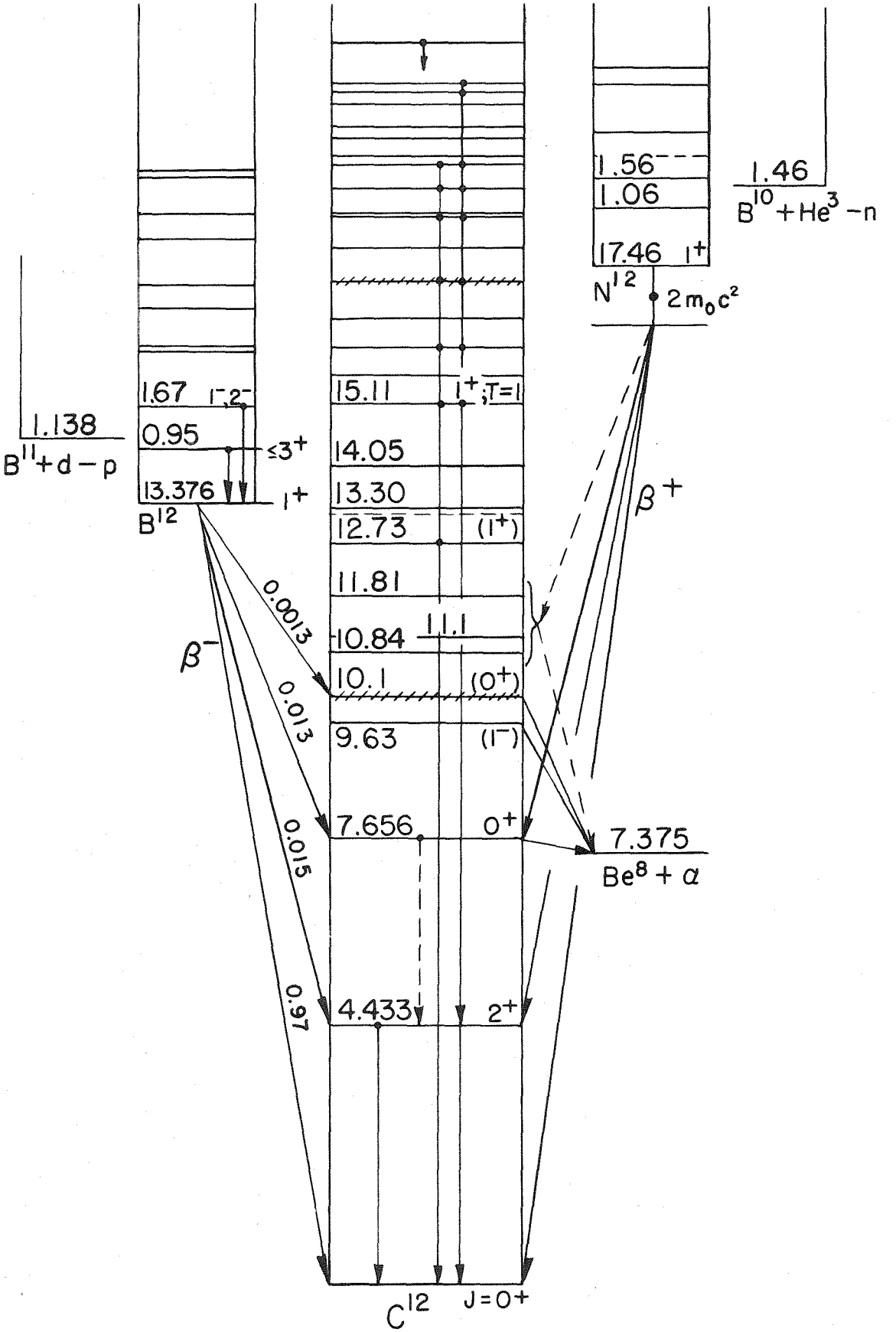
1.56
1.06
17.46 1+
N12
2m0c2
1.46
B10+He3-n
1.67 1-,2-
0.95 ≤3+
13.376 1+
B12
1.138
B11+d-p
15.11 1+;T=1
14.05
13.30
12.73 (1+)
11.81
10.84
11.1
10.1 (0+)
9.63 (1-)
7.656 0+
4.433 2+
C12 J=0+
β+
β-
0.0013
0.013
0.015
0.97
7.375
Be8+α

FIGURE 1

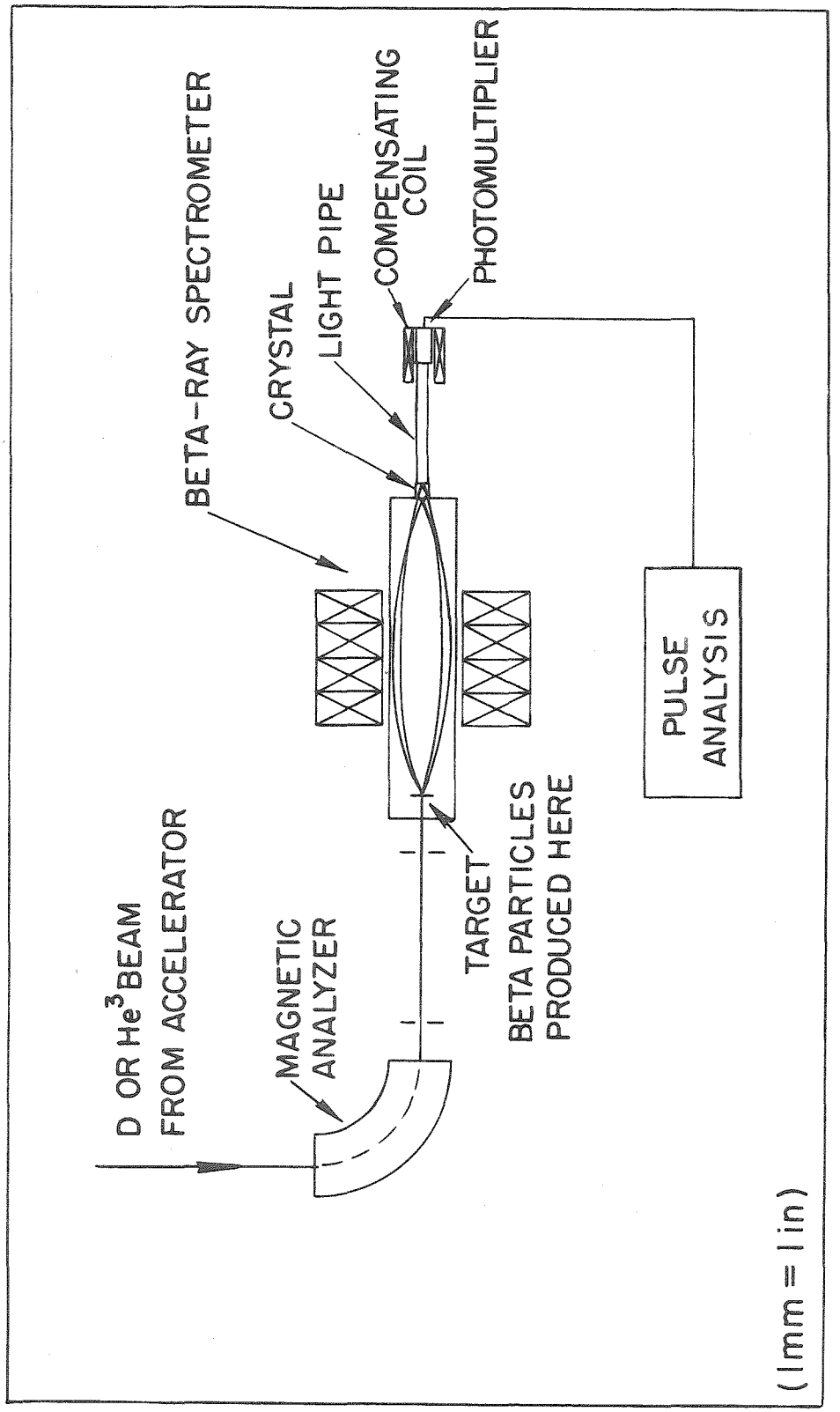

SCHEMATIC OF EXPERIMENT

FIGURE 2

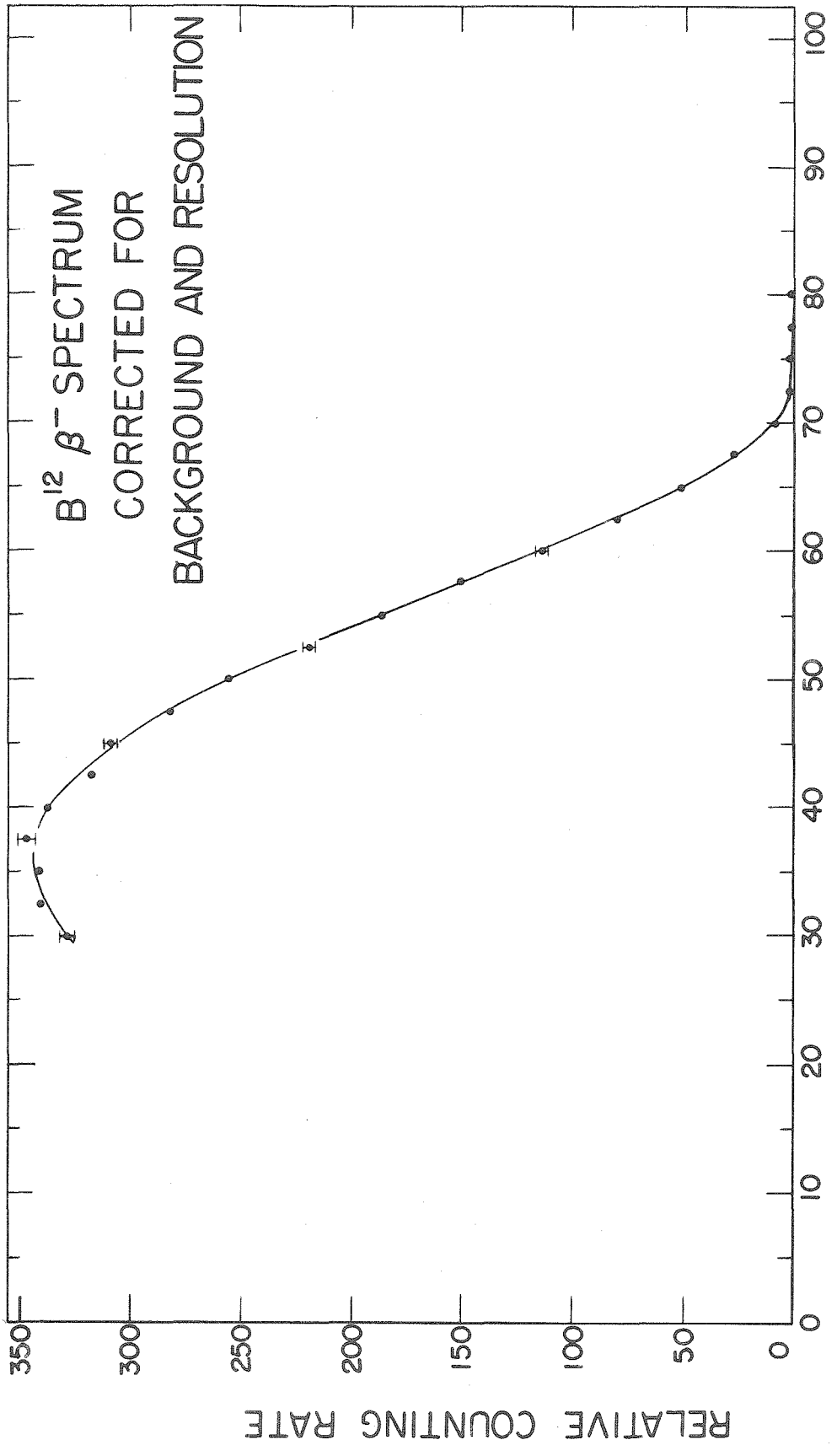
B^{12} β^- SPECTRUM
CORRECTED FOR
BACKGROUND AND RESOLUTION
RELATIVE COUNTING RATE
SHUNT MILLIVOLTS
0
50
100
150
200
250
300
350
0
10
20
30
40
50
60
70
80
90
100

FIGURE 3

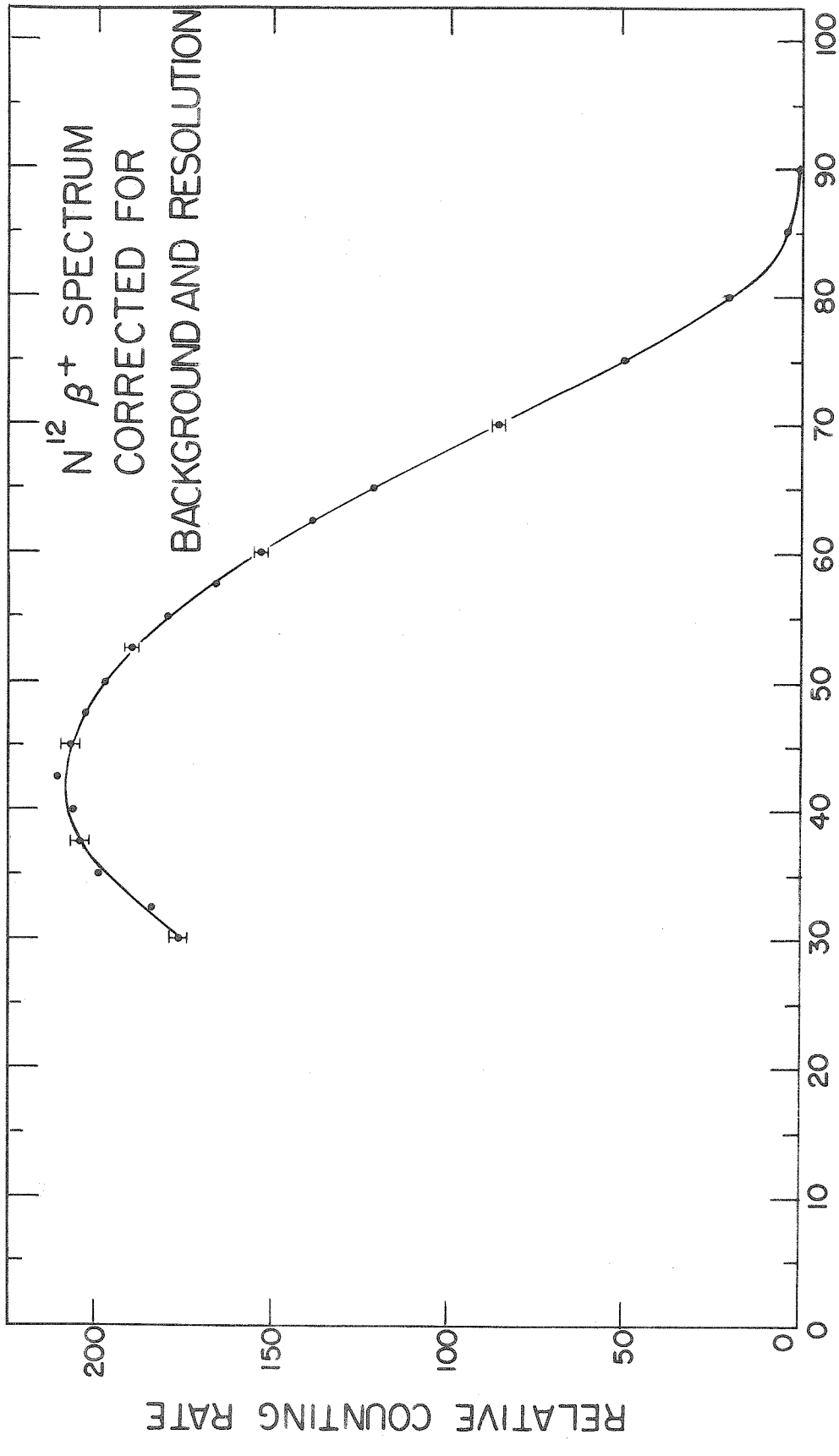
N^{12} β^+ SPECTRUM
CORRECTED FOR
BACKGROUND AND RESOLUTION
RELATIVE COUNTING RATE
SHUNT MILLIVOLTS
0
50
100
150
200
0
10
20
30
40
50
60
70
80
90
100

FIGURE 4

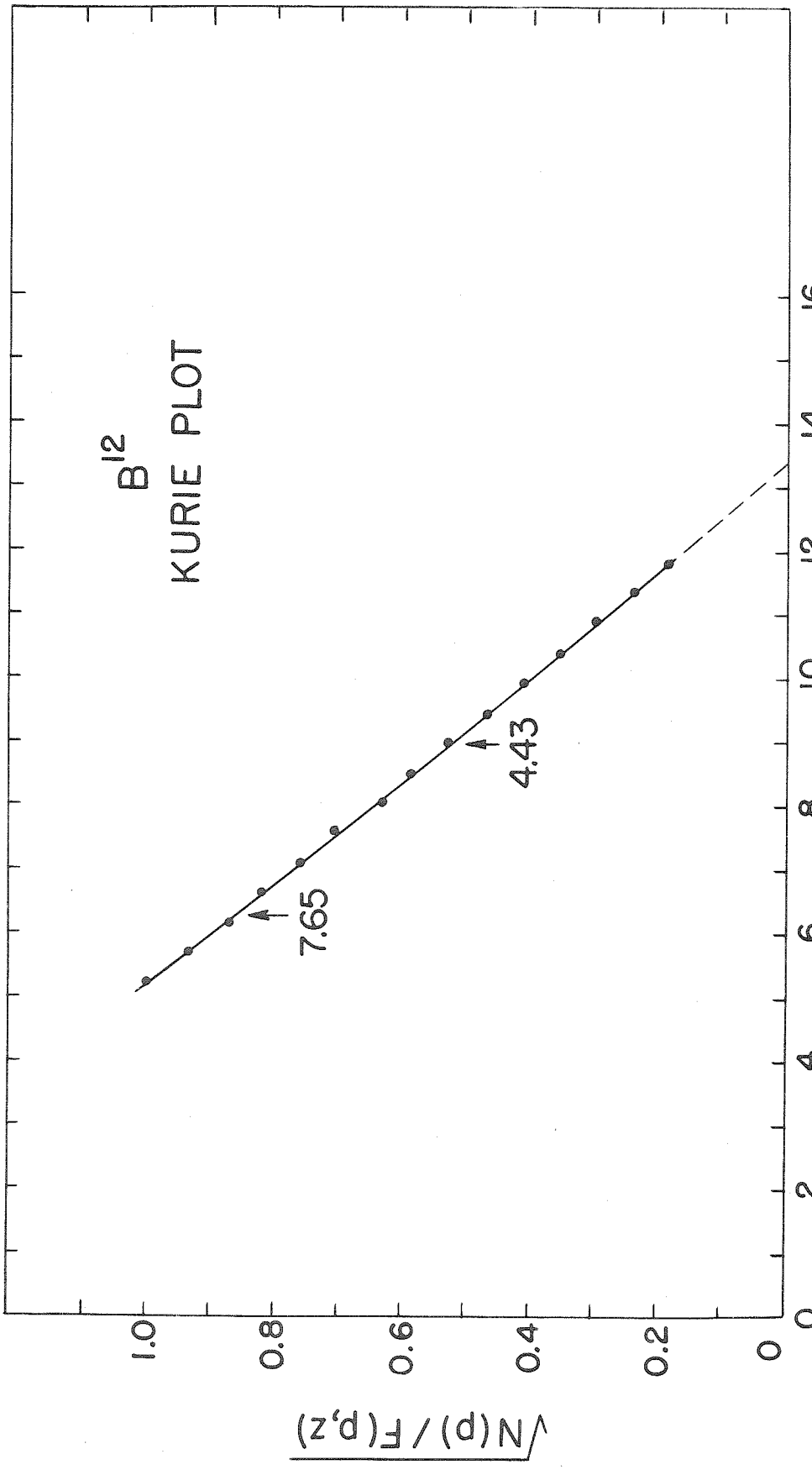
B^{12}
KURIE PLOT
7.65
4.43
$\sqrt{N(p)/F(p,z)}$
ENERGY (Mev)
0
0.2
0.4
0.6
0.8
1.0
0
2
4
6
8
10
12
14
16

FIGURE 5

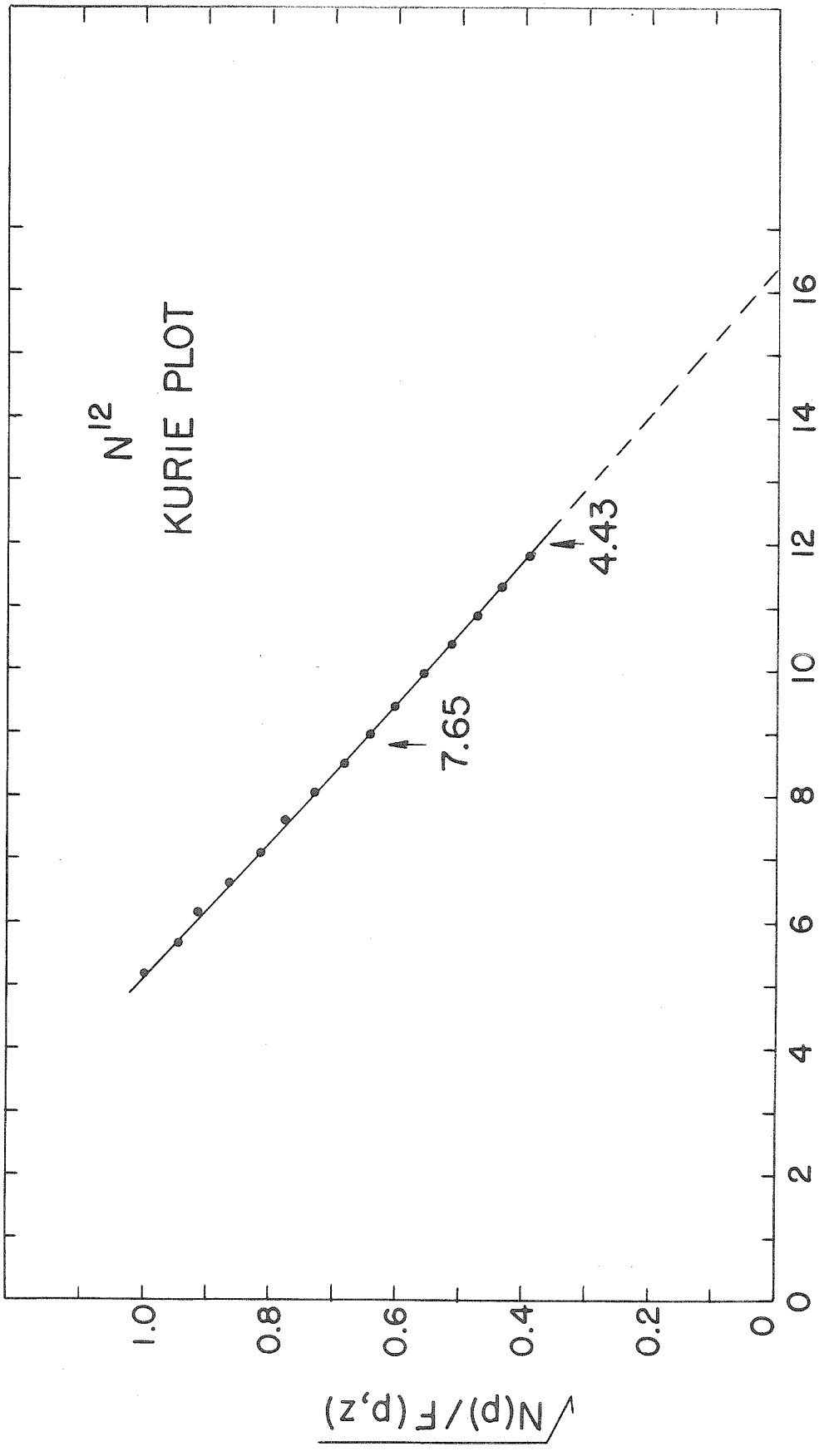
N^{12}
KURIE PLOT
7.65
4.43
$\sqrt{N(p)/F(p,z)}$
ENERGY (Mev)
0
0.2
0.4
0.6
0.8
1.0
0
2
4
6
8
10
12
14
16

FIGURE 6

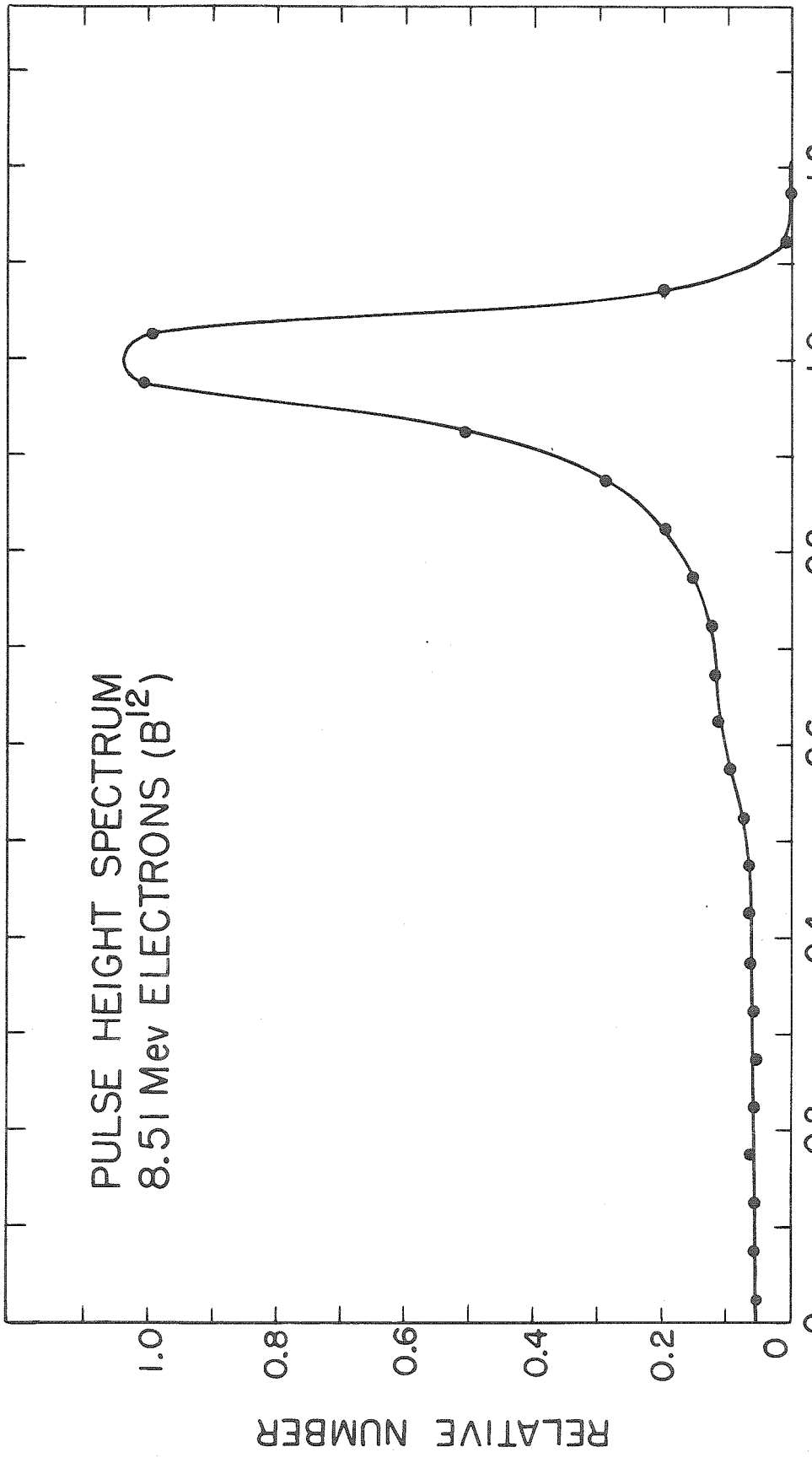
PULSE HEIGHT SPECTRUM
8.51 Mev ELECTRONS (B^{12})
RELATIVE NUMBER
0
0.2
0.4
0.6
0.8
1.0
0
0.2
0.4
0.6
0.8
1.0
1.2
PULSE HEIGHT (Arbitrary Units)

FIGURE 7

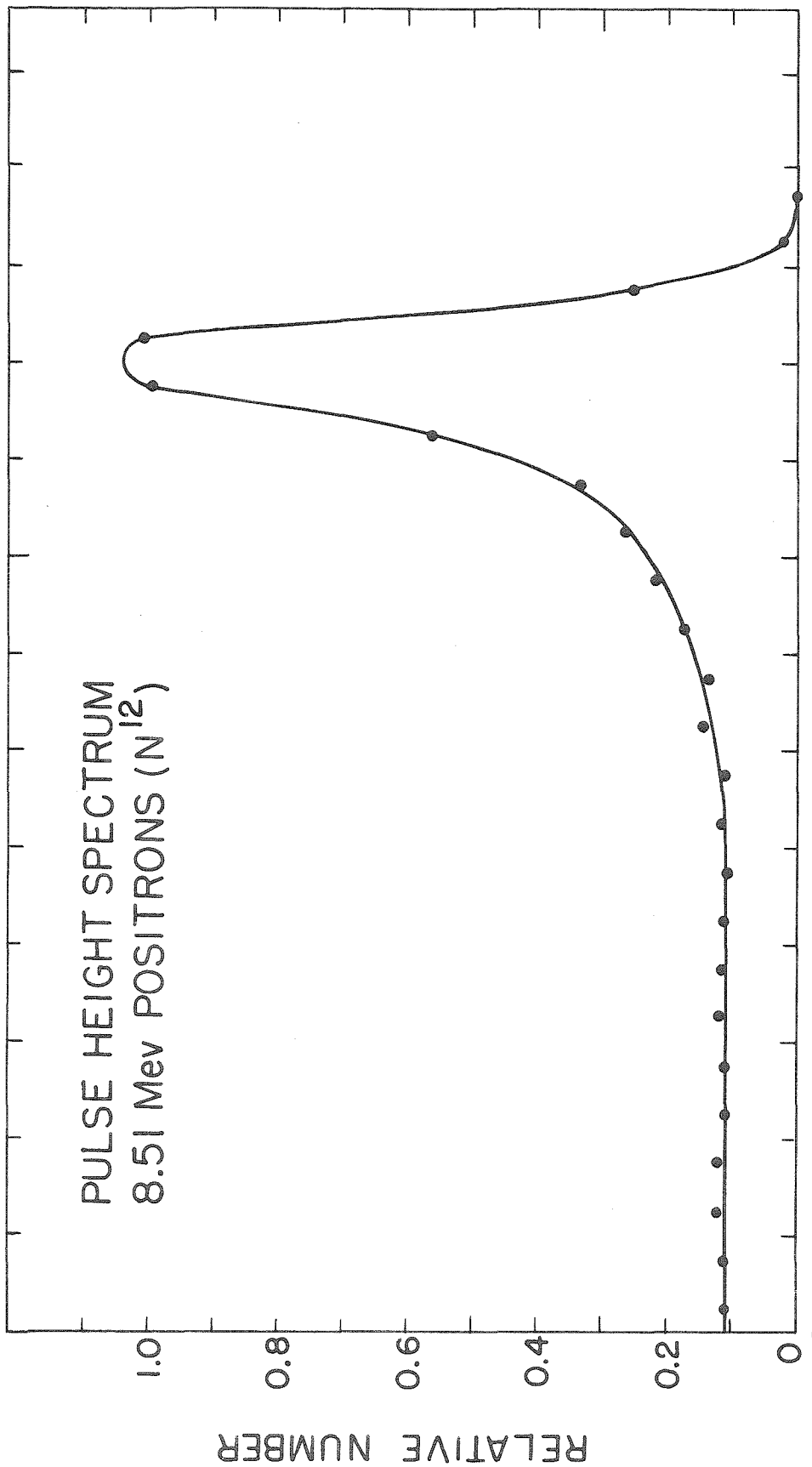
PULSE HEIGHT SPECTRUM
8.51 Mev POSITRONS (N^{12})
RELATIVE NUMBER
1.0
0.8
0.6
0.4
0.2
0
0.2
0.4
0.6
0.8
1.0
1.2
PULSE HEIGHT (Arbitrary Units)

FIGURE 8

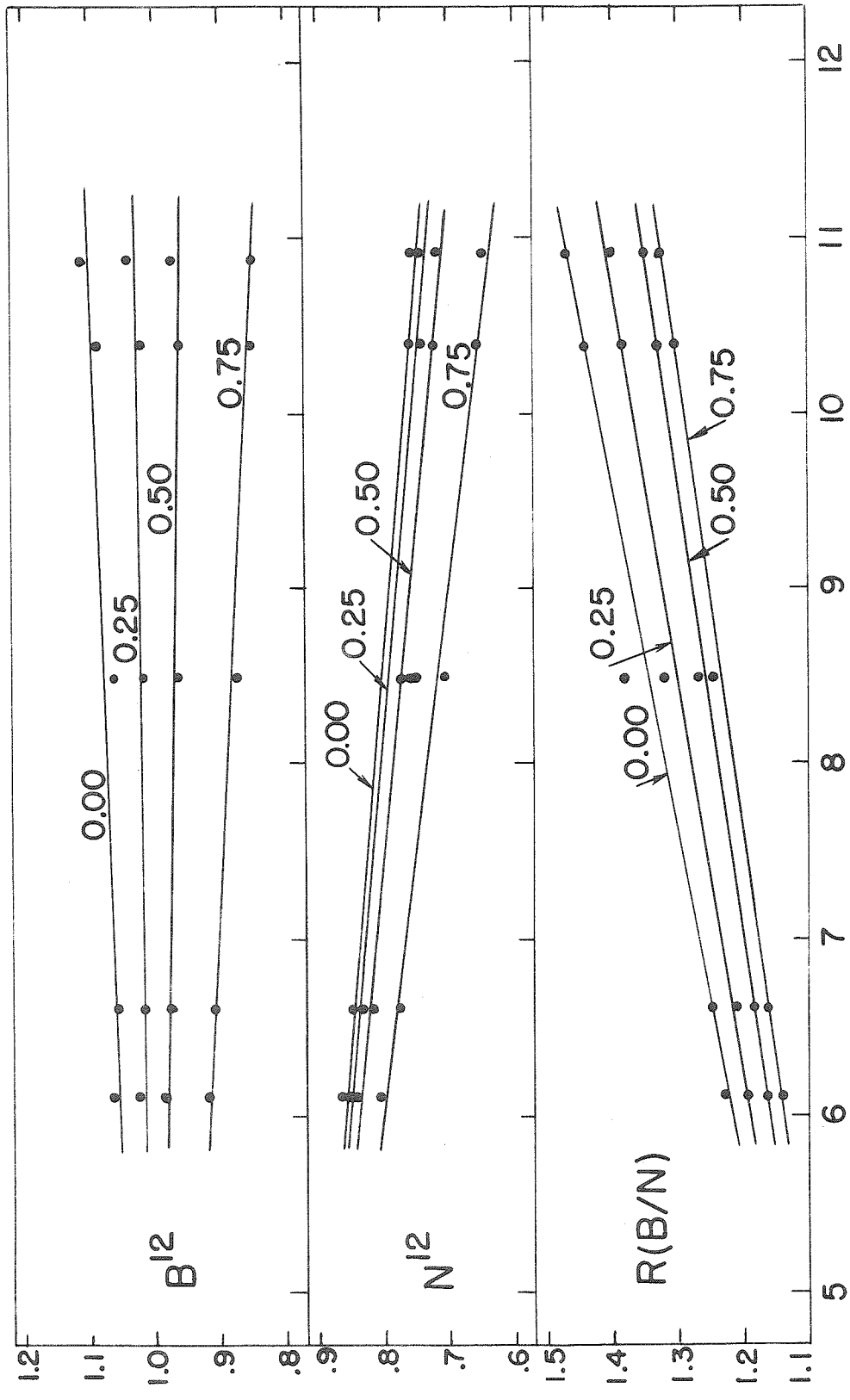

FIGURE 9
EFFECT OF CUT-OFF

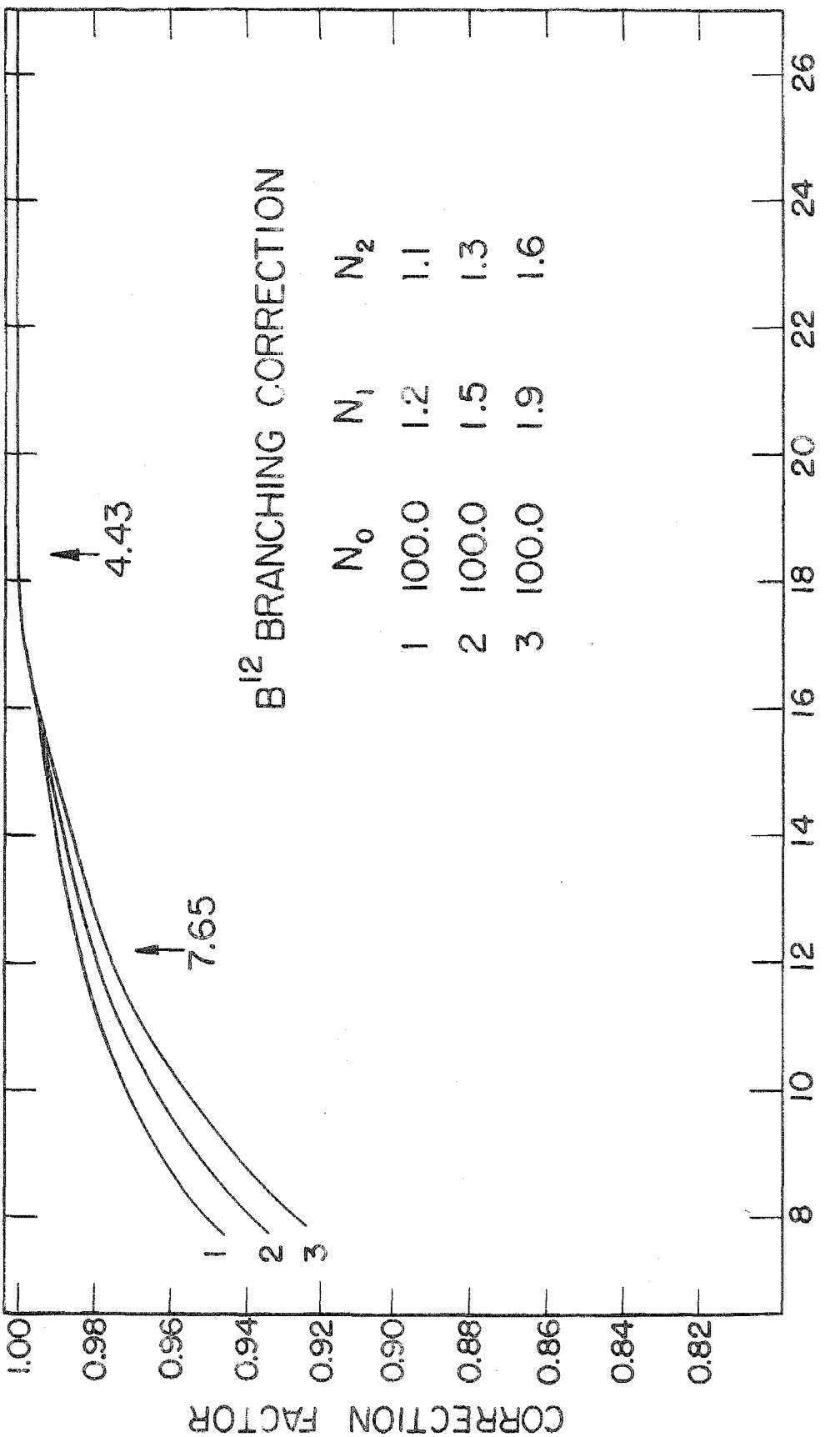
B12 BRANCHING CORRECTION
No N1 N2
1 100.0 1.2 1.1
2 100.0 1.5 1.3
3 100.0 1.9 1.6
4.43
7.65
1
2
3
CORRECTION FACTOR
1.00
0.98
0.96
0.94
0.92
0.90
0.88
0.86
0.84
0.82
8
10
12
14
16
18
20
22
24
26
η (IN UNITS OF mc)

FIGURE 10

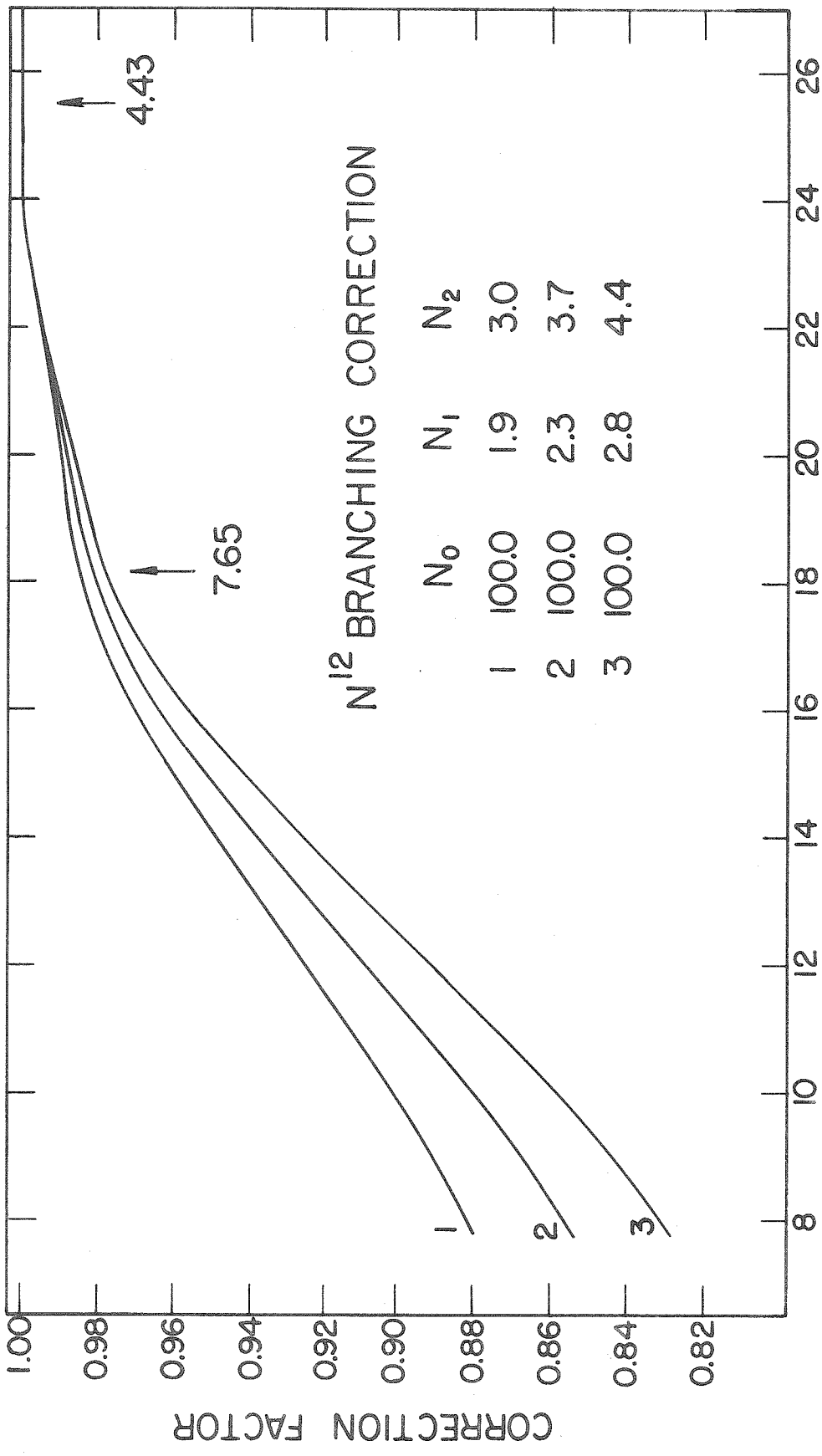
N^{12} BRANCHING CORRECTION
N_0 N_1 N_2
1 100.0 1.9 3.0
2 100.0 2.3 3.7
3 100.0 2.8 4.4
4.43
7.65
1
2
3
CORRECTION FACTOR
1.00
0.98
0.96
0.94
0.92
0.90
0.88
0.86
0.84
0.82
8
10
12
14
16
18
20
22
24
26
η (IN UNITS OF mc)

FIGURE 11

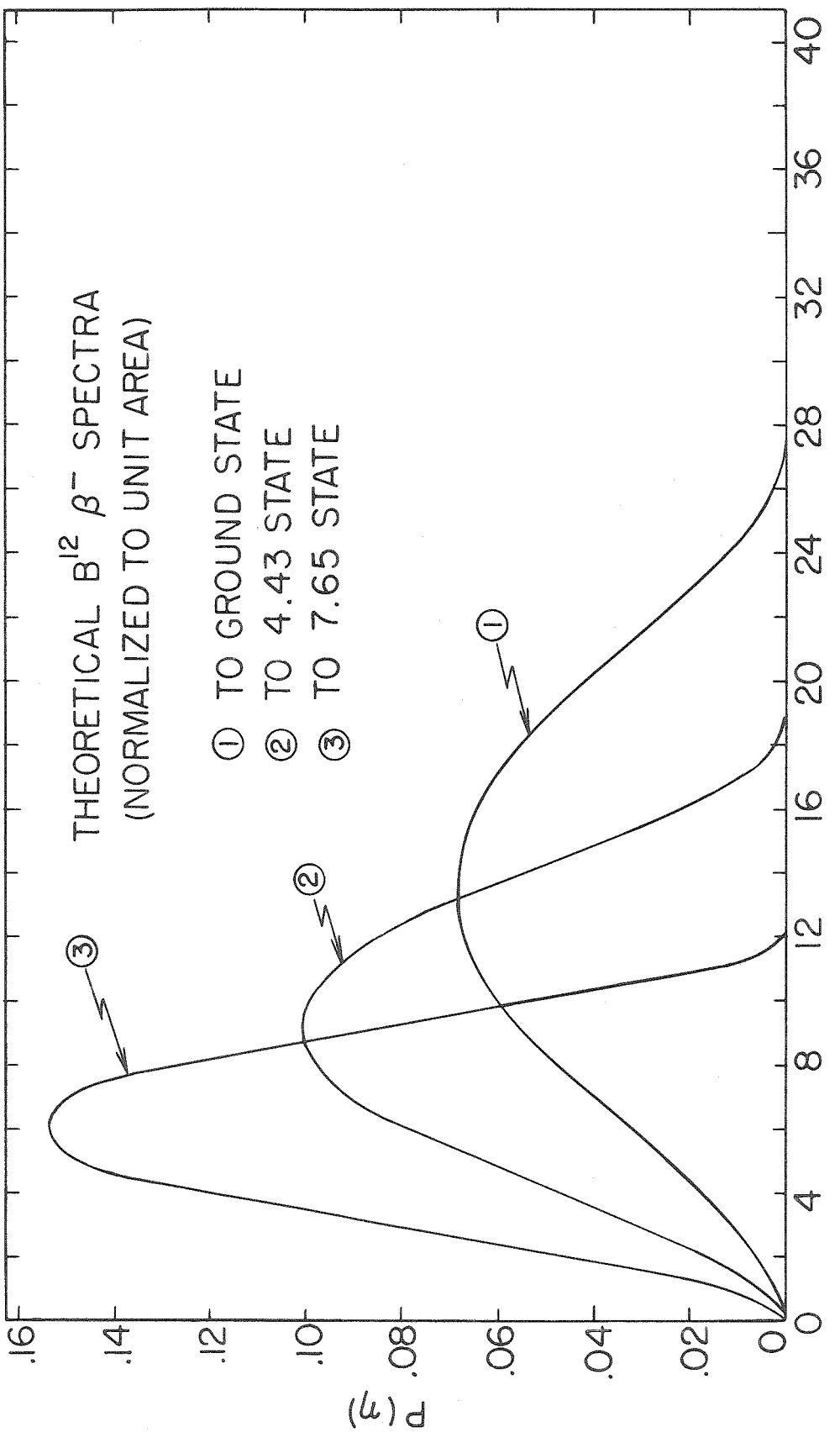
THEORETICAL B^{12} β^- SPECTRA
(NORMALIZED TO UNIT AREA)
① TO GROUND STATE
② TO 4.43 STATE
③ TO 7.65 STATE
P(η)
η (IN UNITS OF mc)
0
.02
.04
.06
.08
.10
.12
.14
.16
4
8
12
16
20
24
28
32
36
40

FIGURE 12

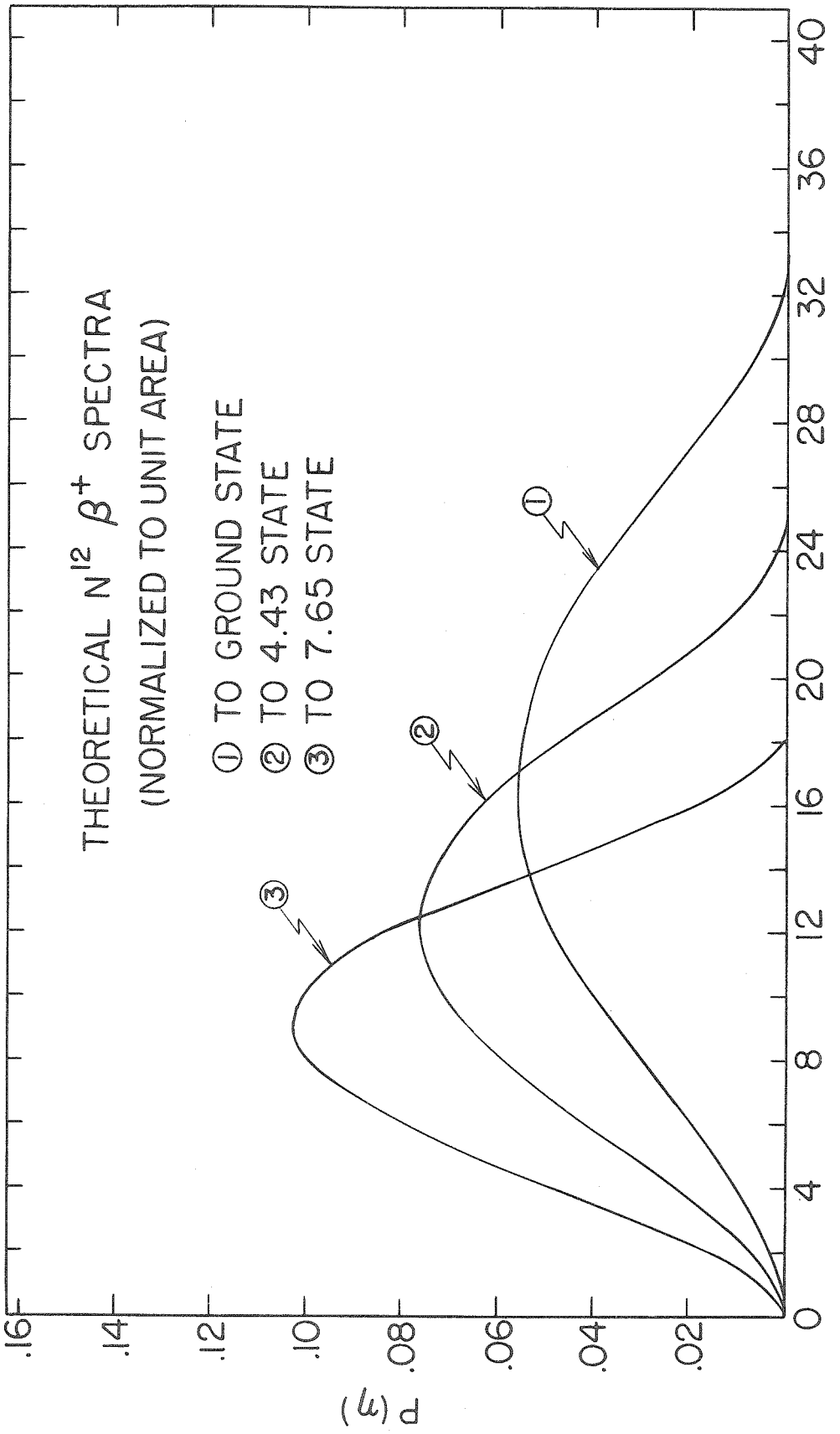
THEORETICAL N^{12} β^+ SPECTRA
(NORMALIZED TO UNIT AREA)
① TO GROUND STATE
② TO 4.43 STATE
③ TO 7.65 STATE
P(η)
η (IN UNITS OF mc)
.16
.14
.12
.10
.08
.06
.04
.02
0
4
8
12
16
20
24
28
32
36
40

FIGURE 13

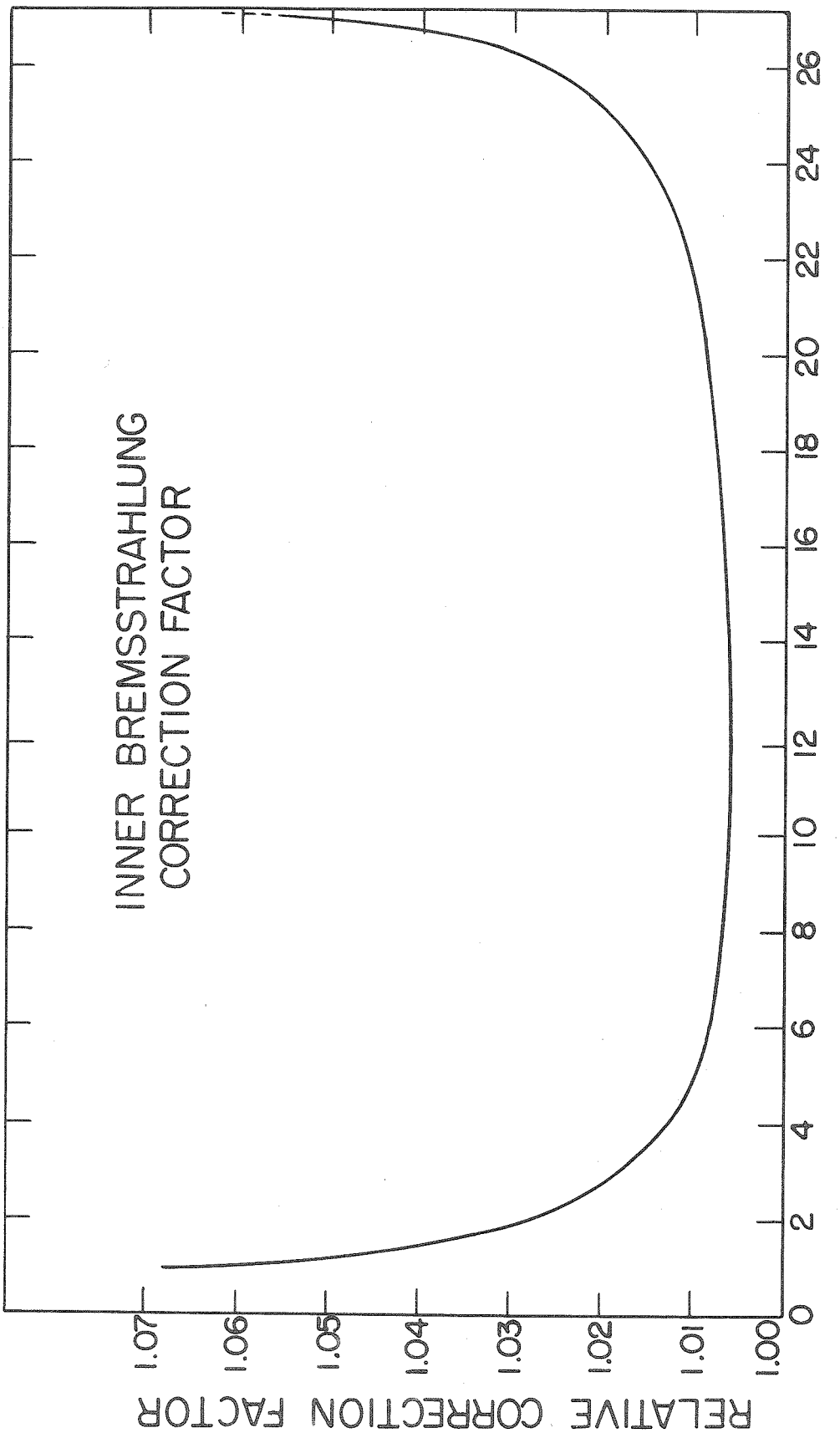
INNER BREMSSTRAHLUNG
CORRECTION FACTOR
RELATIVE CORRECTION FACTOR
1.00
1.01
1.02
1.03
1.04
1.05
1.06
1.07
0
2
4
6
8
10
12
14
16
18
20
22
24
26
W (in units of mc²)

FIGURE 14

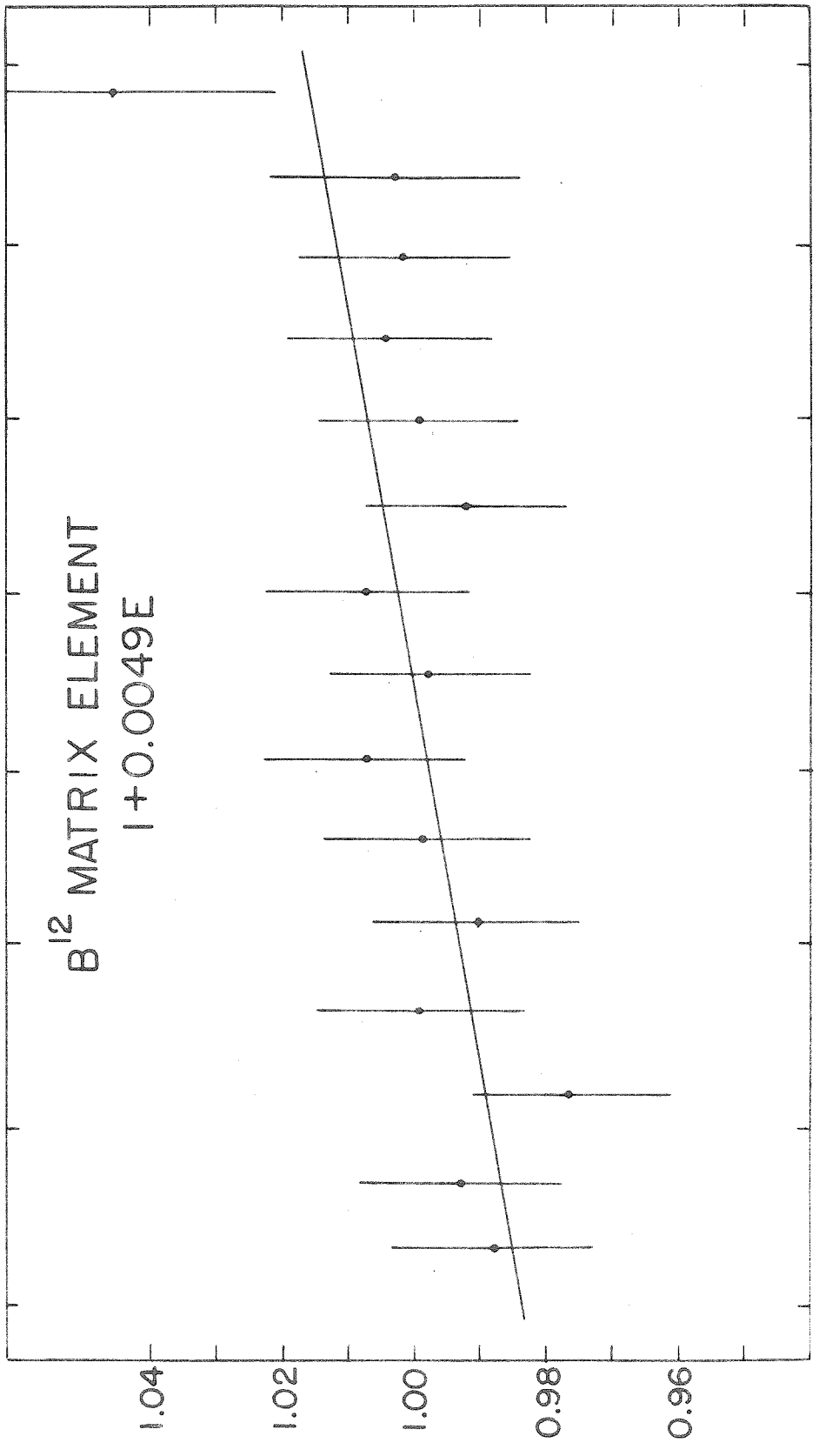
B^{12} MATRIX ELEMENT
1+0.0049E
MATRIX ELEMENT (Normalized to Unity)
1.04
1.02
1.00
0.98
0.96
5
6
7
8
9
10
11
12
ENERGY (Mev)

FIGURE 15

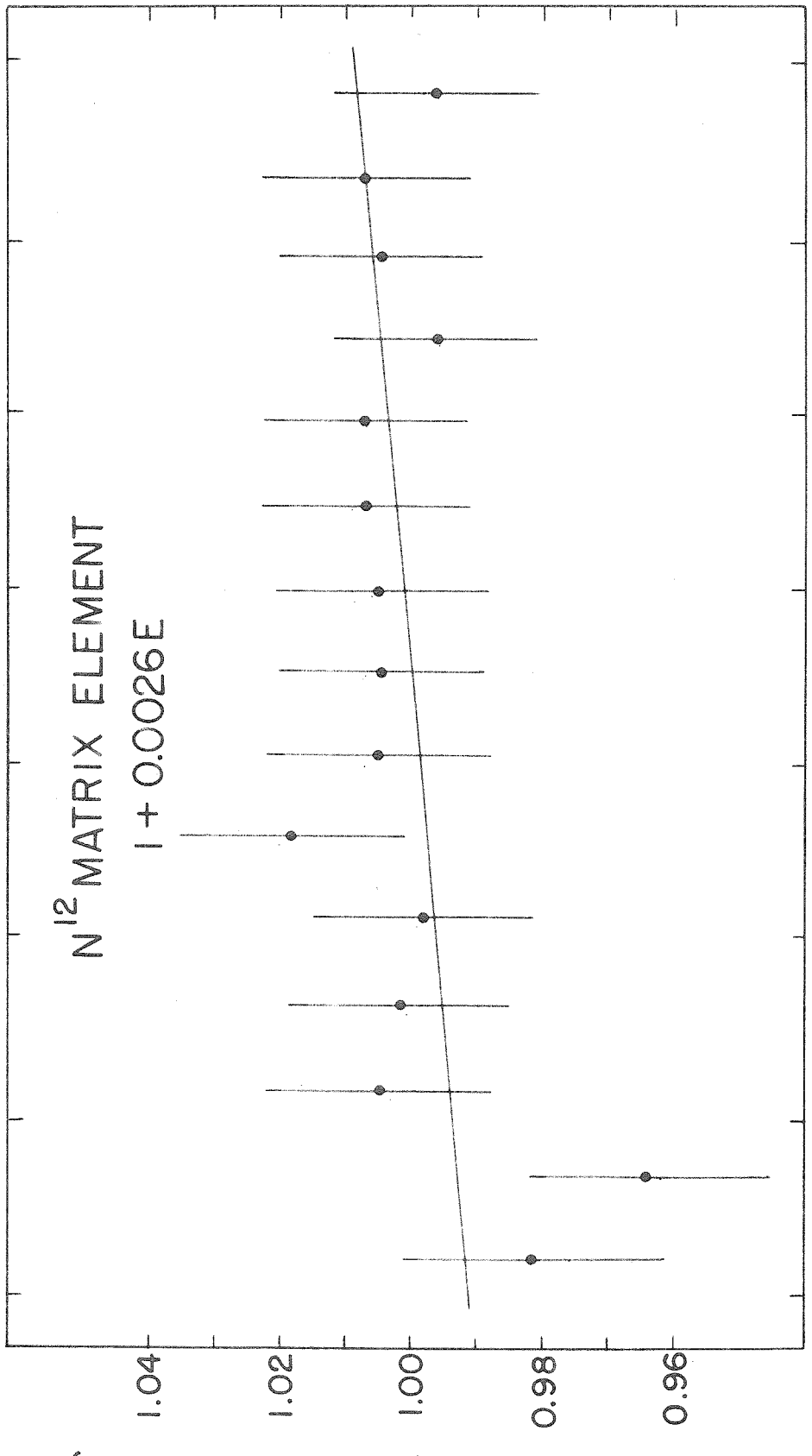
N^{12} MATRIX ELEMENT
1 + 0.0026E
MATRIX ELEMENT (Normalized to Unity)
1.04
1.02
1.00
0.98
0.96
5
6
7
8
9
10
11
12
ENERGY (Mev)

FIGURE 16

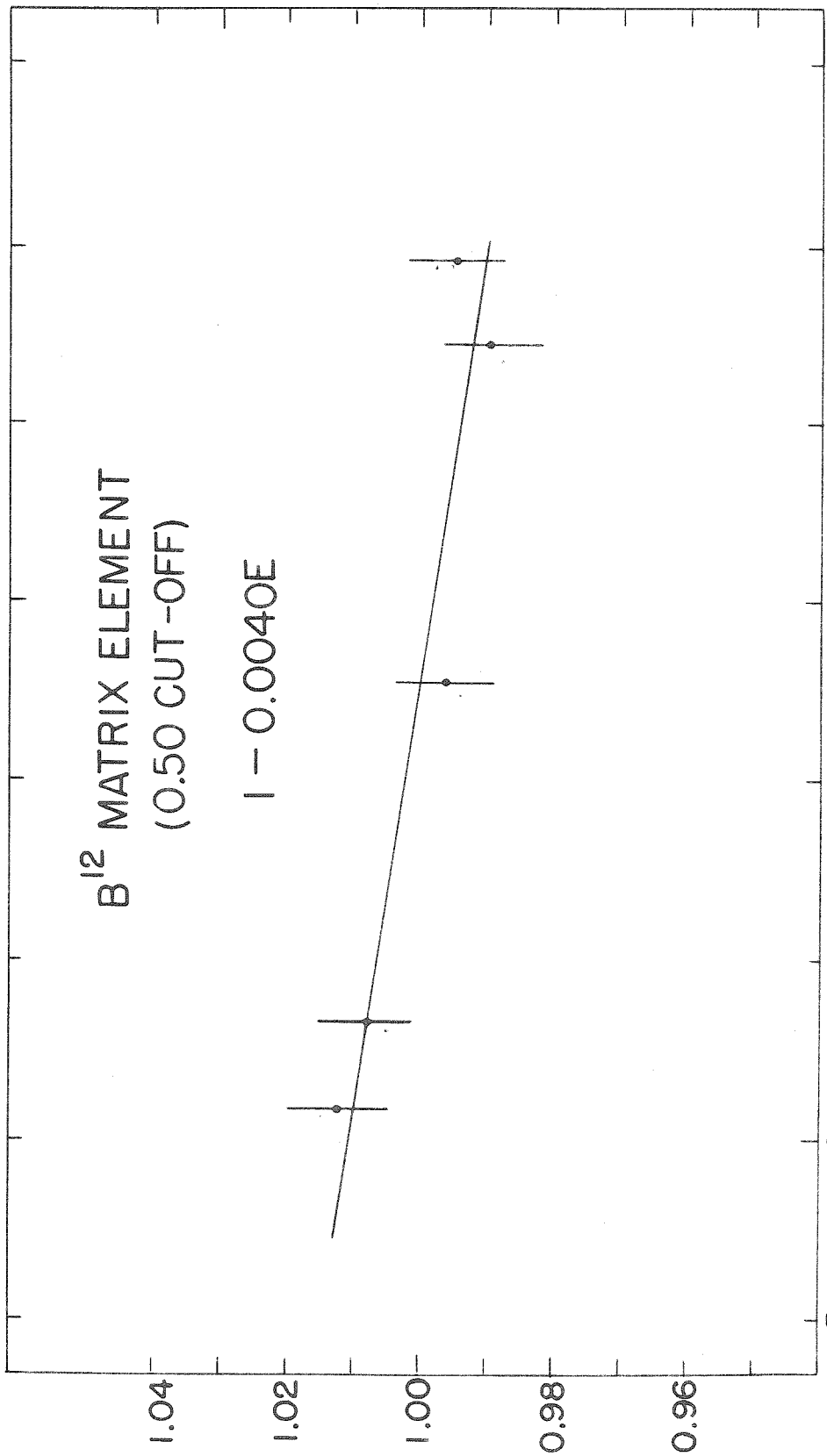
B^{12} MATRIX ELEMENT
(0.50 CUT-OFF)
1 − 0.0040E
MATRIX ELEMENT (Normalized to Unity)
1.04
1.02
1.00
0.98
0.96
5
6
7
8
9
10
11
12
ENERGY (Mev)

FIGURE 17

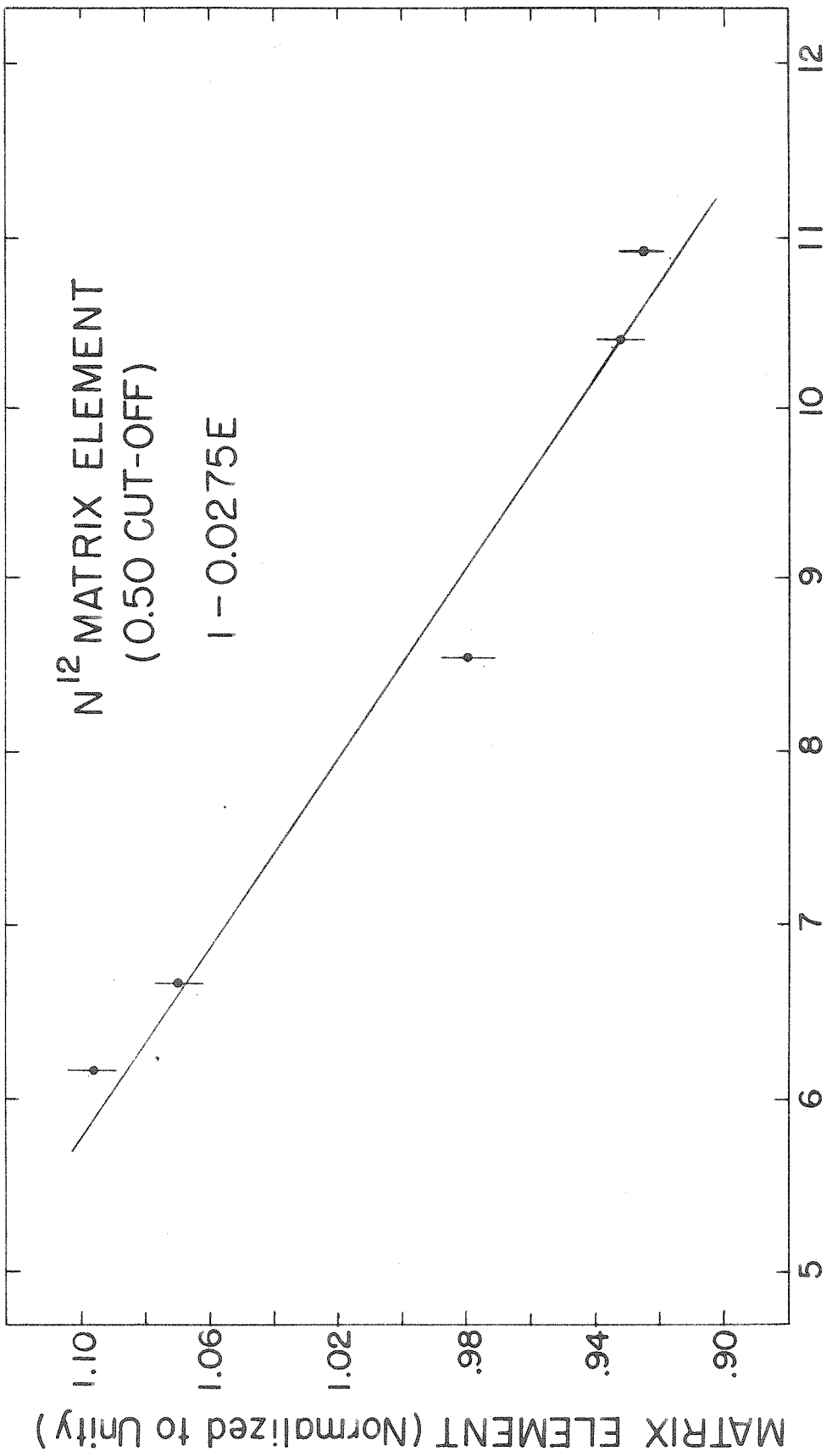
N^{12} MATRIX ELEMENT
(0.50 CUT-OFF)
1 - 0.0275E
MATRIX ELEMENT (Normalized to Unity)
1.10
1.06
1.02
.98
.94
.90
5
6
7
8
9
10
11
12
ENERGY (Mev)

FIGURE 18

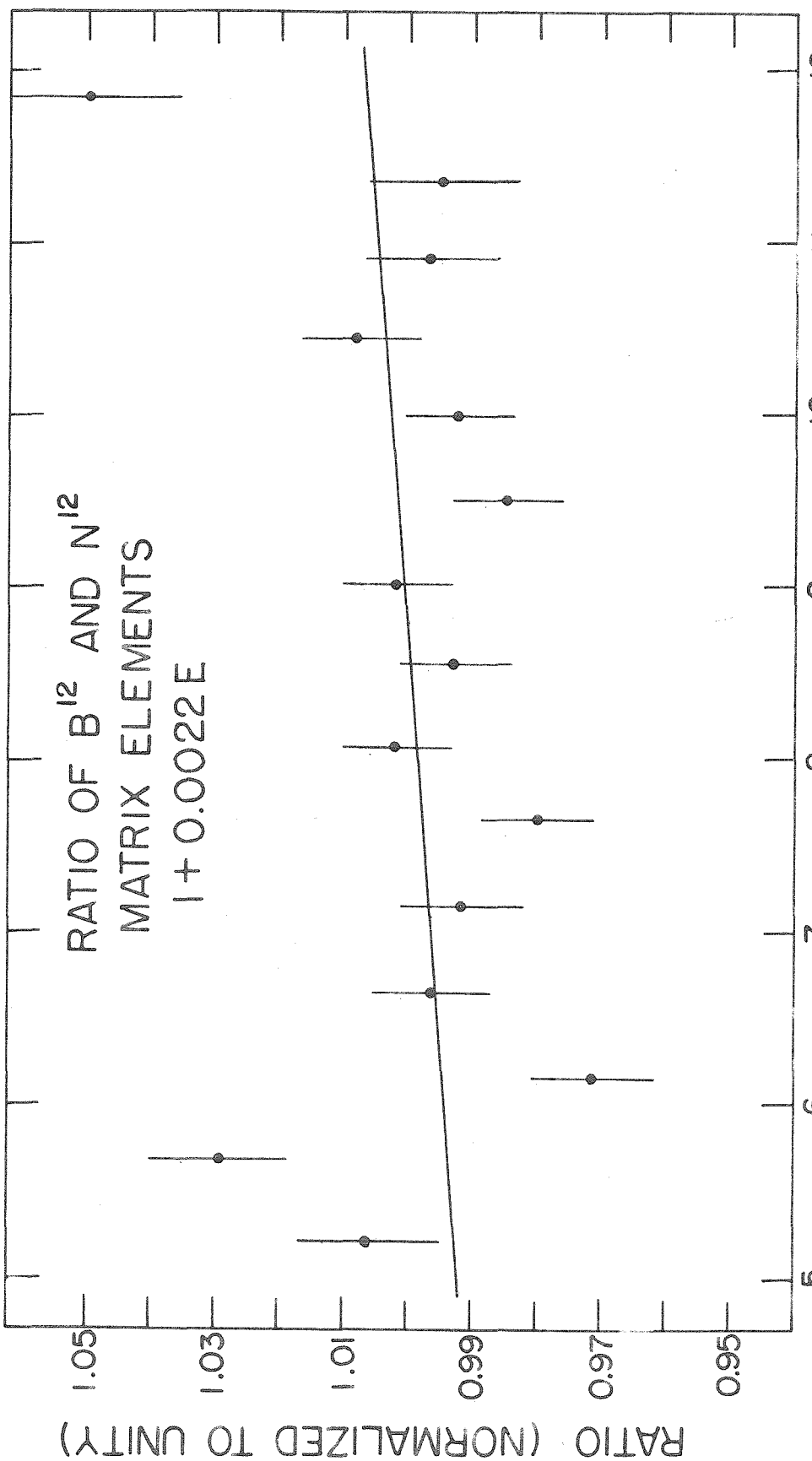
RATIO OF B^{12} AND N^{12}
MATRIX ELEMENTS
1+0.0022E
RATIO (NORMALIZED TO UNITY)
1.05
1.03
1.01
0.99
0.97
0.95
5
6
7
8
9
10
11
12
ENERGY IN MEV

FIGURE 19

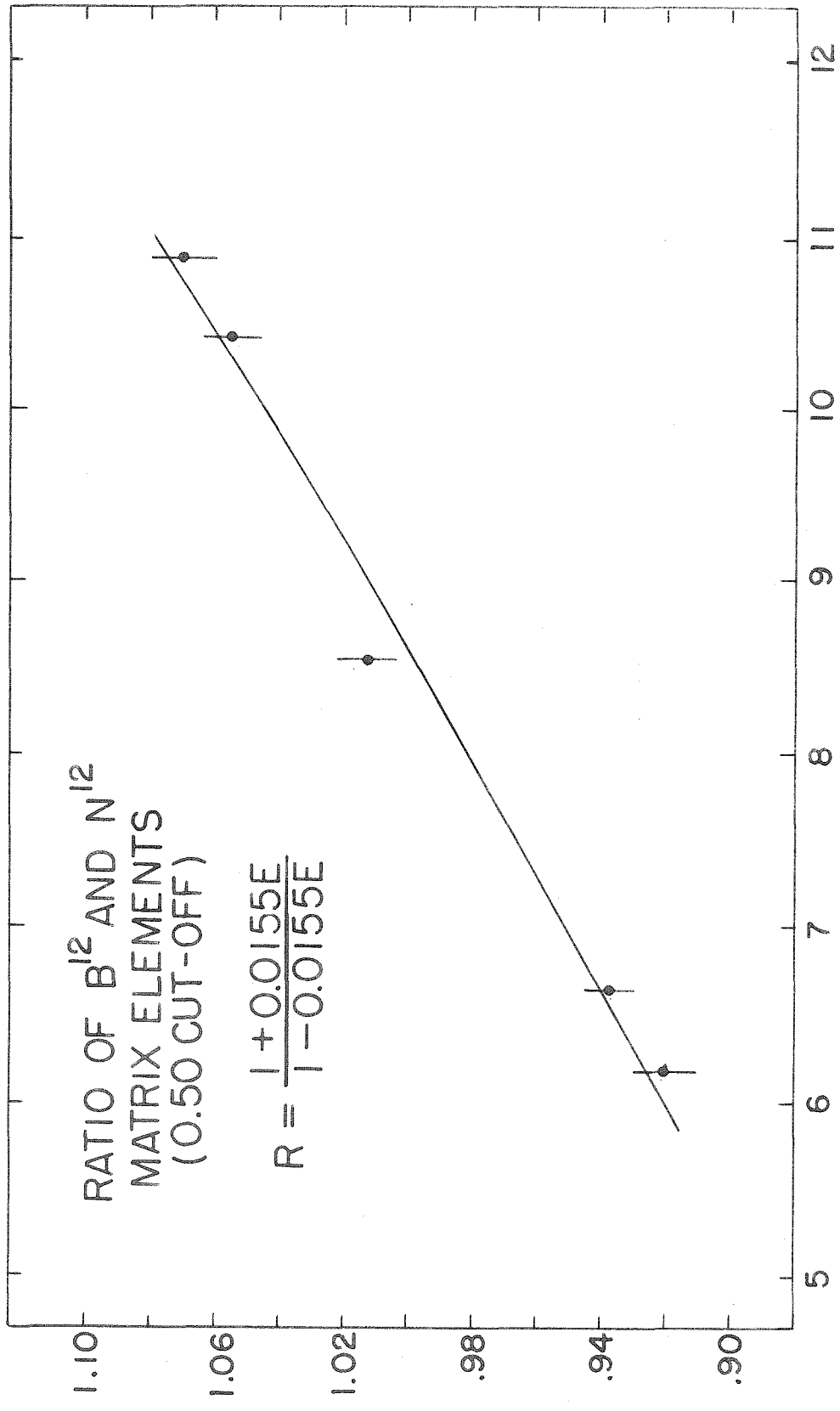
RATIO OF B^{12} AND N^{12}
MATRIX ELEMENTS
(0.50 CUT-OFF)
$R = \frac{1+0.0155E}{1-0.0155E}$
RATIO (Normalized to Unity)
1.10
1.06
1.02
.98
.94
.90
5
6
7
8
9
10
11
12
ENERGY (Mev)

FIGURE 20

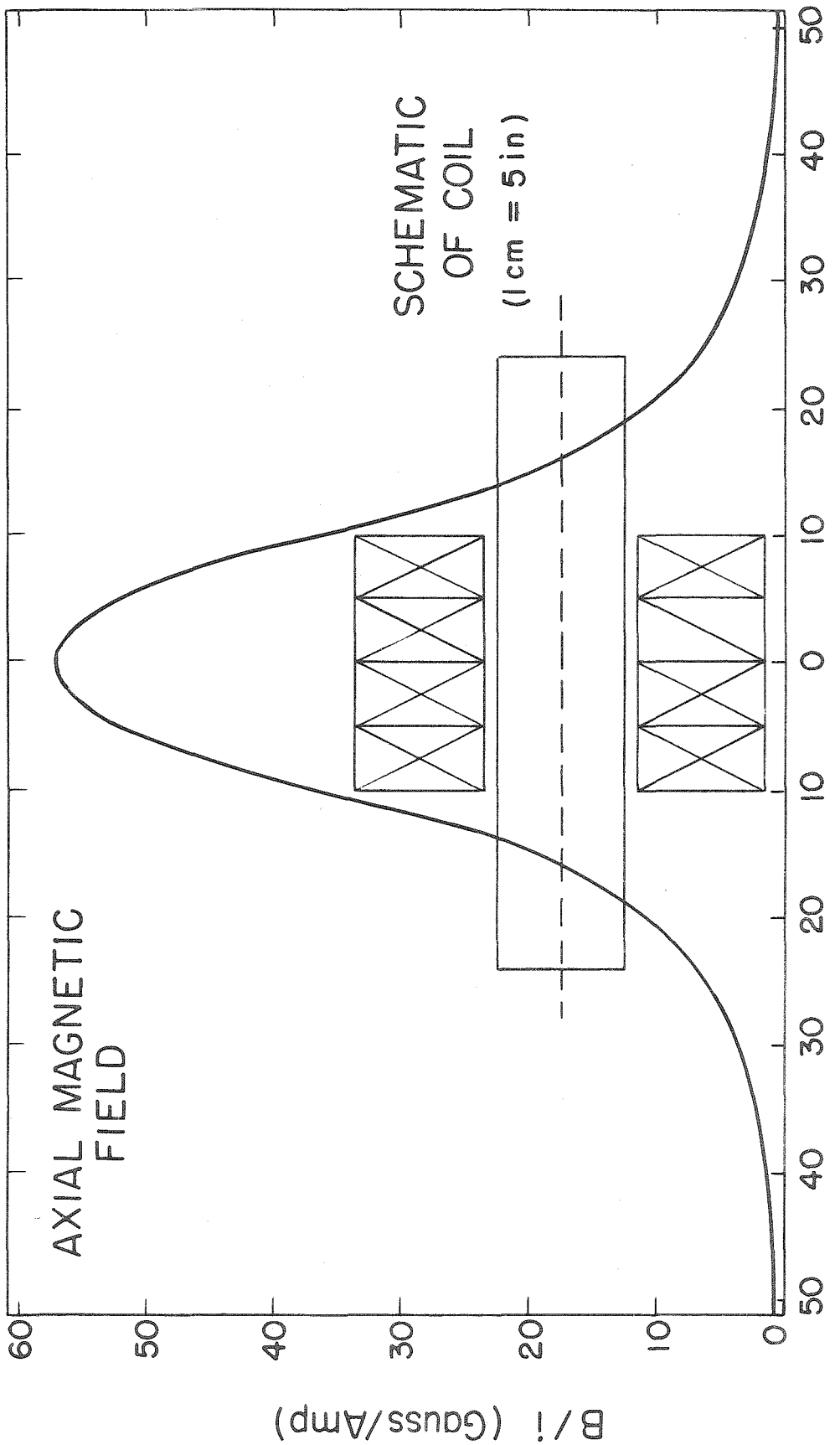
AXIAL MAGNETIC FIELD
SCHEMATIC OF COIL
(1cm = 5in)
B / i (Gauss/Amp)
DISTANCE (INCHES)
0
10
20
30
40
50
60
50
40
30
20
10
0
10
20
30
40
50

FIGURE 21

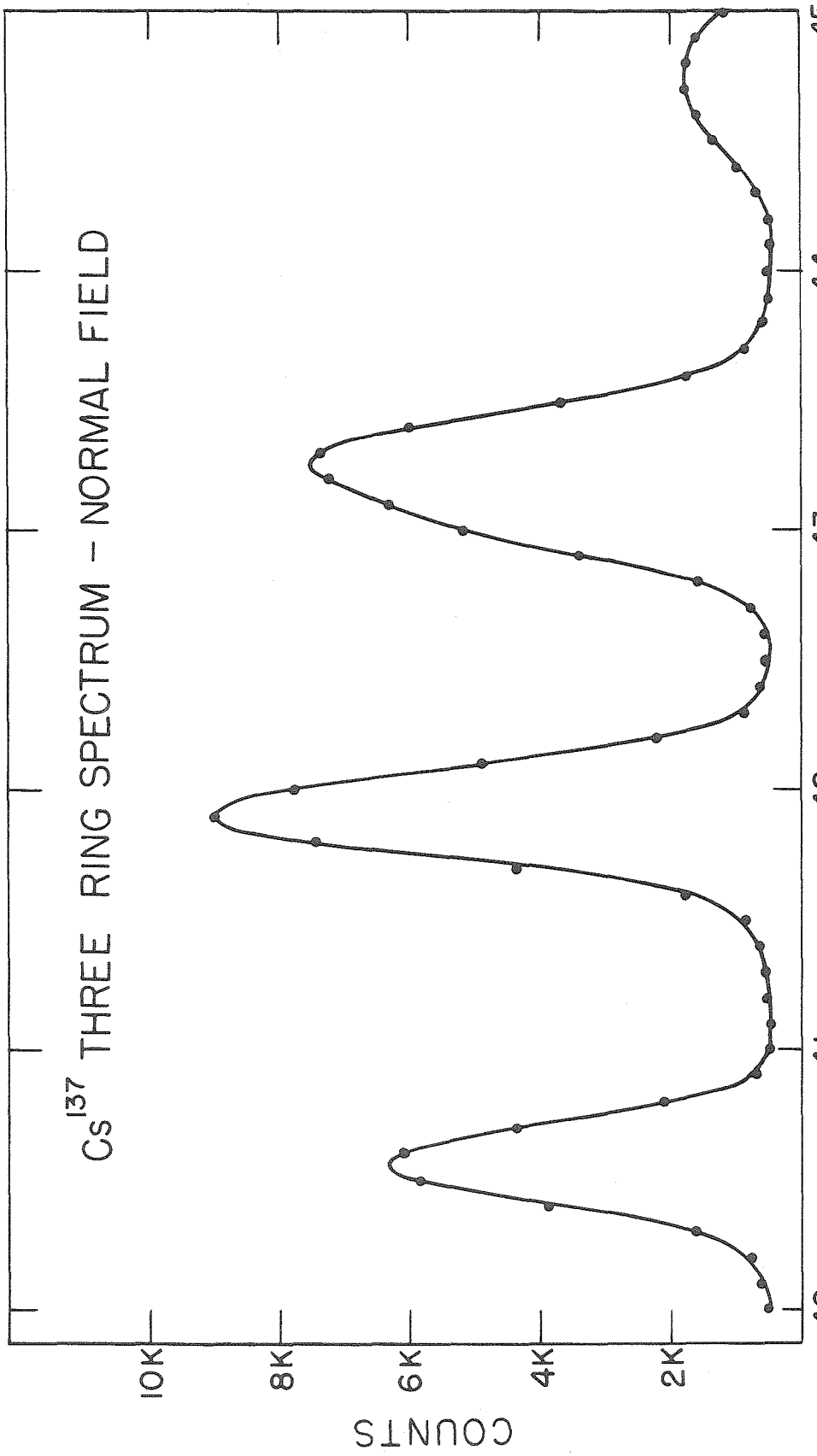
Cs^{137} THREE RING SPECTRUM - NORMAL FIELD
COUNTS
10K
8K
6K
4K
2K
40
41
42
43
44
45
SHUNT MILLIVOLTS

FIGURE 22

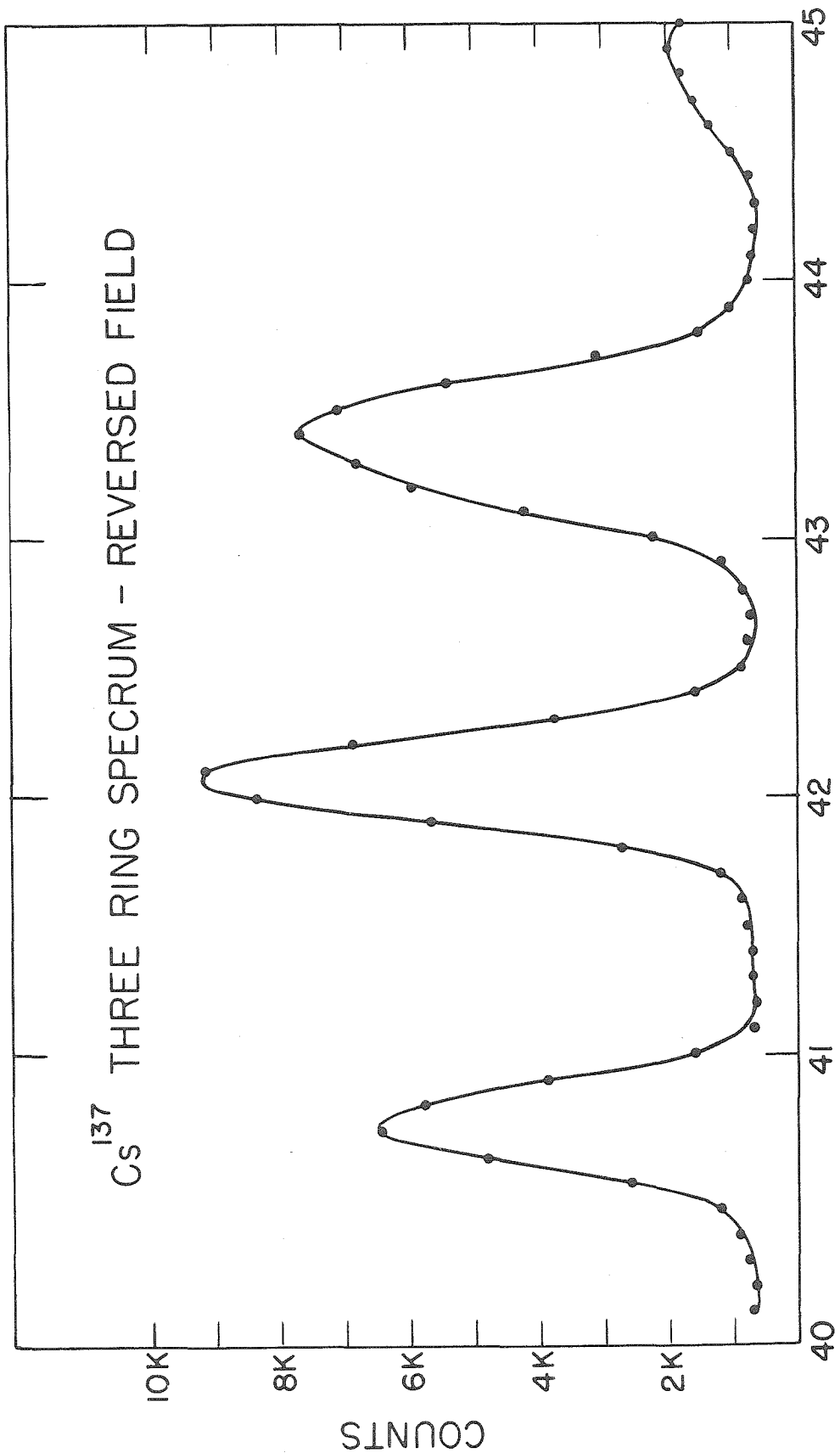
Cs^{137} THREE RING SPECRUM - REVERSED FIELD
COUNTS
10K
8K
6K
4K
2K
40
41
42
43
44
45
SHUNT MILLIVOLTS

FIGURE 23

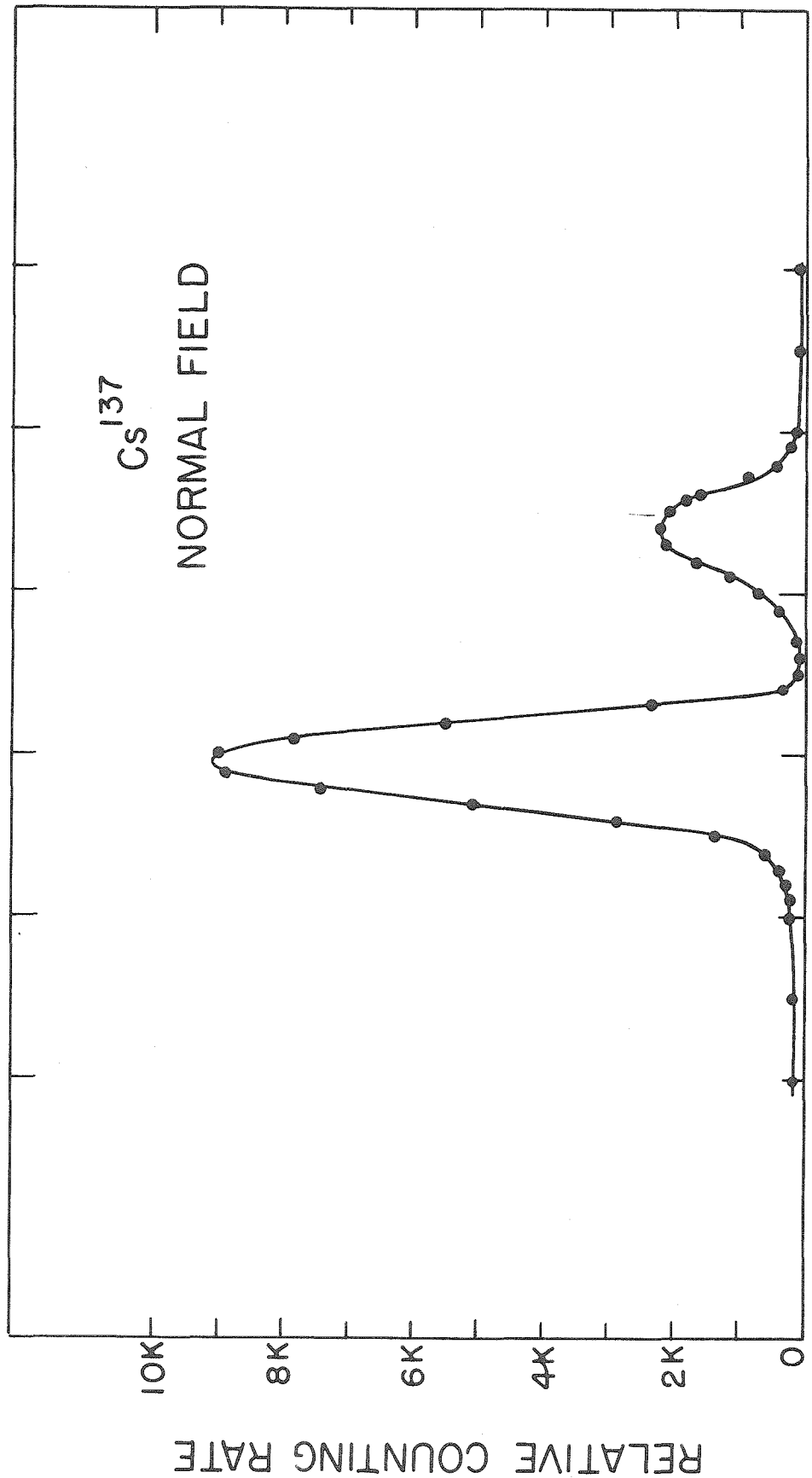
Cs^{137}
NORMAL FIELD
RELATIVE COUNTING RATE
10K
8K
6K
4K
2K
0
38
39
40
41
42
43
SHUNT MILLIVOLTS

FIGURE 24

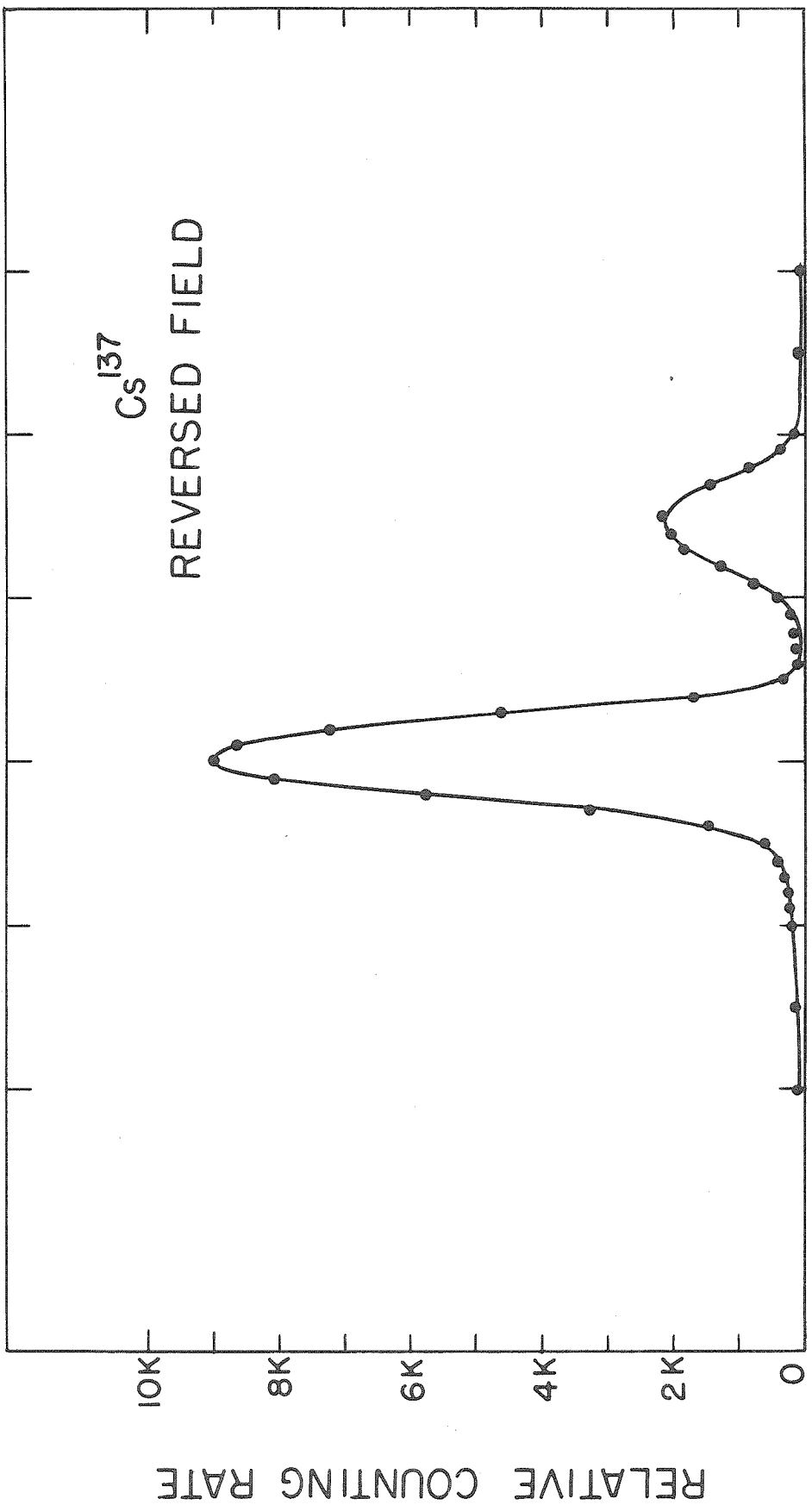
Cs^{137}
REVERSED FIELD
RELATIVE COUNTING RATE
10K
8K
6K
4K
2K
0
38
39
40
41
42
43
SHUNT MILLIVOLTS

FIGURE 25

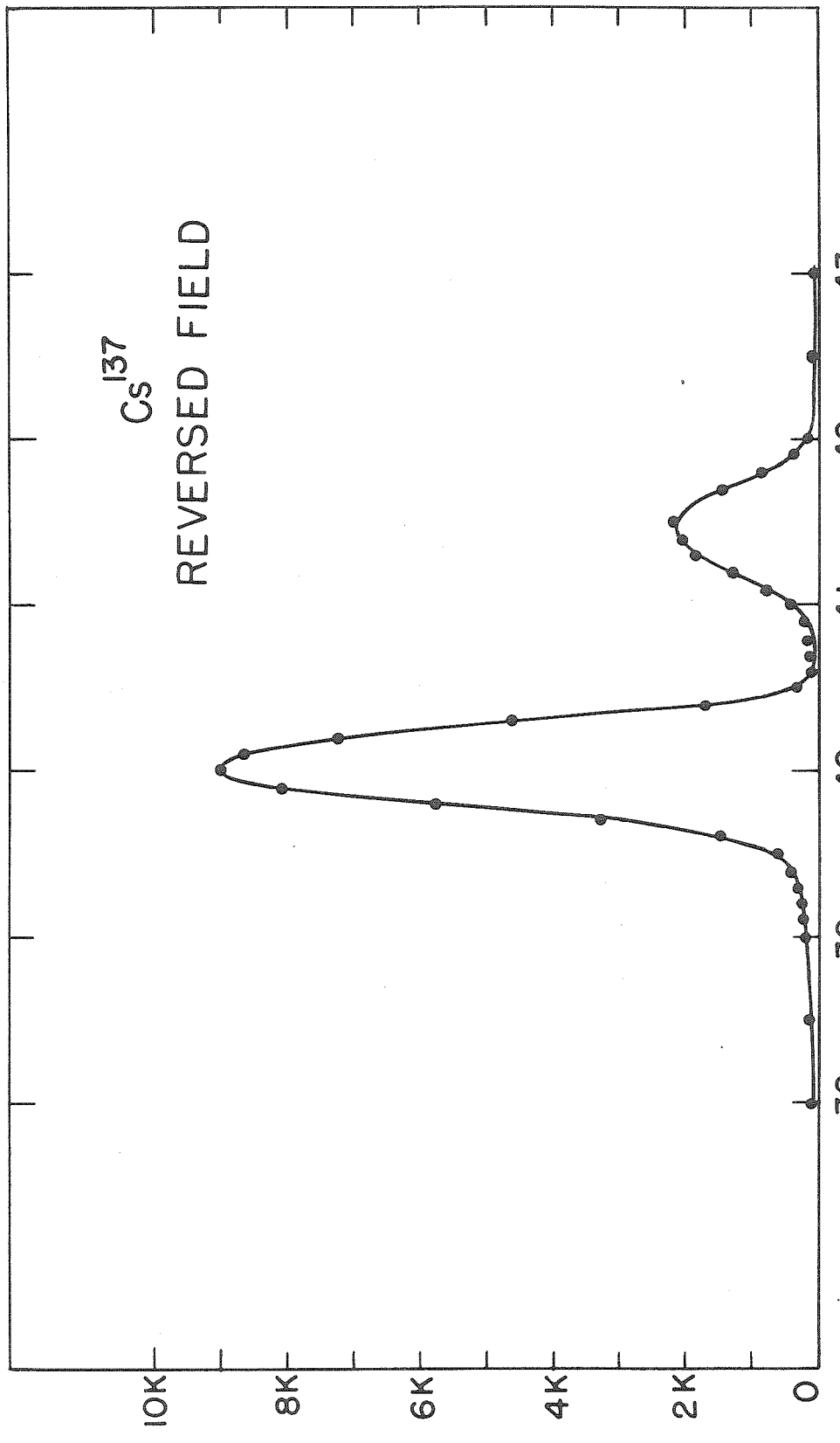
Cs^{137}
REVERSED FIELD
RELATIVE COUNTING RATE
10K
8K
6K
4K
2K
0
38
39
40
41
42
43
SHUNT MILLIVOLTS

FIGURE 25

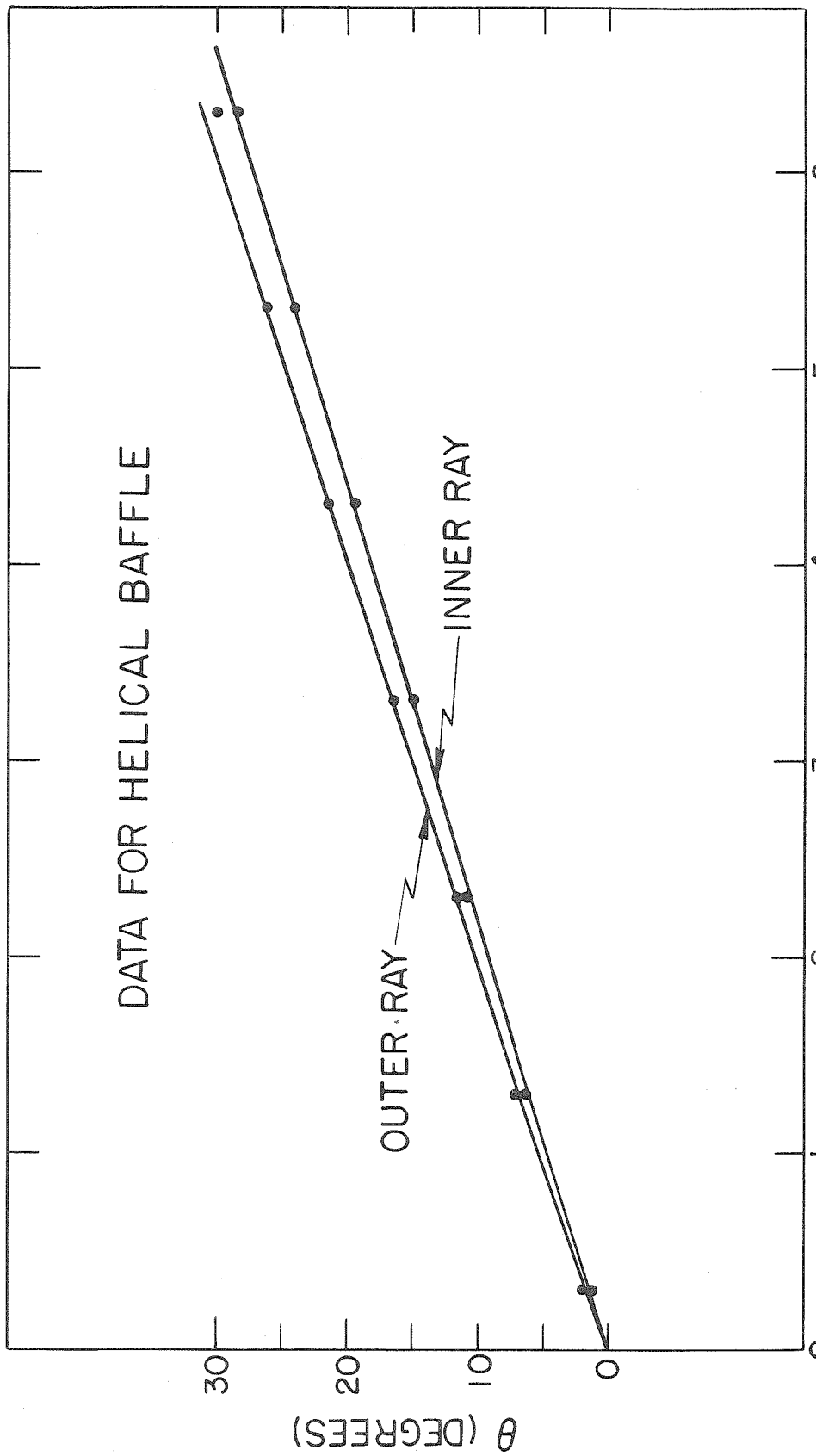
DATA FOR HELICAL BAFFLE
OUTER RAY
INNER RAY
θ (DEGREES)
0
10
20
30
0
1
2
3
4
5
6
AXIAL DISPLACEMENT FROM CENTER OF COIL IN INCHES

FIGURE 26

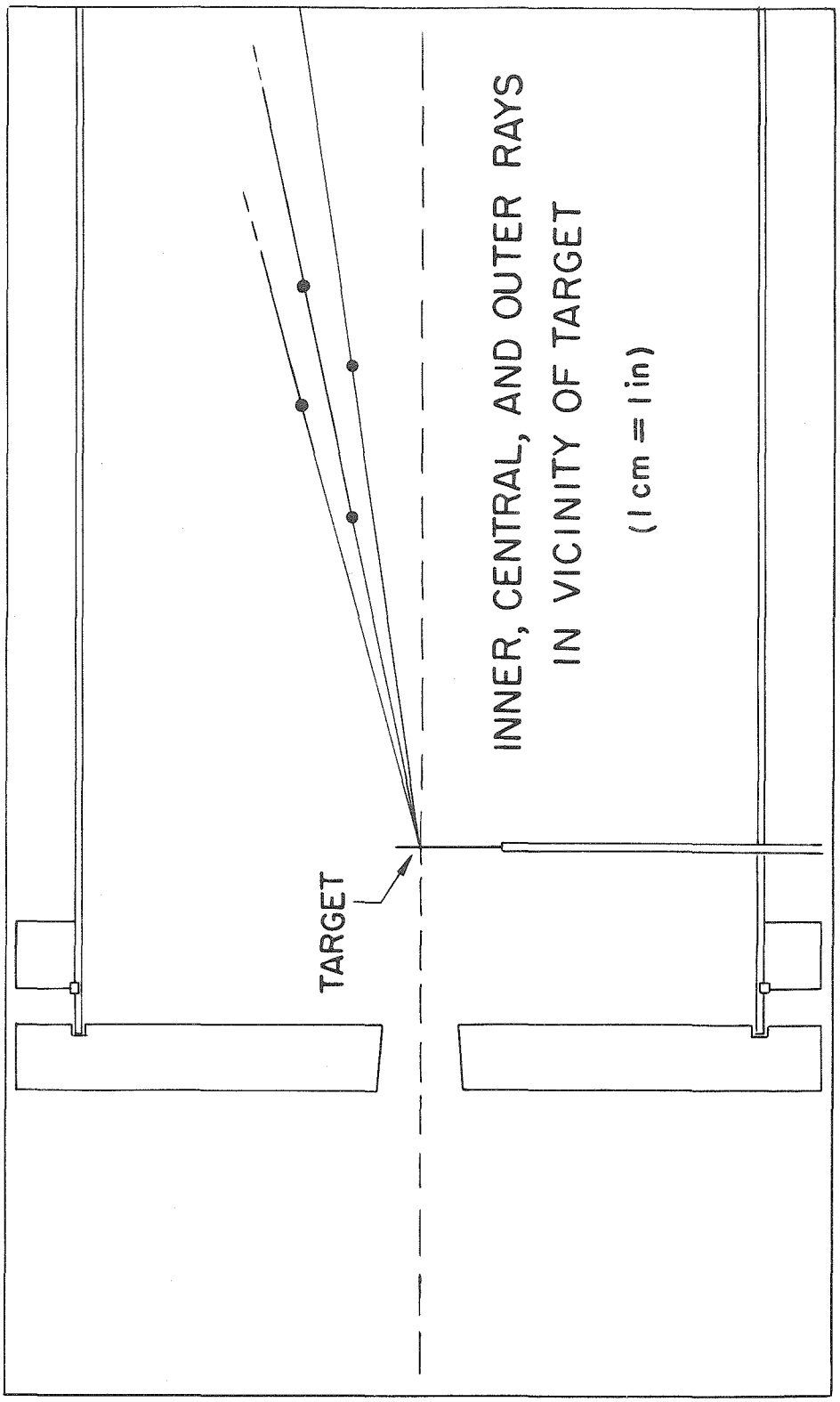
INNER, CENTRAL, AND OUTER RAYS
IN VICINITY OF TARGET
(1 cm = 1 in)
TARGET

FIGURE 27

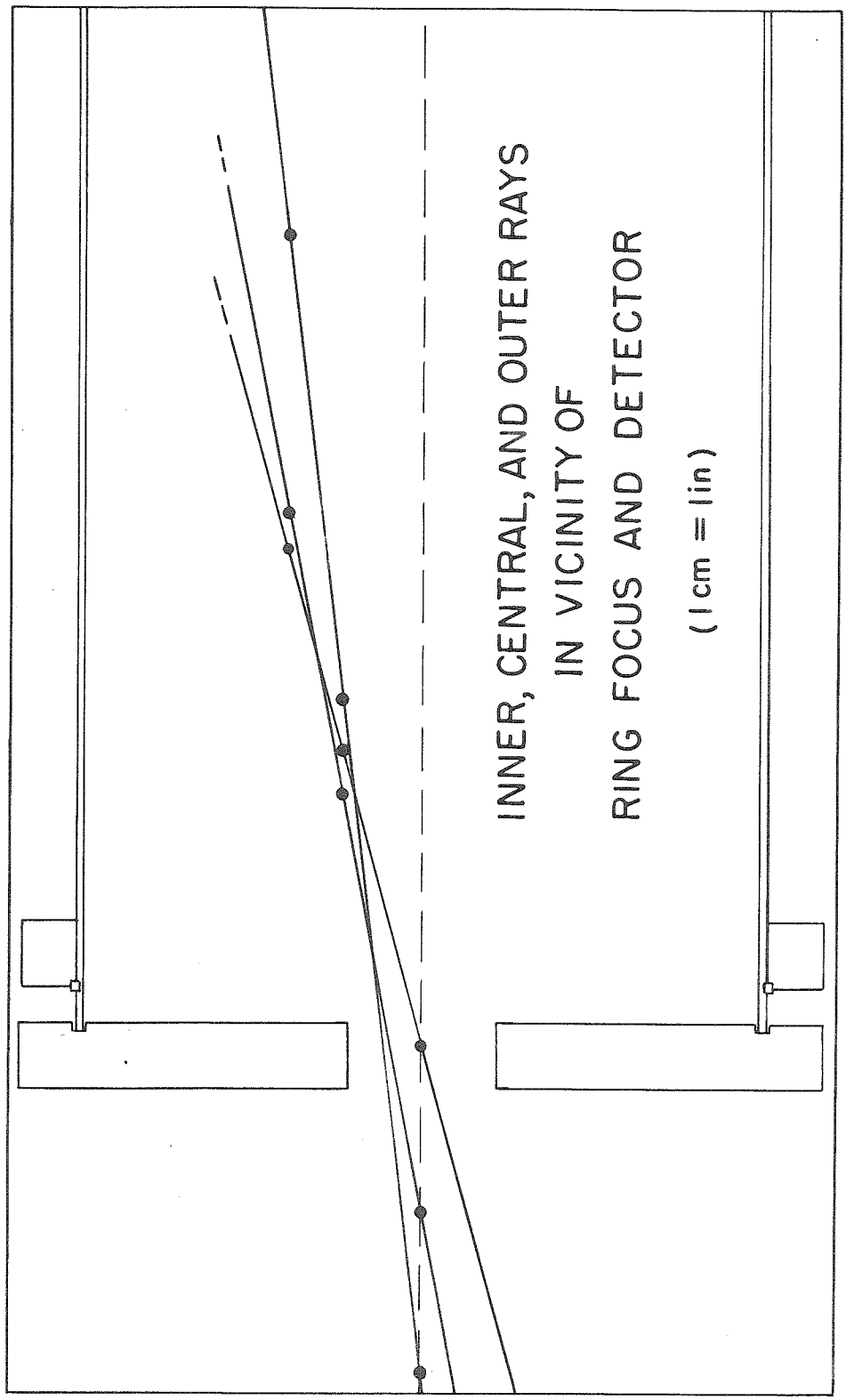
INNER, CENTRAL, AND OUTER RAYS
IN VICINITY OF
RING FOCUS AND DETECTOR
(1 cm = 1 in)

FIGURE 28

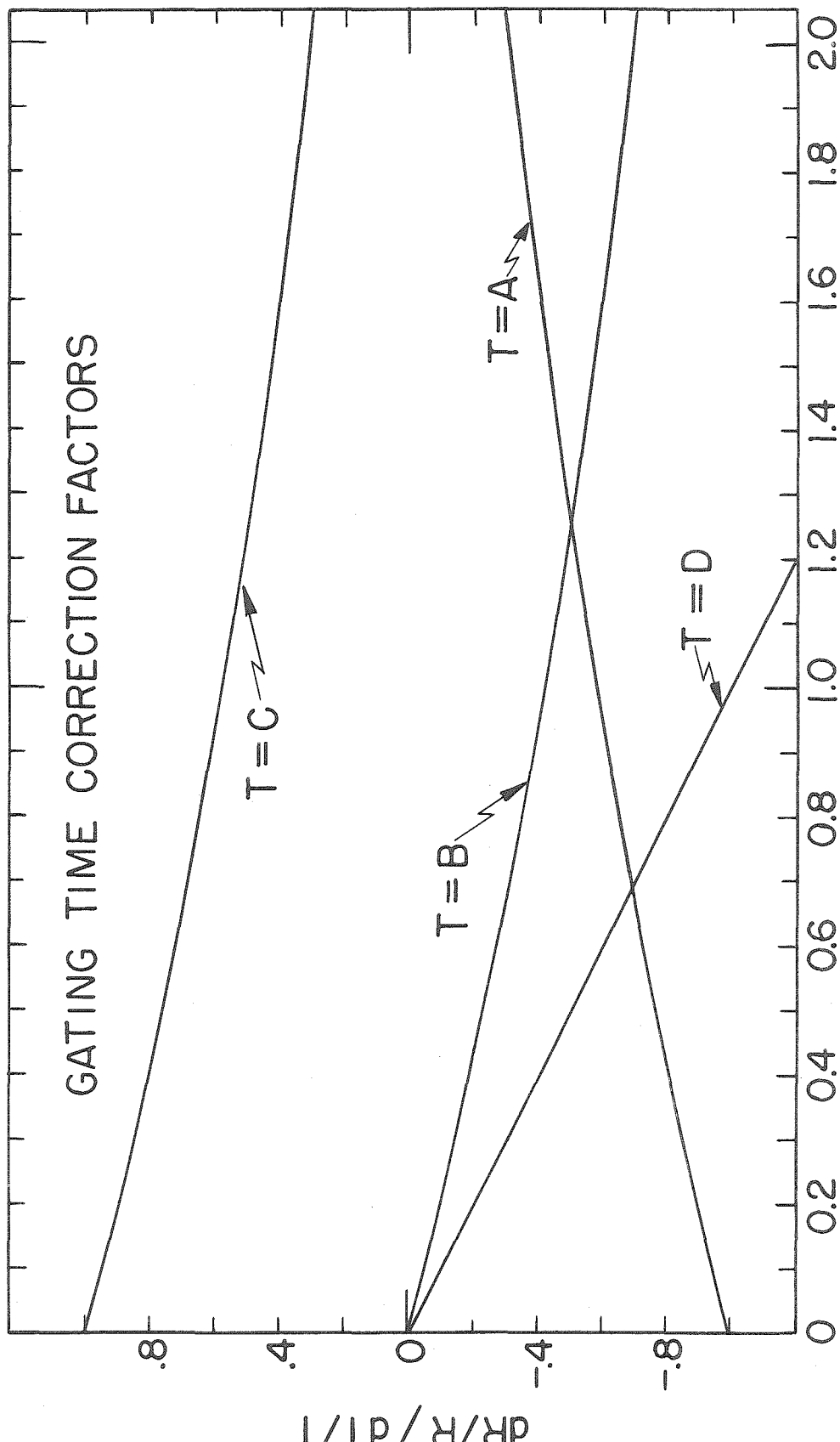
GATING TIME CORRECTION FACTORS
T=C
T=B
T=A
T=D
dR/R / dT/T
x = λT
.8
.4
0
-.4
-.8
0
0.2
0.4
0.6
0.8
1.0
1.2
1.4
1.6
1.8
2.0

FIGURE 29

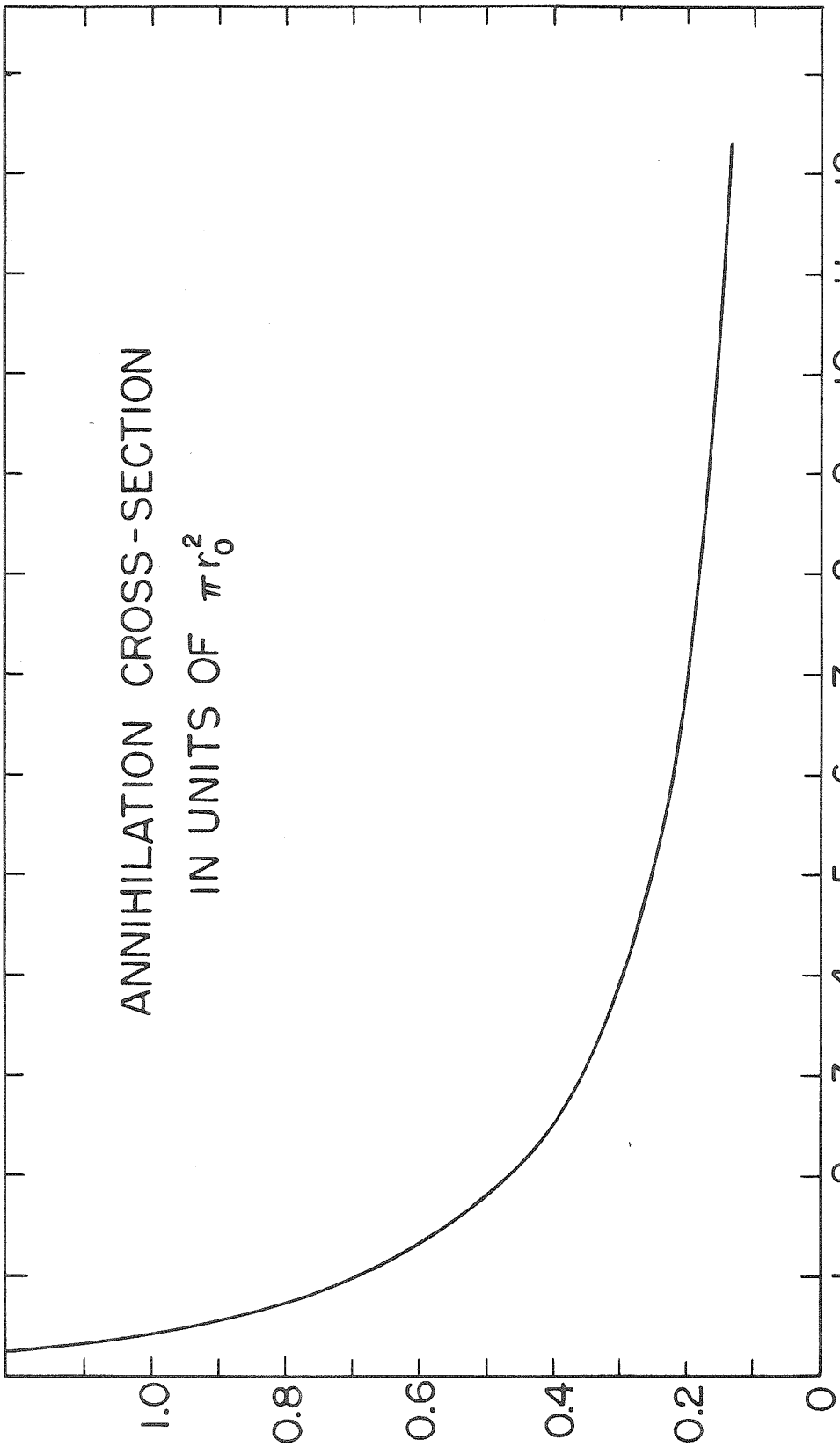
ANNIHILATION CROSS-SECTION
IN UNITS OF πr_o^2
$\phi/\pi r_o^2$
1.0
0.8
0.6
0.4
0.2
0
1
2
3
4
5
6
7
8
9
10
11
12
ENERGY (Mev)

FIGURE 30

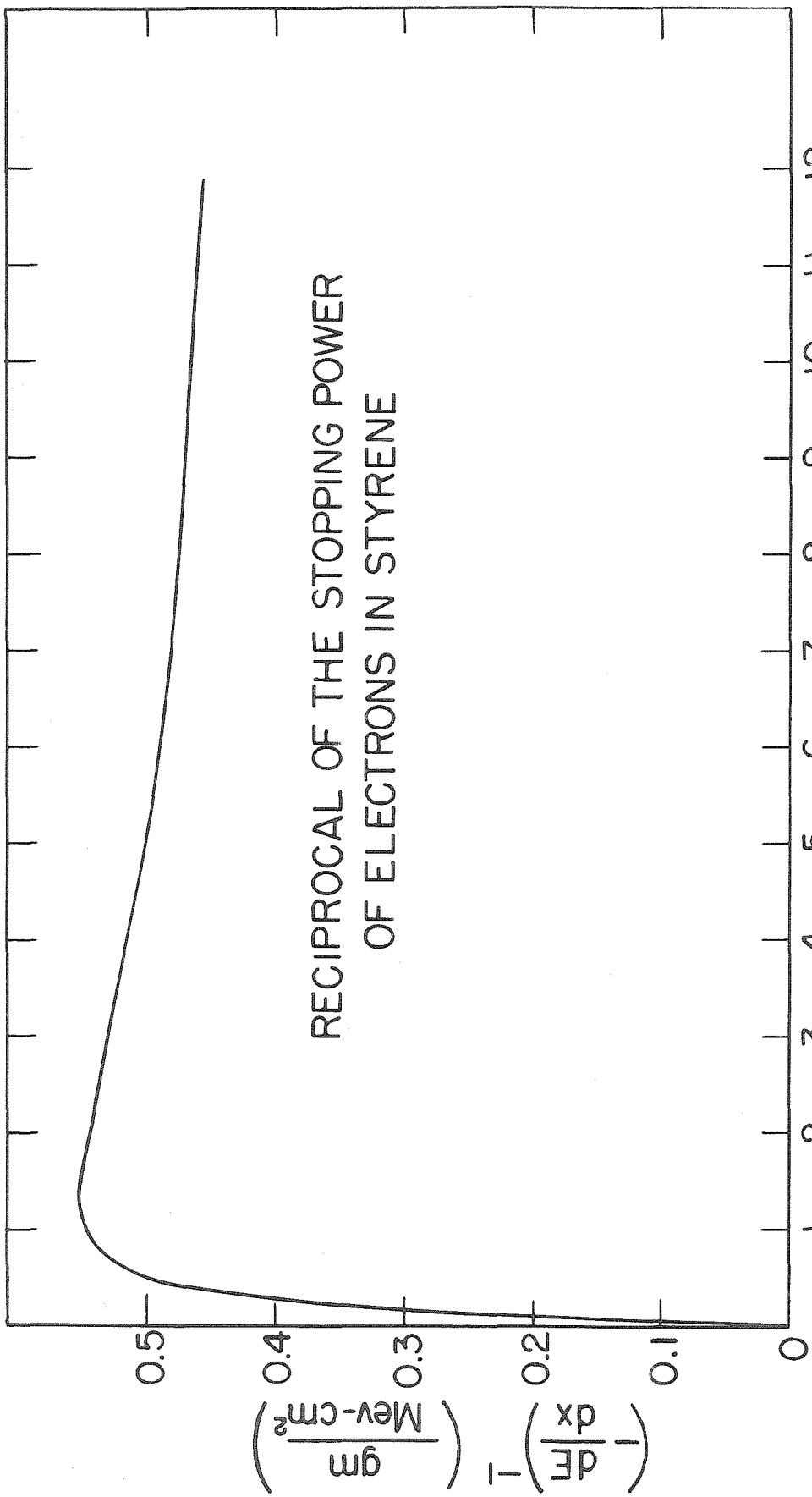
RECIPROCAL OF THE STOPPING POWER
OF ELECTRONS IN STYRENE
$\left(-\frac{dE}{dx}\right)^{-1}$ $\left(\frac{gm}{Mev\text{-}cm^2}\right)^{-1}$
0.5
0.4
0.3
0.2
0.1
0
1
2
3
4
5
6
7
8
9
10
11
12
ENERGY (Mev)

FIGURE 31

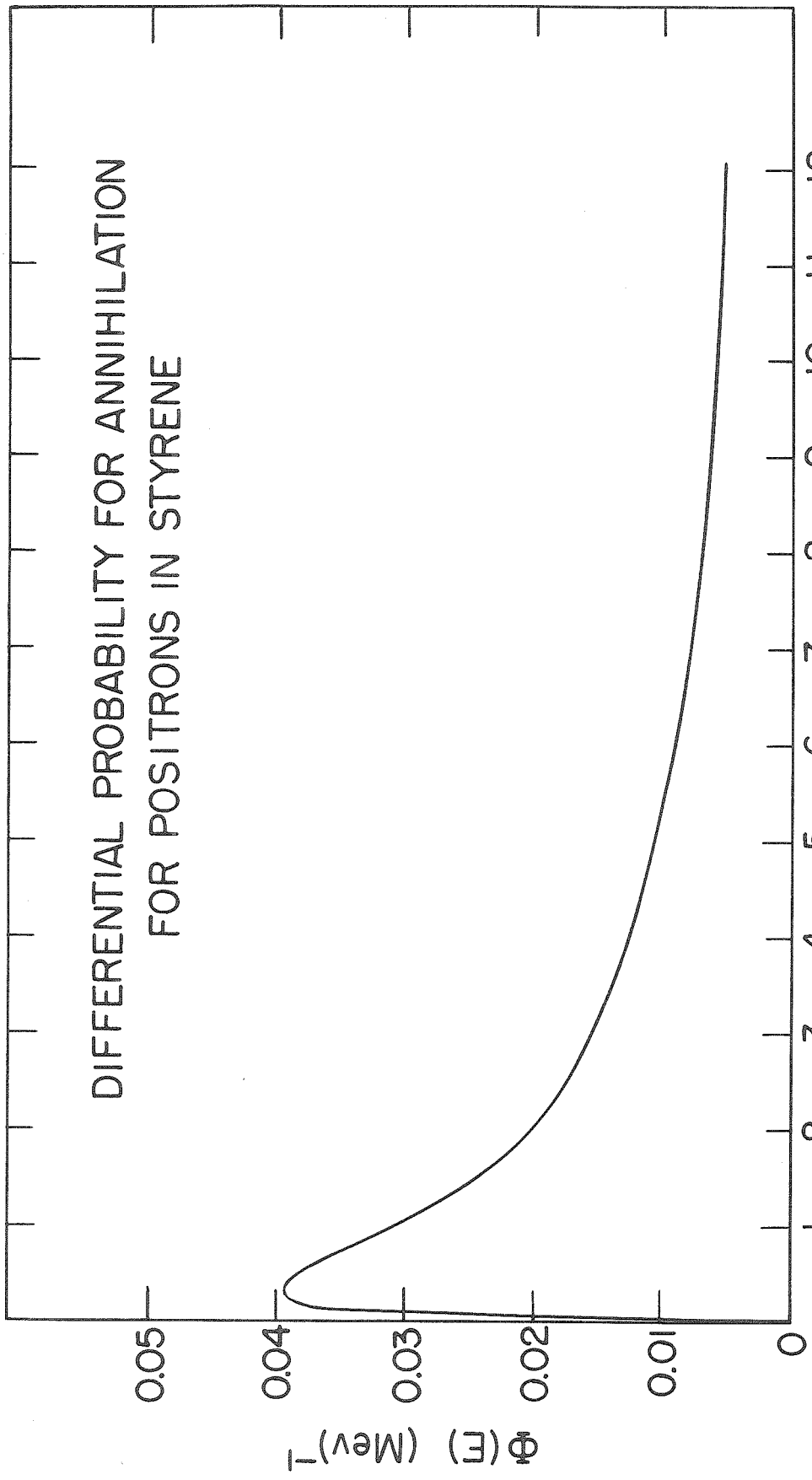
DIFFERENTIAL PROBABILITY FOR ANNIHILATION
FOR POSITRONS IN STYRENE
0.05
0.04
0.03
0.02
0.01
0
Φ(E) (Mev)⁻¹
1
2
3
4
5
6
7
8
9
10
11
12
ENERGY (Mev)

FIGURE 32

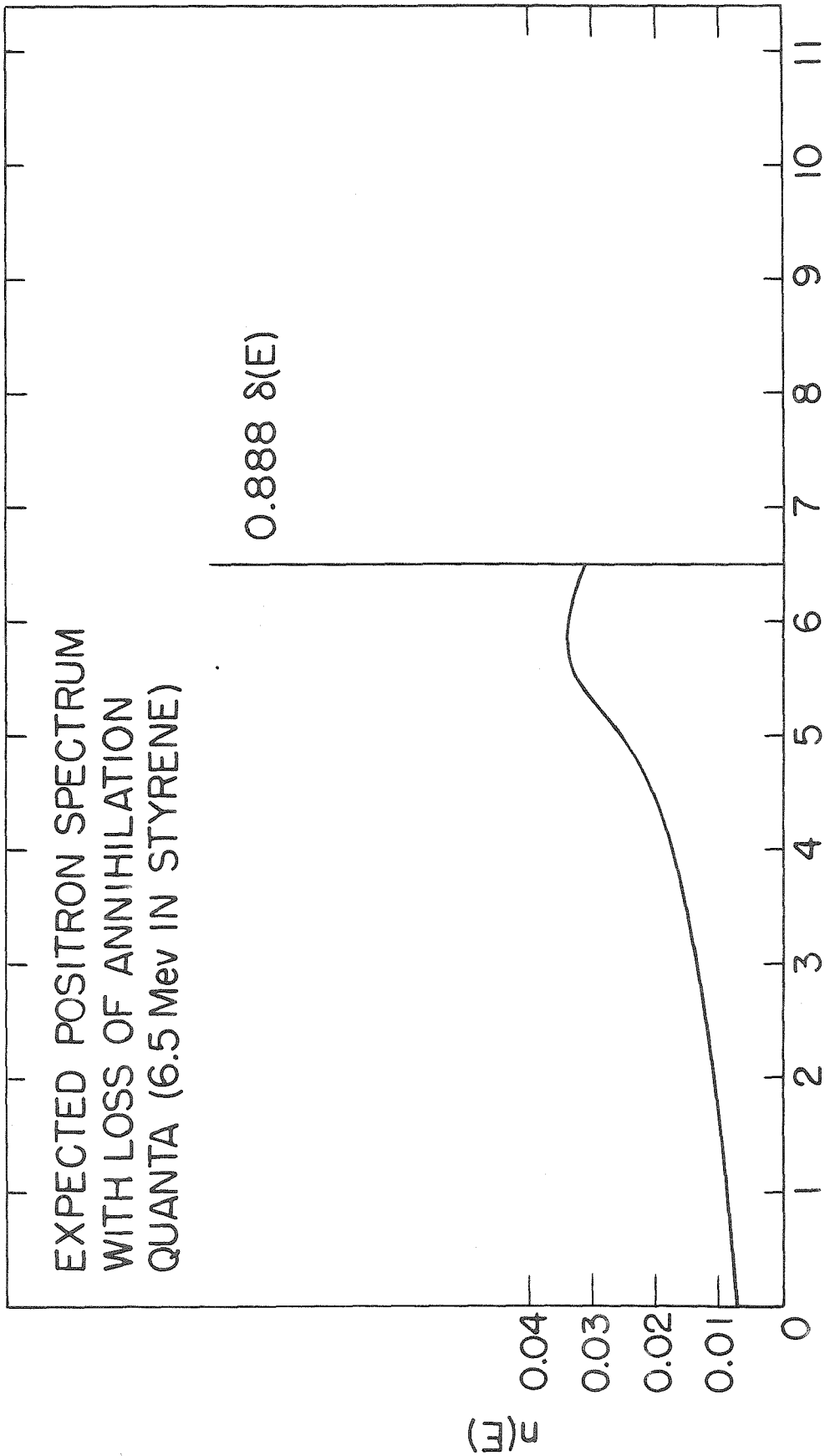
EXPECTED POSITRON SPECTRUM
WITH LOSS OF ANNIHILATION
QUANTA (6.5 Mev IN STYRENE)
0.888 δ(E)
n(E)
0.04
0.03
0.02
0.01
0
1
2
3
4
5
6
7
8
9
10
11
ENERGY (Mev)

FIGURE 33

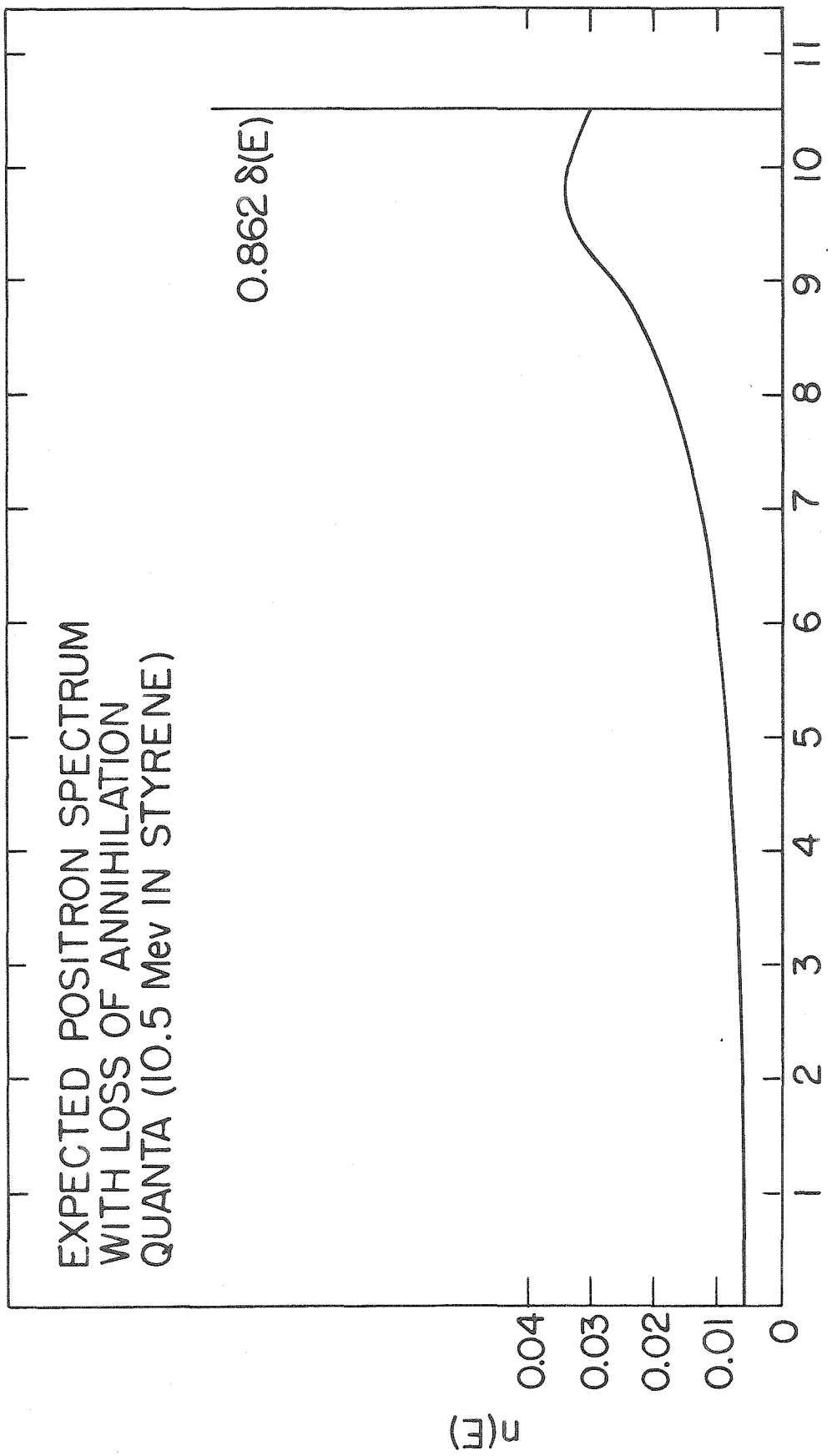
EXPECTED POSITRON SPECTRUM
WITH LOSS OF ANNIHILATION
QUANTA (10.5 Mev IN STYRENE)
0.862 δ(E)
n(E)
0.04
0.03
0.02
0.01
0
1
2
3
4
5
6
7
8
9
10
11
ENERGY (Mev)

FIGURE 34

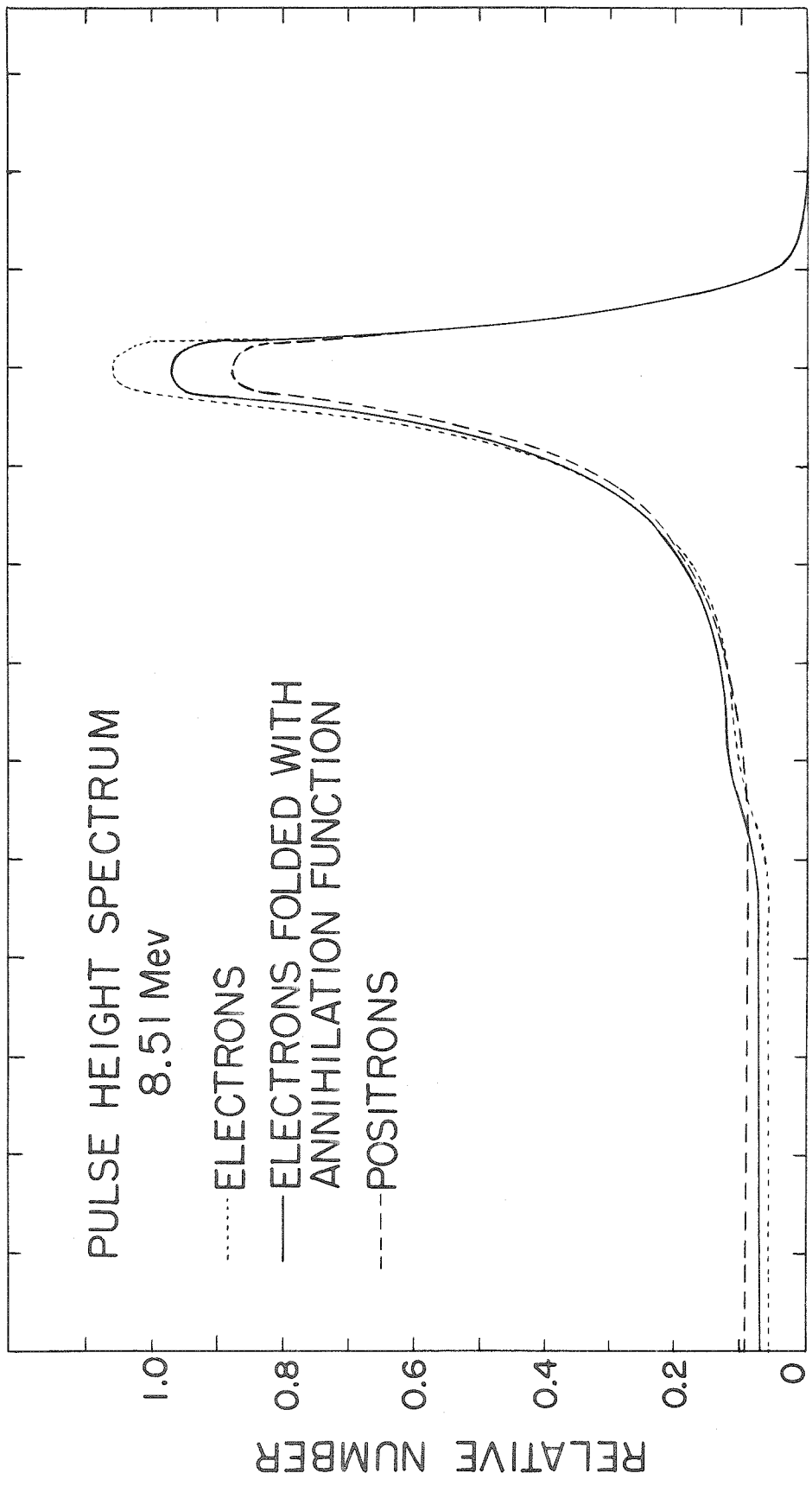
PULSE HEIGHT SPECTRUM
8.51 Mev
ELECTRONS
ELECTRONS FOLDED WITH ANNIHILATION FUNCTION
POSITRONS
RELATIVE NUMBER
0
0.2
0.4
0.6
0.8
1.0
0
0.2
0.4
0.6
0.8
1.0
1.2
PULSE HEIGHT (Arbitrary Units)

FIGURE 35